ASTRONOMY & ASTROPHYSICS
SUPPLEMENT SERIES

Astron. Astrophys. Suppl. Ser. **55,** 179-251 (1984)

A high resolution hydrogen line survey of Messier 31. I. Observations and data reduction

E. Brinks ([1]) and W. W. Shane ([2,1])

([1]) Sterrewacht Leiden, Postbus 9513, 2300 RA Leiden, The Netherlands
([2]) Sterrekundig Instituut, Katholieke Universiteit, Toernooiveld, 6525 ED Nijmegen, The Netherlands

Received April 19, accepted September 23, 1983

Summary. — A new high resolution survey is presented of M31 in the 21-cm line of HI, which gives a more detailed view than has hitherto been available of this nearby galaxy. The observations were made with the Westerbork Synthesis Radio Telescope at an angular resolution of 24″ × 36″, which corresponds to a linear resolution of 80 × 120 pc. The velocity resolution is 8.2 km s^{-1} and velocities are sampled at 4.1 km s^{-1} intervals. The WSRT maps are supplemented by data from the HI survey by Cram *et al.* (1980) with the 100-m Effelsberg telescope to correct for the missing short baselines.
In this paper the calibration and data reduction are described in considerable detail, with emphasis on those parts in the reduction which deviate from standard procedures. The maps are presented in various formats, showing the data from different aspects, in order to give a complete view of the whole data set. Radio photographs of the channel maps are shown at full resolution. At lower resolution, sets of position-velocity maps perpendicular and parallel to the major axis are presented. A radio photo of the total HI surface brightness is also reproduced. A brief discussion is given of the most striking features in this survey, including the presence of many regions which seem devoid of neutral hydrogen. These regions are particularly prominent in the channel maps. In the inner 5 kpc the HI surface density is low. In this region gas clouds are detected at radial velocities which differ by up to 200 km s^{-1} from what one would expect from a simple rotation model. The anomalous velocities in arm 3, which were reported in earlier surveys (e.g. Bajaja and Shane, 1982), can now be traced over a greater extent. At many positions the observed line profile shows multiple peaks. The most likely explanation for this seems to be a warp.

Key words : galaxies : M31 — radio frequency lines : 21-cm radiation.

1. Introduction.

New observations with the Westerbork Synthesis Radio Telescope (WSRT) are presented of the Andromeda galaxy (M31, NGC224) in the 21-cm line of neutral atomic hydrogen (HI). Since its detection in HI by van de Hulst *et al.* (1957), M31 has been the subject of numerous HI surveys. A complete list of such surveys made before 1973 is given by Guibert (1973). Table I extends this list to the present. The observations reported here are a sequel to work by Bajaja and Shane (1982; Shane, 1975, 1978), which was done with the same telescope but with incomplete velocity coverage and modest (27 km s^{-1}) velocity resolution and which was restricted to the central part of the galaxy. After the analogue filter receiver was replaced by a 5120 channel digital back-end, a start could be made with a complete high-resolution survey, covering the galaxy uniformly at a resolution of $\Delta\alpha \times \Delta\delta \times \Delta V = 24'' \times 36'' \times 8.2$ km s^{-1}. The merits of the present data relative to the extensive recent work of Unwin (1980a, 1980b) reside in the higher resolution and higher sensitivity of the Westerbork array. The observations with the 100-m telescope at Effelsberg of Cram *et al.* (1980) are incorporated in order to supply the short-spacing data missing from the WSRT material.

The survey covers most of the optical image of the galaxy. Table II gives some general information on M31. The resolution of the WSRT in the configuration used here corresponds, at the distance of M31, to a linear resolution of about 80 × 120 pc. This is roughly the same linear resolution as is provided by a 25-m single dish, such as the Dwingeloo radio telescope, at the nucleus of our Galaxy. Consequently, galactic structure problems in the Andromeda galaxy can now be studied in detail comparable with that available for studies of the Milky Way galaxy, but from a perspective in some ways more advantageous. The penalty for this high resolution is the quantity of data, which amounts to a few Gigabytes.

We begin with a description of the observations and calibration in section 2. Section 3 is devoted to the various stages of the data reduction, emphasizing the non-standard reduction methods which were employed. The results are presented in various formats in section 4, followed by a brief discussion in section 5. Additional papers are anticipated dealing with the interpretation of the observations.

Send offprint requests to : E. Brinks.

2. Observations and calibration.

2.1 THE 21-CM LINE OBSERVATIONS. — The properties of the WSRT and its operation have been described extensively (Baars and Hooghoudt, 1974; Casse and Muller, 1974; Högbom and Brouw, 1974; Brouw, 1975). Recently the WSRT has undergone some major changes. The analogue receiver system has been replaced by the 5120 channel Digital Line Backend (DLB) and two extra telescopes have been added to extend the WSRT to a 3 km array (Bos *et al.*, 1981). The present observations were all made with the DLB but using the original 1.5 km array. During part of the survey, however, the two new telescopes were temporarily placed on the existing tracks next to the original two movable telescopes, thereby doubling the number of baselines available during a single observation.

Owing to its large angular size of 5° × 1°, many full synthesis fields would be required for full coverage of M31. By restricting the coverage to the optically prominent part of the galaxy, the number of fields required was reduced to five. Figure 1 shows the five field centres together with the corresponding half power circles, superimposed on a blue photograph of M31. The fields are designated Central (C), North East (NE), North West (NW), South East (SE) and South West (SW). The observations were made during four periods : February-March 1978, August-September 1978, January-February 1979, and August-November 1979. All fields suffer more or less from imperfections, mainly due to missing interferometers during part of the observations. Corrections are, where necessary, applied in a later stage of the reduction. Table III gives the instrumental data for each of these fields. All velocities quoted in this paper are heliocentric. Because a high velocity resolution and a wide velocity range were required, the 5120 channels of the DLB were used primarily as velocity channels. This limited the number of polarizations to one and the bit mode to 2 × 2, i.e., 1-bit digitization (Bos *et al.*, 1981). (The slightly more sensitive 2 × 4 mode was not yet implemented when these observations were made.) The channel separation is 4.1 km s^{-1} but before the time-lag to frequency transform, the spectral information was Hanning smoothed to an effective velocity resolution of 8.2 km s^{-1}. Full synthesis with baselines at 18-m intervals was required on each field in order to avoid, as far as possible, the overlapping of grating rings with the synthesized beam response. The resolution across the survey is not exactly uniform. At the time of observing fields C, NE, and NW the fixed telescope which provides the longest baseline was not available because of system tests, resulting in a 10 % decrease in resolution. The noise listed in table III is the noise at the field centre in a single channel map. The noise has, within 10 %, the same value in each field. The systematically higher noise in the two southern fields, after allowance has been made for the difference in beam size, is a combination of two effects. Firstly, when a front-end is tuned to a higher frequency the system temperature increases, resulting in higher noise for the southern fields. Secondly, the telescope and front-end configuration was different for the southern fields. Fields SE and SW were observed using all four movable telescopes. This required simultaneous use of fourteen front-ends, for which the system temperature could vary by up to 30 %. During the rest of the survey only the two original movable telescopes were in use, so that the twelve front-ends having lowest system temperatures could be installed.

2.2 CALIBRATION; CONTAMINATION BY FOREGROUND GALACTIC HI. — The observations were calibrated using the standard WSRT calibration package. Outlines of the calibration procedure are given by Bos *et al.* (1981) and by van Someren Gréve (1974). The sources which were used for calibration are listed in table IV. Source 3C 286, which is polarized, had to be used on one occasion as a flux calibrator (observation date 79035, field SE). The flux density specified is the value which is expected for parallel East-West dipoles. The adopted flux densities of the calibration sources are about 2 % lower than the Baars *et al.* (1977) scale. The amplitude of the signals after calibration, however, is correct. As is explained by de Bruyn and Spoelstra (1983), this 2 % difference is fortuitously compensated in the calibration procedure, because at 21 cm the contribution of the calibrator source to the total power output of the receiver happens to be also about 2 % (see below, formulae (2) and (3)). Source 3C 309.1, although known to be slightly variable, was sometimes used as a flux calibrator. The flux density listed in the table refers to the mean epoch of observation.

Reduction of the other three fields was complicated by the presence of foreground HI from our Galaxy in the passband. The contaminating effect of this HI is threefold :

i) system temperatures are increased by the contaminating HI emission. The resulting decrease in sensitivity varies with the observed field and with frequency;

ii) spectral features are present in the calibrators near $V_{\rm Hel} = 0$ km s^{-1};

iii) channels near a heliocentric velocity of 0 km s^{-1} contain HI emission from our Galaxy. This is quite intense because of the rather low galactic latitude of M31 ($b \simeq -21°$).

The first effect can be illustrated as follows : the total power P measured by one telescope can be written as

$$P = G(T_{\rm A} + T_{\rm S}) \quad (1)$$

where G is a gain factor, $T_{\rm S}$ the system temperature, and $T_{\rm A}$ the antenna temperature, which contains contributions from the object, the sky, the ground, etc. The normalized correlation R_{ij} is given by

$$R_{ij} = \left\{ \frac{T_{{\rm A}i} \, T_{{\rm A}j}}{(T_{{\rm A}i} + T_{{\rm S}i})\,(T_{{\rm A}j} + T_{{\rm S}j})} \right\}^{1/2} \quad (2)$$

where i represents one of the movable telescopes and j one of the fixed ones. Because it is valid to assume that $T_{\rm A} \ll T_{\rm S}$ for almost all uses of the Westerbork telescope, the standard WSRT calibration package contains the approximation

$$R'_{ij} = \left\{ \frac{T_{{\rm A}i} \, T_{{\rm A}j}}{T_{{\rm S}i} \, T_{{\rm S}j}} \right\}^{1/2} . \quad (3)$$

In the case of the M31 survey, however, this approximation does not hold. The radiation entering the telescope will lower the correlation coefficient significantly, or in other words, lower the sensitivity of the system. If the amount of incoming radiation were the same for the observations of the calibrator sources as for the observations of the various M31 fields, it would appear to the calibration programmes that the telescope as a whole had suddenly become somewhat less sensitive as compared to observations on other objects done during the same period. The gain factor which is needed to correct any observation for loss in correlation is the ratio R'_{ij}/R_{ij},

$$F_{ij} = R'_{ij}/R_{ij} = \left\{ \frac{(T_{Ai} + T_{Si})(T_{Aj} + T_{Sj})}{T_{Si}\, T_{Sj}} \right\}^{1/2} . \quad (4)$$

The contribution of T_A to the factor F_{ij} is different for each M31 field, and for each of the calibrator sources and it also varies as a function of the frequency setting and bandwidth used. Because during the observations of M31 the noise source described by Bos *et al.* (1981) was not yet operational, we could not continuously monitor the system temperature, but rather had to rely upon separate total power observations. In principle F_{ij} can be determined for each field and velocity separately, but in practice this is not feasible because it is hard to find a field which contains no HI emission near 0 km s^{-1}. As will be clear from above it is sufficient to determine factors which bring the loss in correlation for the two calibrator sources to the same level as that for the corresponding M31 field. This requires a correction of F^C_{ij} :

$$F^C_{ij} = \left\{ \frac{(T^C_{Ai} + T_{Si})(T^C_{Aj} + T_{Sj})}{(T^M_{Ai} + T_{Si})(T^M_{Aj} + T_{Sj})} \right\}^{1/2} . \quad (5)$$

The superscript C stands for calibrator and M for M31. The factors F^C_{ij} can be obtained by observations of the calibrators and the M31 fields in the total power mode. The total power observations were made on the calibrators at all frequency settings used and with a 5 MHz and 2.5 MHz bandwidth and on the three M31 fields in order to determine these factors.

The second effect, the presence of sharp spectral features in the calibrators near zero velocity, influences both the amplitude and the phase. The amplitude of a calibrator as a function of frequency shows an absorption feature and the phase, especially for the shorter baselines, is influenced primarily by emission features distributed over the field. Figure 2 shows the amplitude and phase of 3C 147 as a function of frequency for a baseline of 36 meters as derived from a calibration measurement. A spectral feature in a calibrator can usually be eliminated by splitting the calibration observation into two parts, each part shifted symmetrically in frequency with respect to the frequency at which the object is observed, so that the contaminating feature falls outside the passband (J. D. Bregman, private communication). For an observation with a narrow total bandwidth, the assumption that the instrumental gain and phase vary linearly as a function of frequency is admissible. For the present observations the bandwidth is too broad to permit this assumption. Instead, each calibrator observation was split into three parts, one at the frequency of the observation of M31, one shifted by + 0.625 MHz and one by − 0.625 MHz. Each of these measurements was corrected separately for loss of correlation as described above. In each measurement the part affected by foreground HI was deleted and, through proper weighting, a featureless calibration spectrum was constructed. A shift of 0.625 MHz is small enough that the instrumental phase and gain vary linearly but large enough to shift the part of the spectrum affected by foreground HI over at least its own width. As the frequency of observation gradually changed over the year, the part of the spectrum of the calibrator which had to be deleted also changed.

The third effect, the presence of foreground HI features in the maps of M31 near 0 km s^{-1}, will be discussed in connection with the further map processing.

The flux calibration is estimated to be more accurate than 2 % and the phases more accurate than 2°, which, after adding another 2° due to the baseline calibration, corresponds to a positional accuracy of 0.5 arcsec.

3. Data reduction.

3.1 Fourier transformation of the data and subtraction of the continuum contribution. — The WSRT observations were Fourier transformed to produce channel maps using standard programmes (Brouw, 1969; Harten, 1979). Ten percent of the channels on the high velocity side of the band are not used because they are too close to the edge of the passband and are subject to severe attenuation. The first five to eight channels on the low velocity side show strong elliptical rings centred on the fringe stopping centre, and these channels were also excluded from the remainder of the reduction. The channel maps contain both line and continuum radiation. A method frequently used to subtract the continuum radiation is to make a continuum map by averaging all channels containing no HI emission. Due to galactic HI in the observations of the central and northern fields, channels on these fields free from line radiation are found only on the low velocity side of the band. The continuum maps based on these channels would have had higher noise, because of the smaller number of contributing channels, than the continuum maps of the southern fields and would have been asymmetric with respect to the global line profile. In order to avoid these inhomogeneities and to restrict the introduction of additional noise, the continuum correction was derived from separate broad-band 21-cm continuum observations (Walterbos, Brinks and Shane, in preparation), made at the same field centres as the line observations.

The broad-band continuum survey, which was done at 1412 MHz with a 10 MHz bandwidth could not be subtracted directly from the line survey, because of the difference in observing frequency. However, this has a measurable effect only on the grating rings of strong sources. We therefore identified the strongest discrete sources in both surveys. The positions and flux densities of these sources from the two surveys were found to agree to within the accuracy with which they could be determined. This agreement shows that the calibration is internally consistent and that effects of foreground HI have been compensated properly. These discrete sources, described by their mean parameters, were subtracted from all line and continuum observations before the Fourier transformation. In the case of strong extended sources, clean components were derived (Högbom, 1974; Harten, 1974; Schwarz, 1978) and subtracted. The continuum emission from M31 itself is weak enough that the corresponding grating rings will be well below the noise so it is not necessary to correct these features for the difference in observing frequency. The continuum maps, with the strongest sources subtracted, were made as identical as possible to the line maps by specifying the same baselines in the Fourier transformation. The continuum maps were then subtracted from all channels of the line survey.

The disadvantage of using independent continuum observations is that small errors in the calibration of the line observations which tend to decrease the dynamic range, are not removed when subtracting the continuum. On four fields the calibration appeared to be consistent, but the HI maps of field SE showed some residual grating rings attributable to the strongest continuum source in the field. We removed these rings as follows : all corrected channel maps containing no HI emission were added to give a continuum recorrection map. This map was transformed to polar coordinates (appropriately compressed in declination) centred on the strongest source and was then convolved in azimuth, thus smoothing away all features except the non-cancelling grating rings. All intensities outside the region with grating rings were then set to zero, and the map was retransformed to the original coordinate grid. The map produced in this way was subtracted from the maps containing line radiation.

3.2 CORRECTION FOR THE MISSING SHORT SPACINGS. — The maximum spacing employed in the survey is 1458 m; the minimum spacing is 36-m. The 0-m and 18-m baselines can not be observed by the WSRT. As a result, the main lobe of the synthesized beam is embedded in a broad depression. The maps have a varying zero level, depending upon the position and amount of emission present. There are two ways to correct for this. One way is to extrapolate the missing spacings from the interferometer data. The other, more satisfactory way, is to include observations made with a different instrument which contain the missing information. For M31, a suitable survey with the 100-m telescope of the Max-Planck-Institut für Radioastronomie (MPIfR) at Effelsberg by Cram *et al.* (1980) was available. These spectra were kindly sent to use by D. T. Emerson at the MPIfR in Bonn. Dr. Emerson convolved the spectra to the WSRT channel width and subsequently produced five sets of channel maps, one for each field, gridded to the sky coordinate system of the WSRT (Brouw, 1975). The missing short spacing data were derived from this survey using the method described by Bajaja and van Albada (1978). These 0-m and 18-m data were incorporated into the WSRT interferometer data during the Fourier transformation.

Figure 3 shows maps and cross cuts made through these maps with and without inclusion of the short-spacing data. The maps are convolved to a larger beam to accentuate the low spatial frequencies. The zero level after correction is flat out to the grating rings. Figure 4 shows the amplitude and phase of the artificial 36-m interferometer derived from the 100-m data as a function of hour-angle compared to the corresponding observed WSRT 36-m data. The phases agree to within 5 to 10 degrees. The 100-m fluxes had to be rescaled slightly in order to make them agree with the WSRT fluxes. In the southern half of the survey the 100-m fluxes are about 5% higher than the Westerbork fluxes; in the North they are on the average 5 % lower. There is evidence that the WSRT flux scale is consistent because sources which were observed in overlapping fields of the WSRT survey agree in both position and flux density. Also, the flux densities of continuum sources found in the WSRT 21-cm line survey are in agreement with the results from the 21-cm continuum survey. The discrepancy between the 100-m and the Westerbork data can probably be attributed to the single dish observations where there appears to be an amplitude jump at the point where the northern and southern surveys overlap. These two surveys were done a year apart and a special calibration scheme was used in the northern survey because of the presence of foreground HI. The 100-m data were recalibrated by comparing the artificial 36-m interferometer data, and in some cases also the 54-m data with the observed WSRT amplitudes. The correction amounts to about 5 %, which is within the accuracy of the absolute calibration. After including the short spacings, the absolute flux density scale of the whole survey is accurate to about 5 %, assuming a 2% error in the WSRT flux calibration, a 2% error in the recalibration of the 100-m amplitudes with respect to the WSRT values and a 4% error in the absolute temperature scale after calibration. The positional accuracy which is largely determined by the WSRT calibration, is 0.5 arcsec (see 2.2). All channels, except the eighteen highest-velocity channels of fields C, NE, and NW, which contain foreground HI, were corrected by adding the 100-m data to the WSRT data. The remaining channels were corrected by extrapolation, as will be explained in the next section.

3.3 CLEANING OF THE MAPS. — The next step in the reduction involved : i) correcting for the missing short spacings on the maps which contain foreground HI; ii) correcting for missing data at certain baselines and hour angles; iii) isolating the HI emission from grating rings in those maps where the HI is so extended that the 40 arcmin grating rings cross the regions of emission. In this stage of the reduction extensive use was made of map cleaning techniques (Högbom, 1974; Harten, 1974; Schwarz, 1978).

3.3.1 *Correction for missing short spacing data by cleaning.* — No short spacings from the 100-m data were added to those channels where foreground HI emission was present. Instead, use was made of the fact that the interferometers do not see large scale features. Only weak emission from our Galaxy is detected in the WSRT channel maps. In order to correct for the missing spacings the maps were cleaned and restored. As we are interested only in large scale structure when making this correction, the maps were first smoothed to four times their original beam dimensions. On these maps the radiation was completely decomposed into components using the standard cleaning procedure. A side-lobe correction antenna pattern was constructed by taking the convolved antenna pattern and setting all points in the central positive area to zero. This antenna pattern was then subtracted from the original full-resolution maps with the central position and intensity described by the above components. In this way the side lobes corresponding to the low spatial frequencies were removed while the original resolution was retained.

In order to test this cleaning procedure, one channel map of field SW (at a radial velocity of -568.6 km s^{-1}) which had been corrected for the missing short spacings by adding the 100-m data, was also corrected by cleaning. After cleaning, the zero level of the map was flat, but comparison of this map with the map corrected by including the short spacings from the 100-m data showed, as expected, that structure at a very large angular scale was missing. An appreciable fraction of the total flux in the map is not found by cleaning. This fraction can vary depending on the complexity of the HI distribution. We estimate that 20 % is a representative figure for the fraction of the total flux in the map which is missed by cleaning, because the test map has an HI distribution quite similar to that of the northern fields at velocities near 0 km s^{-1}.

3.3.2 *Cleaning of side-lobe structure.* — The baseline coverage of each field is fairly complete. The side-lobe structure caused by the deletion of unreliable data points or the absence of some interferometers in the observation is of the order of a few percent of the peak emission in the field and, because most of the missing data fall at intermediate spacings, has a moderate spatial frequency. The same clean technique was applied as above. Because of the moderate spatial frequency involved, the maps and the synthesized beam pattern, which are both corrected for the missing short spacings, were smoothed to twice their original resolution. The maps were cleaned down to about four times the r.m.s. noise on the convolved maps. The components found in this way were cleaned from the full resolution maps using the convolved antenna pattern with the central peak removed.

3.3.3 *Separation of emission from grating rings.* — Separation of emission from grating rings when the grating rings overlap with emission is a very delicate procedure. Using the same clean technique as described above, the maps were cleaned in three steps. First components were determined from the full resolution map and cleaned. The resulting map was convolved to twice the resolution and again components were determined and cleaned. Then the residual map was smoothed to four times the resolution and the emission was decomposed into a final set of components. Each clean step was carried down to about five times the r.m.s. noise on the map to be cleaned, using for each the corresponding convolution of the antenna pattern, always with the central peak set to zero. As above, the short baselines which had been incorporated in the maps, were also included in the antenna patterns.

3.4 COMBINATION OF THE FIELDS. — The final step in the data reduction involved the combination of the five separate fields. Because inadvertently the optical definition for Doppler shift had been used for calculating the observing frequency of the centre of the band instead of the radio definition, $\Delta\nu/\nu_0 = -\Delta V/c$, the velocities of the overlapping channels from the different fields did not match perfectly. This was corrected for by a linear interpolation in velocity between neighbouring channel maps of fields NE, NW, SE and SW to the same frequencies as the central field. The maximum shift is 0.4 km s^{-1} or about 10 % of the channel separation. The reference velocity of the whole survey is now the velocity of the centre of the band of field C, i.e. -263.6 km s^{-1}.

Before the maps could be combined, the HI had to be isolated from its own grating rings. A grating ring in a map of one field could go right across the HI in a map at the same velocity of a neighbouring field. In order to benefit from the increased signal-to-noise ratio in the regions of overlap, an area as large as possible, i.e. up to the grating rings, around the HI emission in each single channel map was selected. A mask, having a value of 1 inside and a value of 0 outside the region to be retained, was made for each channel map. Masks were also made for those channel maps which were contaminated by small-scale foreground HI. For those channels, masks were made which accepted emission from M31 only. Emission from M31 was separated from what was thought to be galactic foreground HI by visual inspection on the Leiden Image Processing System. Groups of six neighbouring channel maps were loaded into the memory of the system. The maps were displayed rapidly in sequence. HI belonging to M31 gradually changed position with velocity following the general pattern of differential rotation, while foreground HI moved almost randomly across the screen.

The five fields could not be combined in a straightforward manner, because they were all observed at different fringe stopping centres, and were therefore generated on different coordinate grids (see e.g. Brouw, 1975). Before combining, the maps were reinterpolated onto the sky coordinate grid defined by the fringe stopping centre of the central field. The maps of the five fields were averaged using weight factors determined on the basis of the primary beam attenuation, which is approximately Gaussian with a half power width of 37.′6. The analytical expression for the primary beam attenuation actually used is $f(r) = \exp(-4.394\, r^4 + 0.7075\, r^3 - 6.875\, r^2)$, where r is the distance from the fringe stopping centre in degrees. This expression has the same functional form as that given by Katgert (1975) but contains slightly improved coefficients. We define :

S_i = intensity at a grid point in a channel map of field i,

f_i = primary beam attenuation at a grid point of field i,

m_i = mask value (0 or 1) at a grid point of field i,

$S_i^c = S_i/f_i$ = intensity corrected for the primary beam attenuation

and

$\sigma_i = \sigma/f_i$ = noise at a grid point in a channel map of field i after correction for primary beam attenuation.

The noise σ_i per channel is constant to within 10 %. When combining the fields, we assumed that σ had the same value in each field. The optimum choice for the total intensity, S^T, at a grid point, corrected for primary beam attenuation, which results in the highest signal-to-noise ratio in the regions of overlap then becomes :

$$S^T = \left(\sum_{i=1}^{n} S_i^c\, m_i/\sigma_i^2\right) \Big/ \left(\sum_{i=1}^{n} m_i/\sigma_i^2\right) \qquad (6)$$

where the summation is over all maps which overlap.

This can be rewritten as :

$$S^{\mathrm{T}} = \left(\sum_{i=1}^{n} S_i m_i f_i\right) \Big/ \left(\sum_{i=1}^{n} m_i f_i^2\right). \tag{7}$$

The noise, σ^{T}, in the combined map at each grid point is

$$\sigma^{\mathrm{T}} = \sigma \Big/ \left(\sum_{i=1}^{n} m_i f_i^2\right)^{1/2}. \tag{8}$$

For some applications it is useful to have maps in which the noise is constant over the whole map and the sensitivity varies accordingly. These are analogous to single field maps before correction for primary beam attenuation. From (7) and (8) it follows that this equal-noise map, S^{E}, is obtained through

$$S^{\mathrm{E}} = \left(\sum_{i=1}^{n} S_i m_i f_i\right) \Big/ \left(\sum_{i=1}^{n} m_i f_i^2\right)^{1/2}. \tag{9}$$

Figure 5 is a contour map of the total sensitivity of the survey if all five fields are combined without masks, $m_i \equiv 1$ for all i.

Because the synthesized beam is slightly smaller for the two southern fields, the fluxes were first converted to brightness temperatures before the channel maps of the five fields were combined. For fields SE and SW, 1 K is 1.20 mJy per beam and for the other fields 1 K is 1.39 mJy per beam. After combination the resolution varies across the maps by some 10 %. We also produced maps at a resolution of 48″ × 72″, i.e. at twice the original resolution. For this purpose the channel maps of the individual fields were smoothed to the desired resolution by convolution with a gaussian function, the two southern fields with a broader gaussian to compensate for the difference in beam size, after which the fields were combined. On these maps 1 K corresponds to 5.55 mJy per beam and the r.m.s. noise at the field centre of the central field is 0.60 K. At each resolution a set of combined channel maps with and without correction for the primary beam was produced.

In order to reduce the contribution by noise to maps of the total HI surface density, the combined channel maps were again masked. The equal-noise maps at 48″ × 72″ were smoothed to four times their original resolution. Masks were constructed which accepted only emission above a level of two times the r.m.s. noise, on these maps 0.20 K, compromising between accepting too many spurious peaks and excluding genuine emission belonging to M31. These masks, M_i, were made without taking account of the fact that neighbouring channels are correlated through the Hanning taper. To reduce the number of noise peaks and to enhance continuity between successive channel maps new masks were defined as :

$$M_i' = M_{i-1} \cap M_i \cap M_{i+1} \tag{10}$$

thus accepting emission only if it occurred in three consecutive channel maps. This procedure reduced the number of spurious peaks but also affected the emission of M31, which shifts in position as a function of channel. To compensate for this, final masks were defined as :

$$M_i'' = M_{i-1}' \cup M_i' \cup M_{i+1}'. \tag{11}$$

These masks were applied to the various sets of combined maps mentioned above.

The final results are represented by the following set of data cubes :

a) 147 channel maps at a resolution of $\Delta\alpha \times \Delta\delta \times \Delta V =$ 24″ × 36″ × 8.2 km s^{-1}. The maps are sampled at velocity intervals of 4.1 km s^{-1} and corrected for the primary beam ;

b) as *a*, but with equal-noise ;

c) 147 channel maps at a resolution of $\Delta\alpha \times \Delta\delta \times \Delta V =$ 48″ × 72″ × 8.2 km s^{-1}. The maps are sampled at velocity intervals of 4.1 km s^{-1} and corrected for the primary beam ;

d) as *c*, but with equal-noise.

In due time these maps will be made available in FITS-format. Upon request, maps at other stages of the reduction, for instance, unmasked versions of datasets *a* to *d*, may be obtained. It is anticipated that about 45 tapes with 1600 BPI will be needed to transport data cubes *a* and *b* and 12 tapes for data cubes *c* and *d*. The total amount of data is of the order of 1 Gigabyte.

4. The results.

Because the data set is so voluminous, it is not possible to present it as a complete set of intensity maps, nor is it possible to present all of the data in a quantitative way. The maps given here are selected to give an overview of the HI survey, showing the data from various aspects. Figure 6 is a collection of channel maps, showing the data at full resolution (dataset *a*) as radio photographs. Because neighbouring channels are correlated, the maps are shown at 8.2 km s^{-1} intervals. The maps were photographed from the monitor of the Leiden Image Processing System which is based on a COMTAL® Vision 1 system. The largest data matrix which can be displayed by this system is 512 × 512 pixels. As the full resolution maps measure 1024 × 1024 pixels, they were first rotated around the central pixel, $\alpha_c = 0^h40^m00^s$ and $\delta_c = 41°00'00''$, so that the major axis of M31 was vertical. The data then fit into 512 × 1024 matrices, out of which 512 × 512 matrices were subsequently extracted, centred on one of three positions along the major axis, 32.′26 North of the nucleus, on the nucleus, or 32.′26 South of the nucleus. These matrices were displayed on the monitor. *X* and *Y* coordinates are given in a rectangular grid centred on the nucleus of M31 with *X* measured along the major axis and *Y* along the minor axis. To avoid ambiguity in sign, the axes are labeled N, S, and E, W following Bajaja and Shane (1982). Due to distortion of the monitor the coordinate grid is only approximate and deviations of 1 or 2 arcmin can occur, particularly at the edges of the map. The heliocentric velocity is indicated on top of each frame. The resolution can be judged from the size of a single noise peak. The resolution is slightly higher in the South. Because the maps are corrected for primary beam attenuation the noise varies across the maps, being highest at the extreme North and South end of the major axis. The displayed intensities range from 2.5 K at the r.m.s. noise level to about 50 K at the HI peaks.

It is difficult from figure 6 to see the continuity in velocity. This is better illustrated by maps which show the brightness temperature as a function of position and velocity along a cross cut through the galaxy. We have constructed two such sets of position-velocity maps, one set at regular intervals of 1.2 arcmin perpendicular to the major axis (Fig. 7) and the other at the same intervals parallel to the major axis (Fig. 8). The cross cuts were made through the maps at the lower resolution, dataset *c*. In this way extended low level emission is better seen and the distance between cross cuts can be made larger than would be the case for the full resolution maps. The resolution is $54'' \times 8.2$ km s^{-1} for the maps in figure 7 and $60'' \times 8.2$ km s^{-1} for figure 8. The total HI surface density map of M31 is shown in figure 9 as a radio photograph. The beam is indicated in the lower right corner. Again the coordinates are only approximate. The noise varies across this map and is highest at the extreme northern and southern ends of the galaxy.

Although figures 6 to 9 show the available data from various aspects it is still hard to visualize continuity along the three coordinates simultaneously. Therefore the maps were recorded on 16-mm film. The production of this film is described by Shostak and Brinks (1983). The film was made using the facilities of the Groningen Image Processing System (GIPSY), which is described by Shostak and Allen (1979). Maps analogous to those of figures 6 to 9, but now at smaller intervals were recorded on film. The filmed sequences are black and white. Some static shots, like the total HI surface brightness map, are in color. The duration of the film is about 8 minutes, including brief titles describing the sequences. Copies of the film may be obtained at cost (about 250 Dutch guilders) from the first author.

5. Discussion.

A full analysis of the data presented here is in progress and will be presented in due course. Only a brief discussion will be given here of the most striking features in the maps.

5.1 Hydrogen distribution. — The individual channel maps of figure 6 show a wealth of detail. Many filaments, arcs and shell-like structures are found delineating regions which seem devoid of neutral hydrogen. At present some 250 of these have been listed, and a detailed study of their correlation with OB-associations, HII-regions, etc. is in progress. One large structure, coinciding with the bright OB-association NGC 206 (OB78 of van den Bergh, 1964) has already been studied in more detail (Brinks, 1981), and results on a few others are given by Brinks and Bajaja (1983a, 1983b). From these studies it appears that the HI structures are similar to the shells and supershells in our own Galaxy described by Heiles (1976, 1979) and the supergiant shells in the Large Magellanic Cloud reported by Meaburn (1980).

The HI structures can also be seen in the total surface density map (Fig. 9), which shows numerous arcs and filaments. Comparison of our map with the maps by Unwin (1980a, 1980b) shows good general agreement. Thanks to the improved sensitivity, HI arms well inside 5 kpc can now be traced. Especially clear is the arm at 5 kpc northwest of the nucleus, which coincides with the highly contrasted dust arm seen on optical maps. This arm has an anomalous velocity of about 50 km s^{-1} (see also Bajaja and Shane, 1982).

5.2 Anomalous velocities in the central region. — It has been known for some time that the HI near the centre of M31 is moving with anomalous velocities (Whitehurst and Roberts, 1972; Bajaja and Shane, 1982). This is most dramatically illustrated by the maps in figure 7 which cross the inner part of the disk, i.e. $12'\mathrm{N} < X < 12'\mathrm{S}$. Velocities deviating by as much as 200 km s^{-1} from the expected values for differential rotation are found. The location of some of the highest velocity structures can be read from the channel maps near $-$ 20 km s^{-1} or, on the low velocity side, near $-$ 600 km s^{-1}. Some implications of these findings are discussed by Brinks (1983).

5.3 Multi-peaked velocity profiles. — The position-velocity maps made parallel to the major axis, figure 8, show that across almost the whole galaxy there are at least two and sometimes more structures present which are separated in velocity. The main structures seem to be one which roughly follows the pattern of differential rotation and one which appears almost as a straight line in each of the maps and shows a more shallow velocity gradient than expected from differential rotation. Both components were noted by Cram *et al.* (1980) and by Bajaja and Shane (1982). The most likely interpretation seems to be the one suggested by Shane (1978) and developed by Henderson (1979), in which the first component lies in the inner disk, and is associated with the spiral arms, whereas the second originates in the outer disk, which exhibits a warp. (Emerson and Newton (1978) discuss a different sort of warp.) This warp may be represented as a tilting of the outer disk about a line roughly coincident with the apparent major axis of M31 and such that the outer disk is seen more nearly edge on. In this way we can see both parts of the galaxy along a single line of sight.

Acknowledgements.

A project of this size can only be accomplished by team work. However the help of one person, Mrs. H. Versteege-Hensel, who assisted with the reduction at Leiden Observatory was of particular importance. Her patient, painstakingly accurate, and efficient help brought the reduction of the survey to a successful conclusion. We are also grateful for the help of the Telescope Group at Westerbork during the observations and the assistance and advice of the Reduction Group at Dwingeloo regarding the non-standard calibration of the data. In particular, discussions with Drs. R. Harten, H. van Someren Gréve, T. Spoelstra, and A. Willis and the help of Mr. P. van de Velde are acknowledged. Of vital importance were the short spacing data from the 100-m survey, which were put at our disposal before publication by Dr. Cram. A special word of thanks goes to Dr. Emerson who regridded the complete 100-m survey to the Westerbork format. Thanks are also due to Dr. R. Walterbos for providing specially adapted 21-cm continuum maps.

All reduction done at Leiden was performed at the University Computing Center (CRI), where night and day the crews of operators took special care of the hundreds of tapes required. Problems with or changes in the standard reduction programmes were always quickly taken care of by the programmers Messrs. T. Hoekema, D. Hogeweg, K. Lugtenborg and K. Weerstra. This manuscript has benefitted from constructive remarks on an earlier version by Drs. E. Bajaja, W. Burton, H. van der Laan and R. Walterbos. The drawings were made by Mr. J. Ober. The hundreds of photographic reproductions which were needed during the reduction phase, of which only a limited portion are shown here, were accurately and skillfully made by Mr. W. Brokaar.

E. B. was supported financially by the Netherlands Foundation for Astronomical Research (ASTRON). The Westerbork Synthesis Radio Telescope is operated by the Netherlands Foundation for Radio Astronomy (SRZM). Both Foundations are supported by the Netherlands Organization for the Advancement of Pure Research (ZWO).

References

BAADE, W., ARP, H. : 1964, *Astrophys. J.* **139,** 1027.
BAADE, W., SWOPE, H. H. : 1963, *Astron. J.* **68,** 435.
BAARS, J. W. M., HOOGHOUDT, B. G. : 1974, *Astron. Astrophys.* **31,** 323.
BAARS, J. W. M., GENZEL, R., PAULINY-TOTH, I. I. K., WITZEL, A. : 1977, *Astron. Astrophys.* **61,** 99.
BAJAJA, E., ALBADA, G. D. VAN : 1979, *Astron. Astrophys.* **75,** 251.
BAJAJA, E., SHANE, W. W. : 1982, *Astron. Astrophys. Suppl. Ser.* **49,** 745.
BERGH, S. VAN DEN : 1964, *Astrophys. J. Suppl. Ser.* **9,** 65.
BOS, A., RAIMOND, E., SOMEREN GRÉVE, H. W. VAN : 1981, *Astron. Astrophys.* **98,** 251.
BRINKS, E. : 1981, *Astron. Astrophys.* **95,** L1.
BRINKS, E. : 1983, in *Internal Kinematics and Dynamics of Galaxies* (IAU Symp. No. 100), ed. E. Athanassoula, Reidel, Dordrecht, p. 27.
BRINKS, E., BAJAJA, E. : 1983a, in *Internal Kinematics and Dynamics of Galaxies* (IAU Symp. No. 100), ed. E. Athanassoula, Reidel, Dordrecht, p. 139.
BRINKS, E., BAJAJA, E. : 1983b, in *Surveys of the Southern Galaxy*, eds. W. B. Burton and F. P. Israel (Reidel, Dordrecht) p. 247.
BROUW, W. N. : 1969, *Netherlands Foundation for Radio Astronomy, Int. Techn. Rep.* **79.**
BROUW, W. N. : 1975, in *Methods in Computational Physics* **14,** 131, eds. B. Alder, S. Fernbach and M. Rotenberg, Academic Press, New York.
BRUYN, A. G. DE, SPOELSTRA, T. A. Th. : 1983, *Netherlands Foundation for Radio Astronomy, User Note* **47** (in preparation).
CASSE, J. L., MULLER, C. A. : 1974, *Astron. Astrophys.* **31,** 333.
CRAM, T. R., ROBERTS, M. S., WHITEHURST, R. N. : 1980, *Astron. Astrophys. Suppl. Ser.* **40,** 215.
EMERSON, D. T. : 1974, *Mon. Not. R. Astron. Soc.* **169,** 607.
EMERSON, D. T., NEWTON, K. : 1978, in *Structure and Properties of Nearby Galaxies* (IAU Symp. No. 77), eds. E. M. Berkhuijsen and R. Wielebinski, Reidel, Dordrecht, p. 183.
GUIBERT, J. : 1973, *Astron. Astrophys. Suppl. Ser.* **12,** 263.
HARTEN, R. H. : 1974, *Netherlands Foundation for Radio Astronomy, Int. Techn. Rep.* **121** (revised 1975).
HARTEN, R. H. : 1979, *Netherlands Foundation for Radio Astronomy, Int. Techn. Rep.* **151** (version 2).
HEILES, C. : 1976, *Astrophys. J. Lett.* **208,** L137.
HEILES, C. : 1979, *Astrophys. J.* **229,** 533.
HENDERSON, A. P. : 1979, *Astron. Astrophys.* **75,** 311.
HÖGBOM, J. A. : 1974, *Astron. Astrophys. Suppl. Ser.* **15,** 417.
HÖGBOM, J. A., BROUW, W. N. : 1974, *Astron. Astrophys.* **33,** 289.
HOLMBERG, E. : 1958, *Medd. Lunds Astron. Obs., Ser. II*, Nr. 136.
HULST, H. C. VAN DE, RAIMOND, E., WOERDEN, H. VAN : 1957, *Bull. Astron. Inst. Netherl.* **14,** 1.
KATGERT, P. : 1975, *Astron. Astrophys.* **38,** 87.
LANDECKER, T. L. : 1978, in *Structure and Properties of Nearby Galaxies* (IAU Symp. No. 77), eds. E. M. Berkhuijsen and R. Wielebinski, Reidel, Dordrecht, p. 173.
MEABURN, J. : 1980, *Mon. Not. R. Astron. Soc.* **192,** 365.
NEWTON, K., EMERSON, D. T. : 1977, *Mon. Not. R. Astron. Soc.* **181,** 573.
PELLET, A., ASTIER, N., VIALE, A., COURTÈS, G., MAUCHERAT, A., MONNET, G., SIMIEN, F. : 1978, *Astron. Astrophys. Suppl. Ser.* **31,** 439.
POOLEY, G. G. : 1969, *Mon. Not. R. Astron. Soc.* **144,** 101.
ROBERTS, M. S., WHITEHURST, R. N. : 1975, *Astrophys. J.* **201,** 327.
SCHWARZ, U. J. : 1978, *Astron. Astrophys.* **65,** 345.
SHANE, W. W. : 1975, in *La Dynamique des Galaxies Spirales* (Colloque International C.N.R.S. No. 241), ed. L. Weliachew, Editions du CNRS, Paris, p. 257.
SHANE, W. W. : 1978, in *Structure and Properties of Nearby Galaxies* (IAU Symp. No. 77), eds. E. M. Berkhuijsen and R. Wielebinski, Reidel, Dordrecht, p. 180.
SHOSTAK, G. S., ALLEN, R. J. : 1980, in *Proceedings of the ESO Workshop on Two Dimensional Photometry*, eds. P. Crane and K. Kjär, Noordwijkerhout, p. 169.
SHOSTAK, G. S., BRINKS, E. : 1983, in *Surveys of the Southern Galaxy*, eds. W. B. Burton and F. P. Israel (Reidel, Dordrecht) p. 243.
SOMEREN GRÉVE, H. W. VAN : 1974, *Astron. Astrophys. Suppl. Ser.* **15,** 343.
UNWIN, S. C. : 1980a, *Mon. Not. R. Astron. Soc.* **190,** 551.
UNWIN, S. C. : 1980b, *Mon. Not. R. Astron. Soc.* **192,** 243.
DE VAUCOULEURS, G., DE VAUCOULEURS, A., CORWIN, H. G., Jr. : 1976, *Second Reference Catalogue of Bright Galaxies*, University of Texas Press, Austin.
WHITEHURST, R. N., ROBERTS, M. S. : 1972, *Astrophys. J.* **175,** 347.

TABLE I. — *List of HI observations of M31, updating the list by Guibert (1973).*

Authors	Telescope	HPBW	Velocity Resolution (km s^{-1})	Sensi-tivity (K)	Notes
Whitehurst and Roberts, 1972	Green Bank, 140 ft	21'	5.5	-	(1)
Emerson, 1974	Cambridge Half Mile	1'.5x2'.2	39	1.5	(2)
		6' x9'.4	39	0.2	(3)
Roberts and Whitehurst, 1975	Green Bank, 300 ft	10'	6.6	-	(4)
Newton and Emerson, 1977	Cambridge Half Mile	3'.6x5'.5	16	0.3	(5)
Landecker, 1978	Penticton,Synthesis Telecope	2' x 3'	5	2.0	
Cram, Roberts,and Whitehurst, 1980	Effelsberg, 100-m	8'.8	5.5	0.1	
Unwin, 1980	Cambridge Half Mile	0'.8x1'.2	16	3.6	
Bajaja and Shane, 1982	WSRT, 1.5 km	24" x 36"	27	1.4	(6)
This paper, 1983	WSRT, 1.5 km	24" x 36"	8.2	2.5	

(1) Single profile on the nucleus
(2) Northern and central part
(3) Southern part
(4) South West major axis
(5) Two fields on the major axis, centred 150' on each side of the nucleus.
(6) Central region (field C in the nomenclature of this paper). Velocities undersampled.

TABLE II. — *General information on M31.*

Position of the optical nucleus	: $\alpha_{1950} = 0^h\ 40^m\ 00^s.28$	Baade and Arp (1964),
	: $\delta_{1950} = 40^\circ\ 59'\ 42''.9$	precessed to 1950.0
Line of nodes	: $\theta_{1950} = 37^\circ\ 46'.6$	
Galactic coordinates	: $l = 121^\circ.18$	
	: $b = -21^\circ.57$	de Vaucouleurs et al. (1976)
Systemic velocity	: -299 km s^{-1}	
Inclination	: $77^\circ\ 30'$	Pellet et al. (1978)
Distance	: 690 kpc[(1)]	Baade and Swope (1963)
Holmberg radius	: 19.8 kpc	Holmberg (1958)
HI radius	: 30 kpc	Newton and Emerson (1977)

[(1)] At this distance 1 arcmin corresponds to 200 pc.

TABLE III. — *Instrumental data.*

Field	C	NW	NE	SW	SE
Right ascension (1950.0)	$0^h40^m00^s$	$0^h40^m30^s$	$0^h43^m18^s$	$0^h36^m42^s$	$0^h39^m30^s$
Declination (1950.0)	41°00'	41°40'	41°15'	40°44'	40°20'
Heliocentric velocity of centre of the band (km s^{-1})	-263.6	-160.4	-160.4	-420.6	-420.6
Total Bandwidth (MHz)	5	2.5	2.5	2.5	2.5
Number of channels	256	128	128	128	128
Number of interferometers per 12 hour observation	9	18	18	20	20
Number of 12 hour observations per full synthesis	8	4	4	4	4
Baselines (meter) shortest(incr.)largest	36(18)1314	36(18)1314	36(18)1314	36(18)1458	36(18)1458
Fraction of baseline data missing due to malfunctioning	2.7%	0.0%	1.7%	0.3%	1.8%
R.m.s. noise in a channel (mJy)	2.7	2.8	2.8	3.0	3.0
map at the field centre (K)	1.9	2.0	2.0	2.5	2.5
Mean synthesized beamwidth	24" x 36"	24" x 36"	24" x 36"	22" x 34"	22" x 34"

Radius of first grating ring	40'.4 x 60'.6
Half power beamwdith of primary beam	37'.6
System noise temperature (K)	80-100
Channel separation (km s^{-1})	4.1
Velocity resolution (km s^{-1})	8.2
Frequency taper	Hanning
Bit mode (degradation factor)	2 x 2 (1.57)
Polarization direction	East-West
Halfpower width of a Gaussian source with a fringe amplitude of 0.5 when observed at the shortest spacing.	9 x 13'.5

TABLE IVa. — *Position and fluxes of the calibrator sources used for the observations of fields SE and SW.*

Name	α(1950)	δ(1950)	Flux density (Jy)	Notes
3C 48	23.70761	32.90573	15.67	
3C 147	84.68126	49.82858	21.57	
3C 286	202.20689	30.76633	(13.70)	(1)
3C 309.1	224.73602	71.86977	-	(2)
3C 380	277.05630	48.71137	-	(2)

TABLE IVb. — *Position and fluxes of the calibrator sources used for the observations of fields C, NE, and NW.*

Name	α(1950)	δ(1950)	Flux density (Jy)	Notes
3C 147	84.681275	49.828564	21.57	
3C 309.1	224.736017	71.869764	7.84	(3)

(1) Polarized source. The flux density depends on the dipole setting. It is used only as a phase calibrator, except on day 79035 where it is used as a flux calibrator for observations of field SE.

(2) Source is used only as a phase calibrator.

(3) Slightly variable source. The flux density listed is valid only for the epoch of these observations.

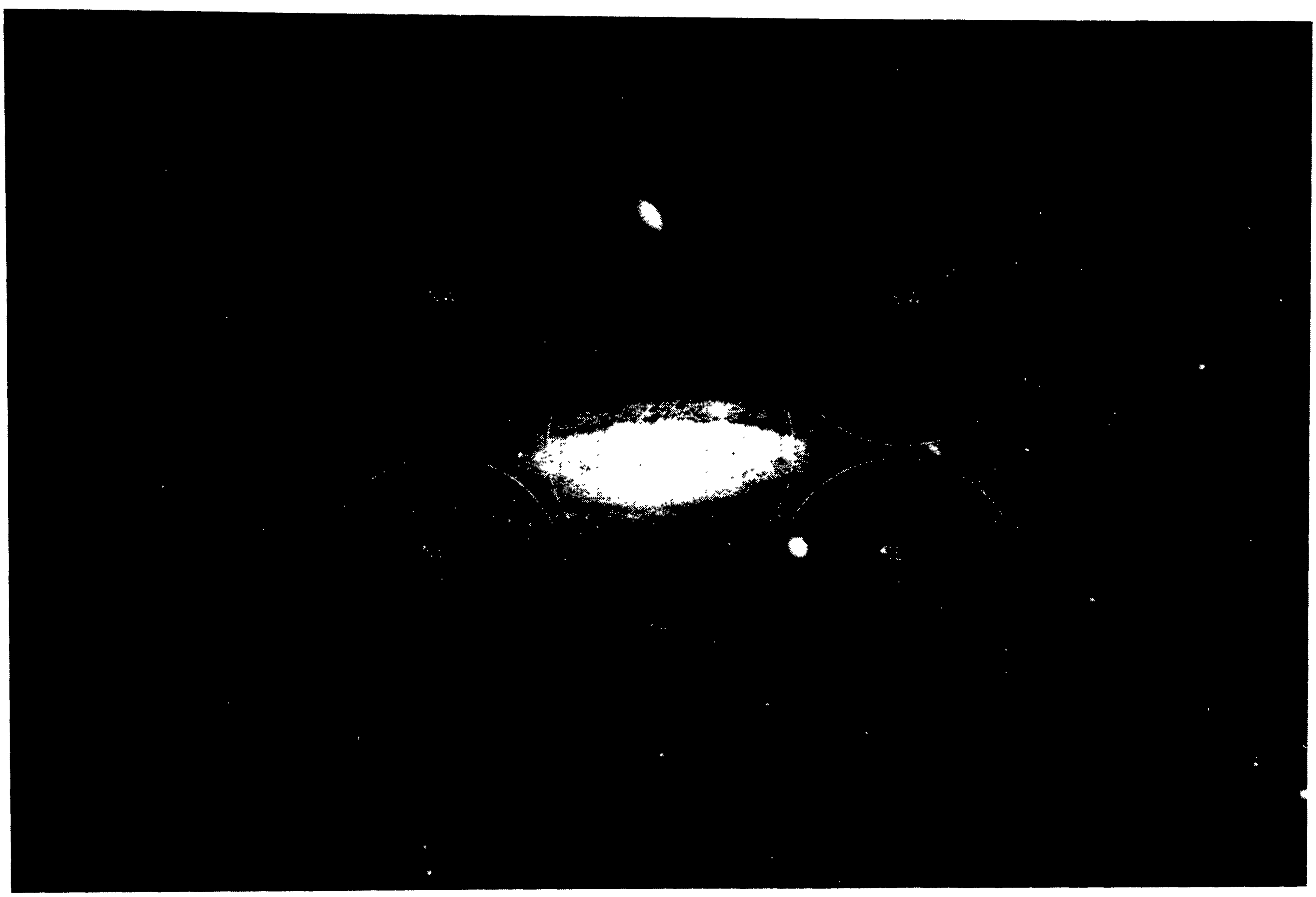

FIGURE 1. — Optical picture of M31 (Blue plate, 48" Palomar Schmidt; courtesy of A. G. de Bruyn) with superimposed the half-power beams of the five survey fields. The centre of field C coincides with the nucleus of M31, the centres of the other four fields are indicated by larger crosses. Small crosses indicate orientation star positions.

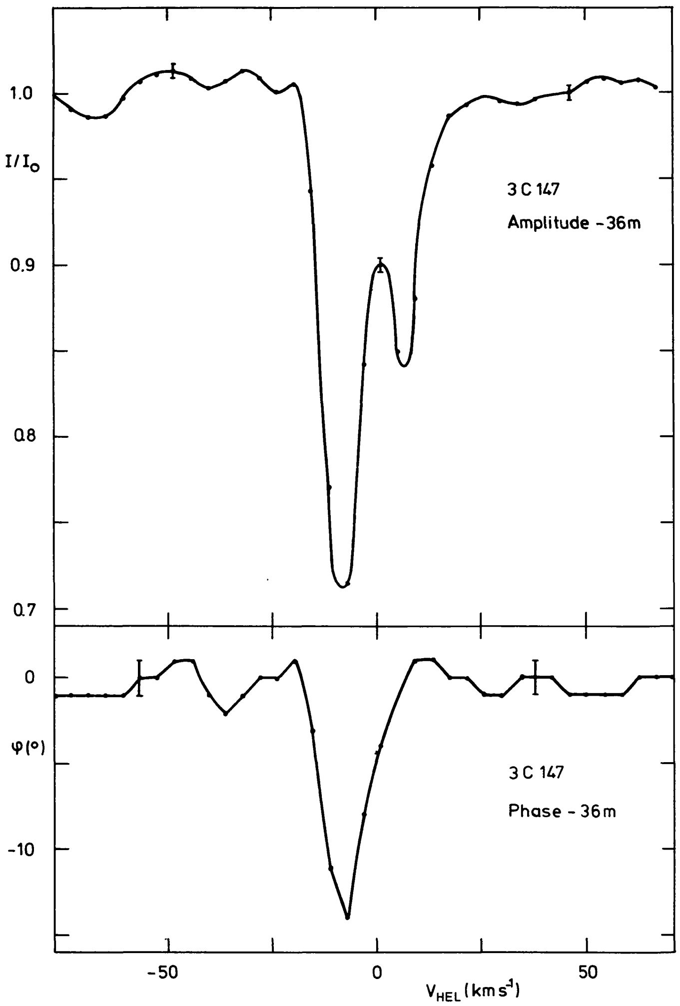

FIGURE 2. — Normalized amplitude and phase of the calibrator source 3C 147, plotted as a function of velocity, showing the spectral features caused by foreground HI from the Galaxy. The amplitude shows an absorption feature against the source, whereas the phase is mostly affected by emission which is present elsewhere in the field of view.

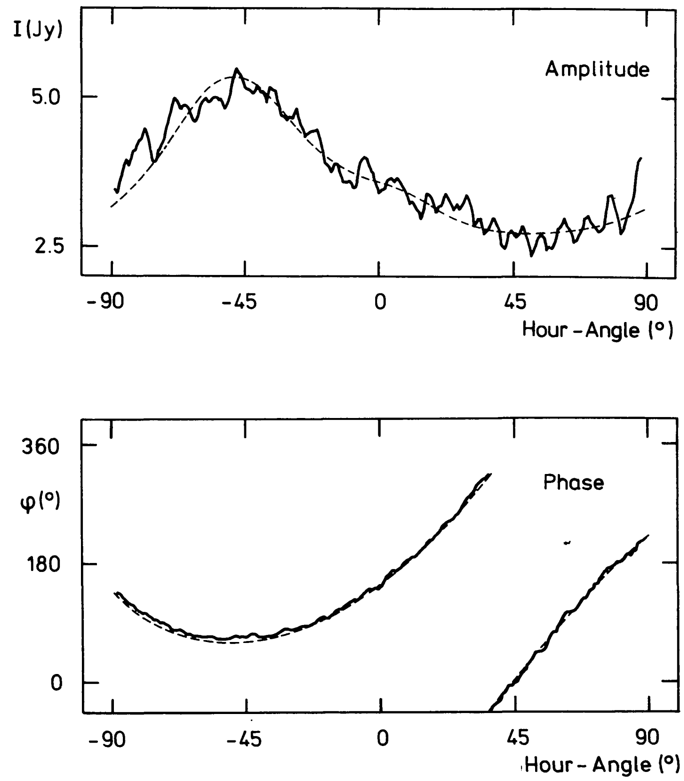

FIGURE 4. — Amplitude and phase as a function of hour-angle for the 36-m baseline data corresponding to the maps shown in figure 3. Dashed line : the reconstructed amplitude and phase derived from the single dish observations done with the 100-m telescope at Effelsberg. Solid line : the values as observed with the WSRT.

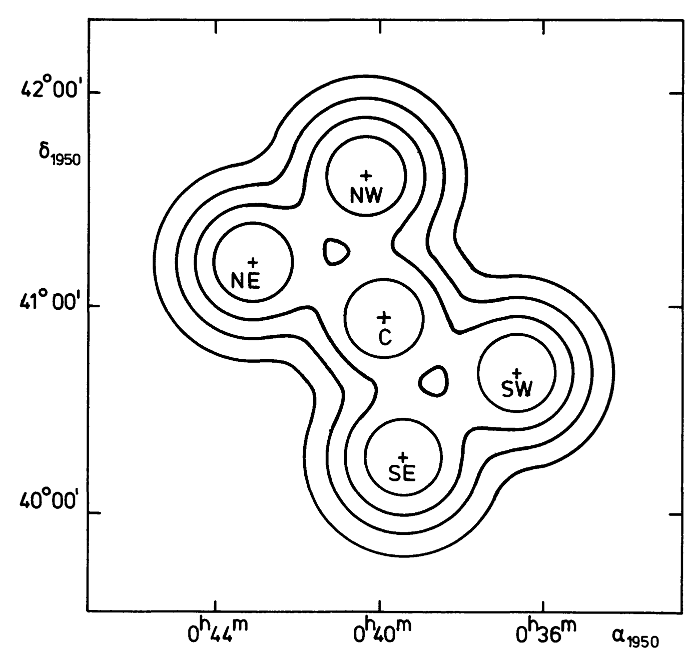

FIGURE 5. — Relative sensitivity pattern of the survey if all fields are combined without any masks applied. The contour levels are at 20 %, 40 %, 60 % and 80 % of the maximum. The [illegible] centres are indicated by crosses. Within the central part of the survey the sensitivity nowhere drops below 50 % of the sensitivity at the field centres.

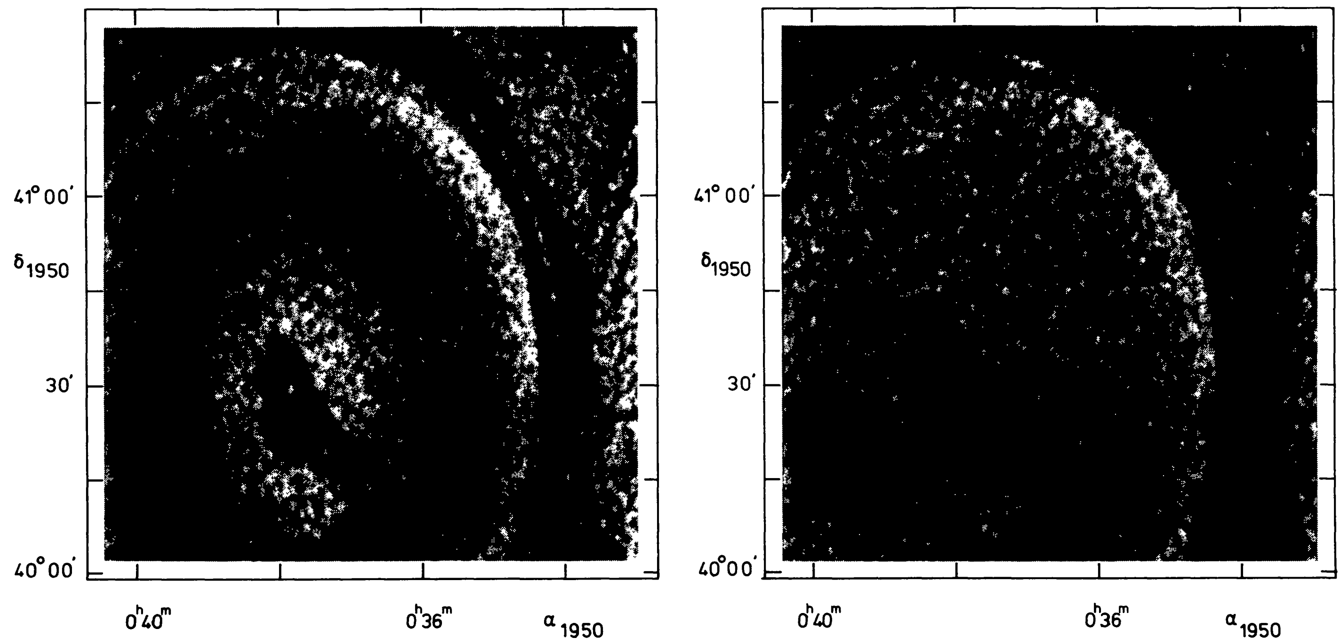

FIGURE 3a. — Channel map at V_{HEL} = − 568.6 km s^{-1} before (left) and after (right) inclusion of the short spacing data. The maps are convolved to 48″ × 72″ to accentuate the low spatial frequencies. The maps are shown as radio photographs, where the brightness and contrast have been optimized for intensities near the zero level. The coordinates are only approximate.

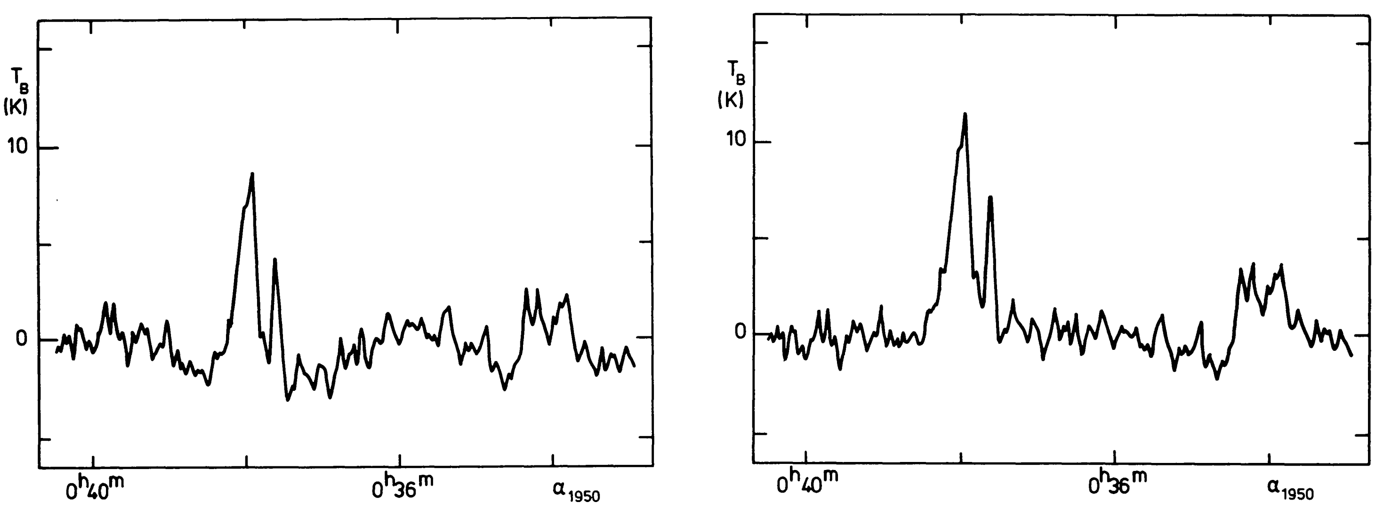

FIGURE 3b. — Intensity profiles through the channel maps of figure 3a along a line at a constant declination of δ = 40°30′.

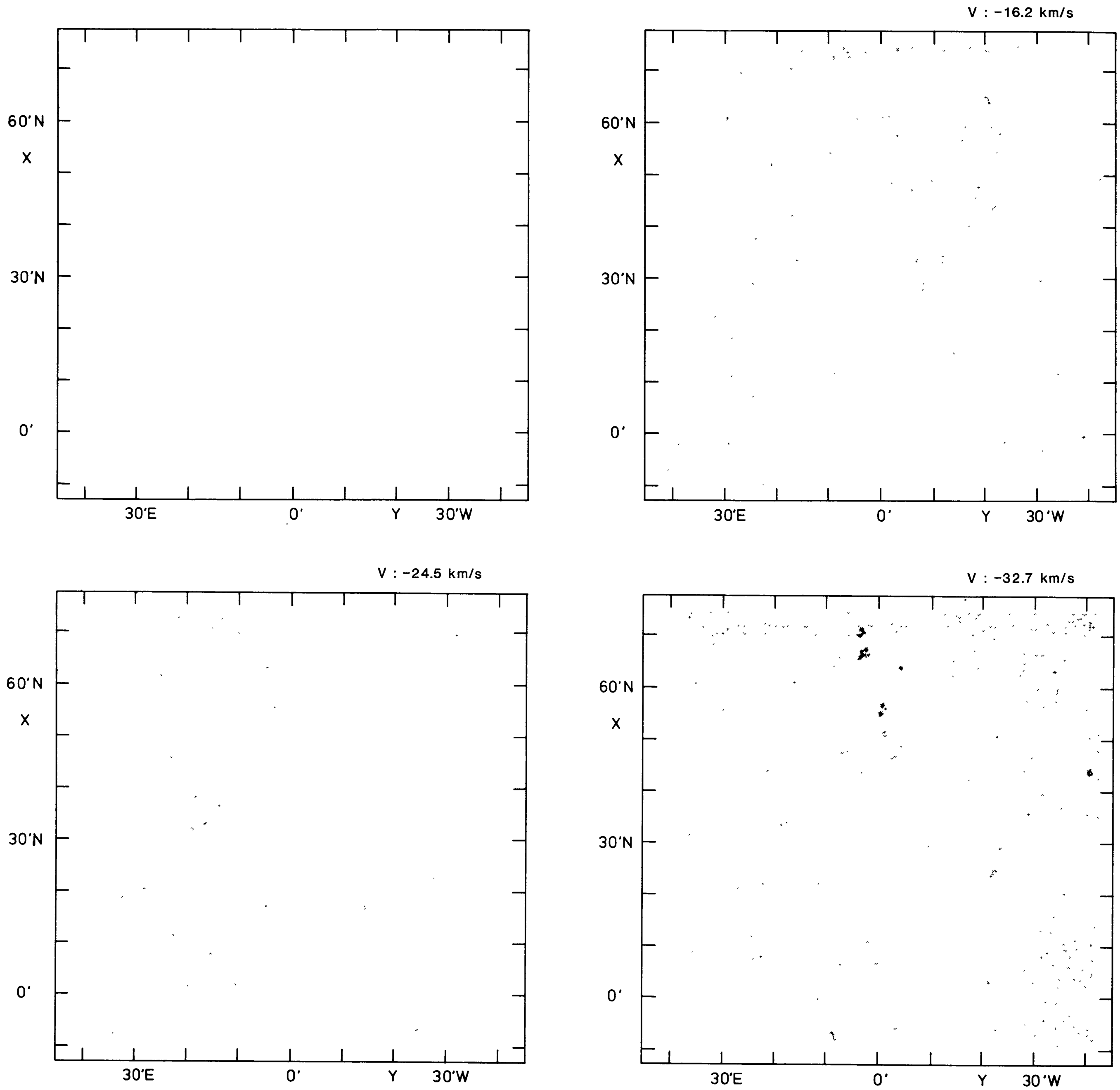

FIGURE 6. — Series of channel maps at a resolution of 24″ × 36″. The maps are rotated so that the major axis is vertical, with north-following upward. The interval between channels is 8.2 km s^{-1}. The maps were produced by photographing the monitor of the Leiden Image Processing System. Distortions in the monitor render the coordinate system only approximately correct. Coordinates are rectangular *X*-*Y* coordinates with *X* measured along the major axis and *Y* along the minor axis, with labels N, S, and E, W. In producing the figures, three map centres were used in order to follow the HI as a function of velocity.

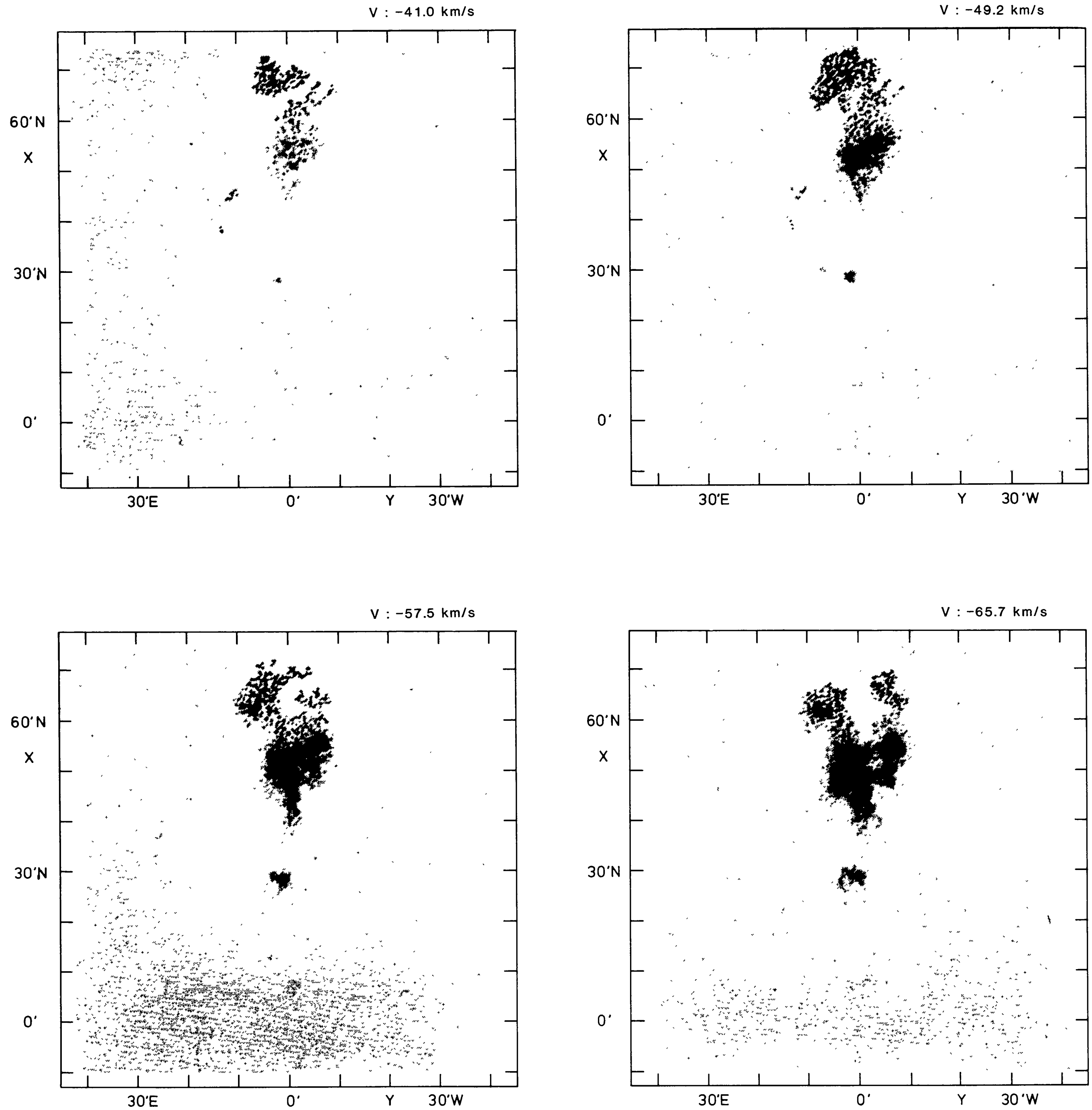

FIGURE 6 *(continued)*.

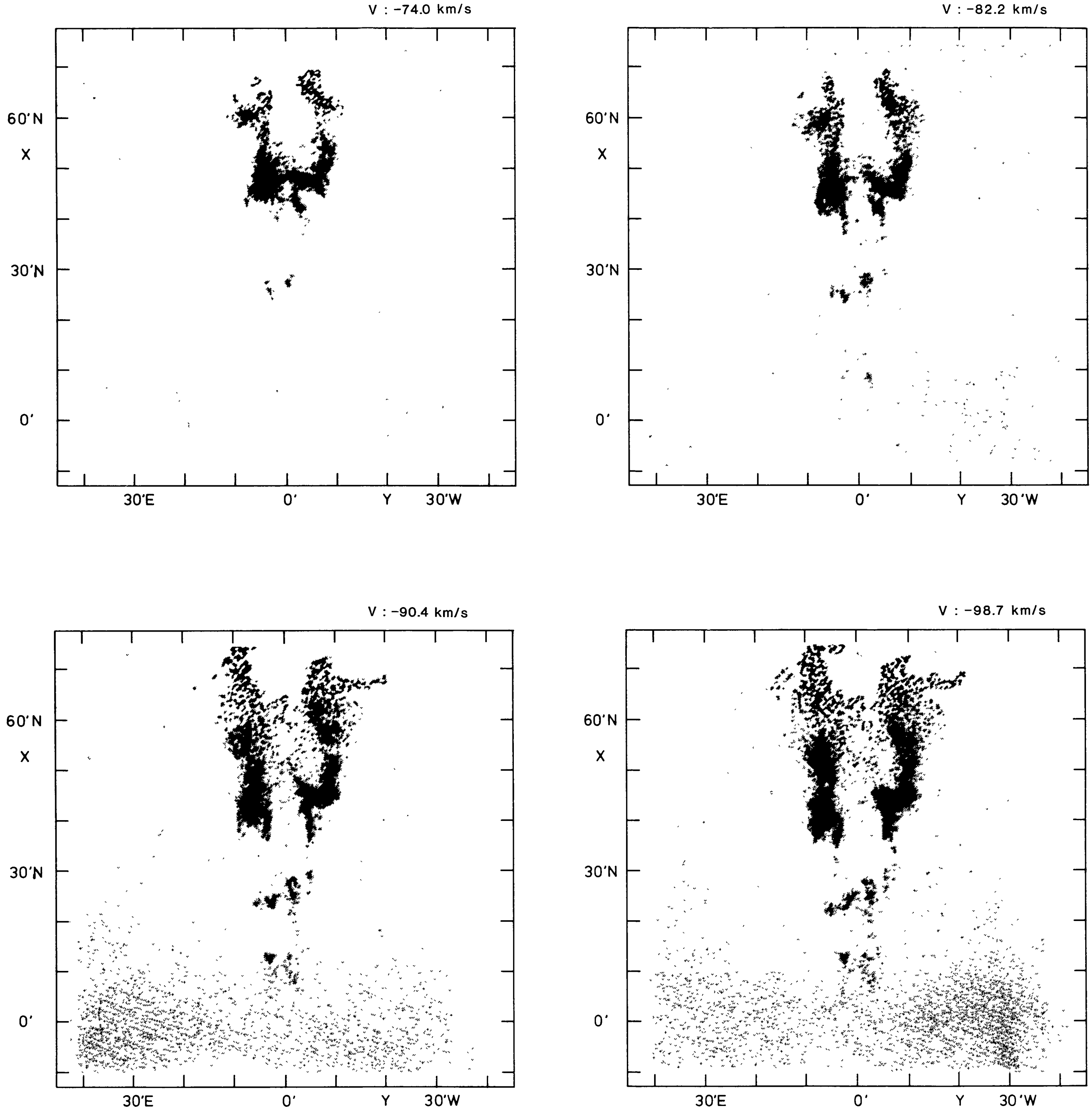

FIGURE 6 *(continued)*.

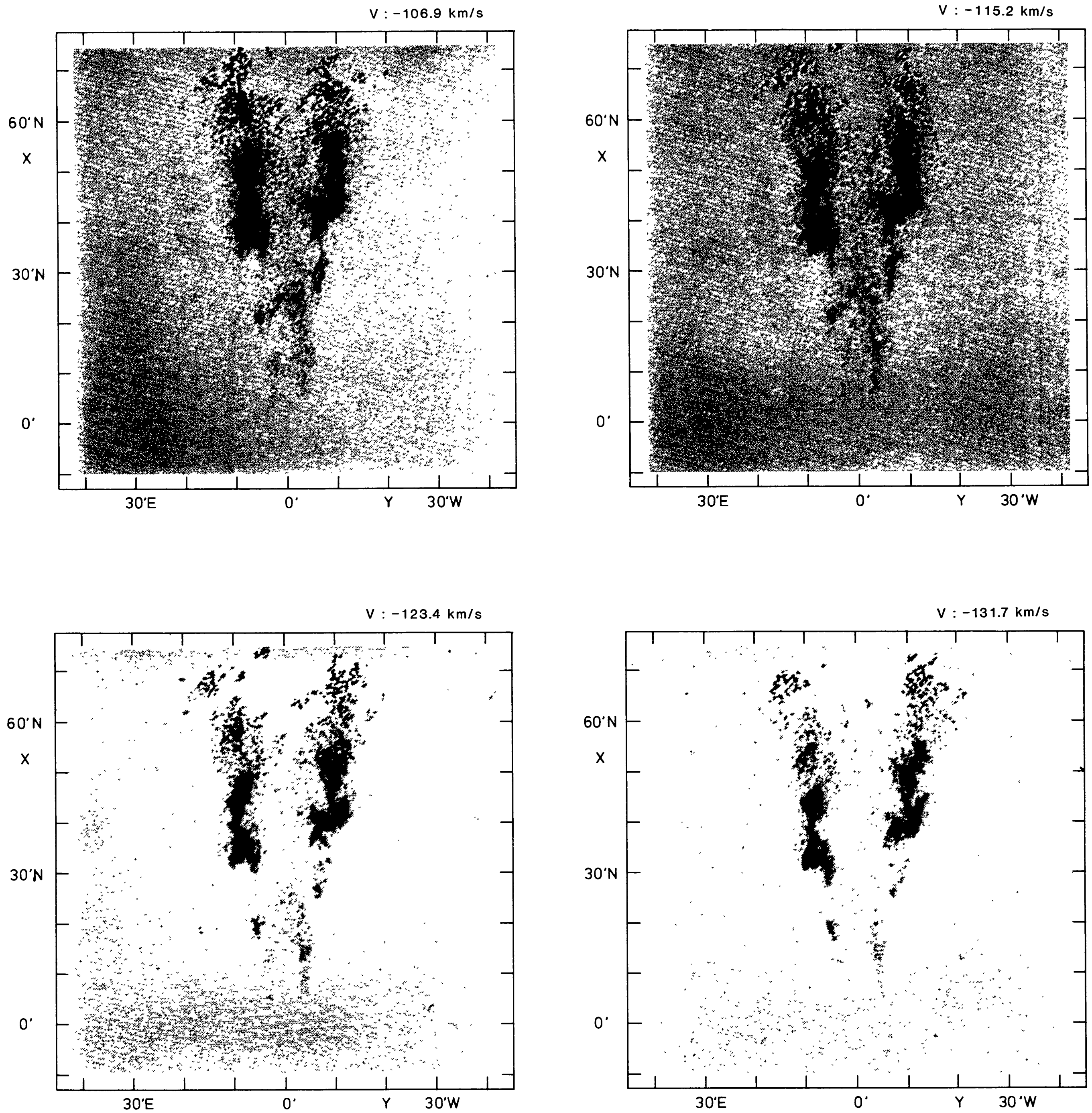

FIGURE 6 *(continued)*.

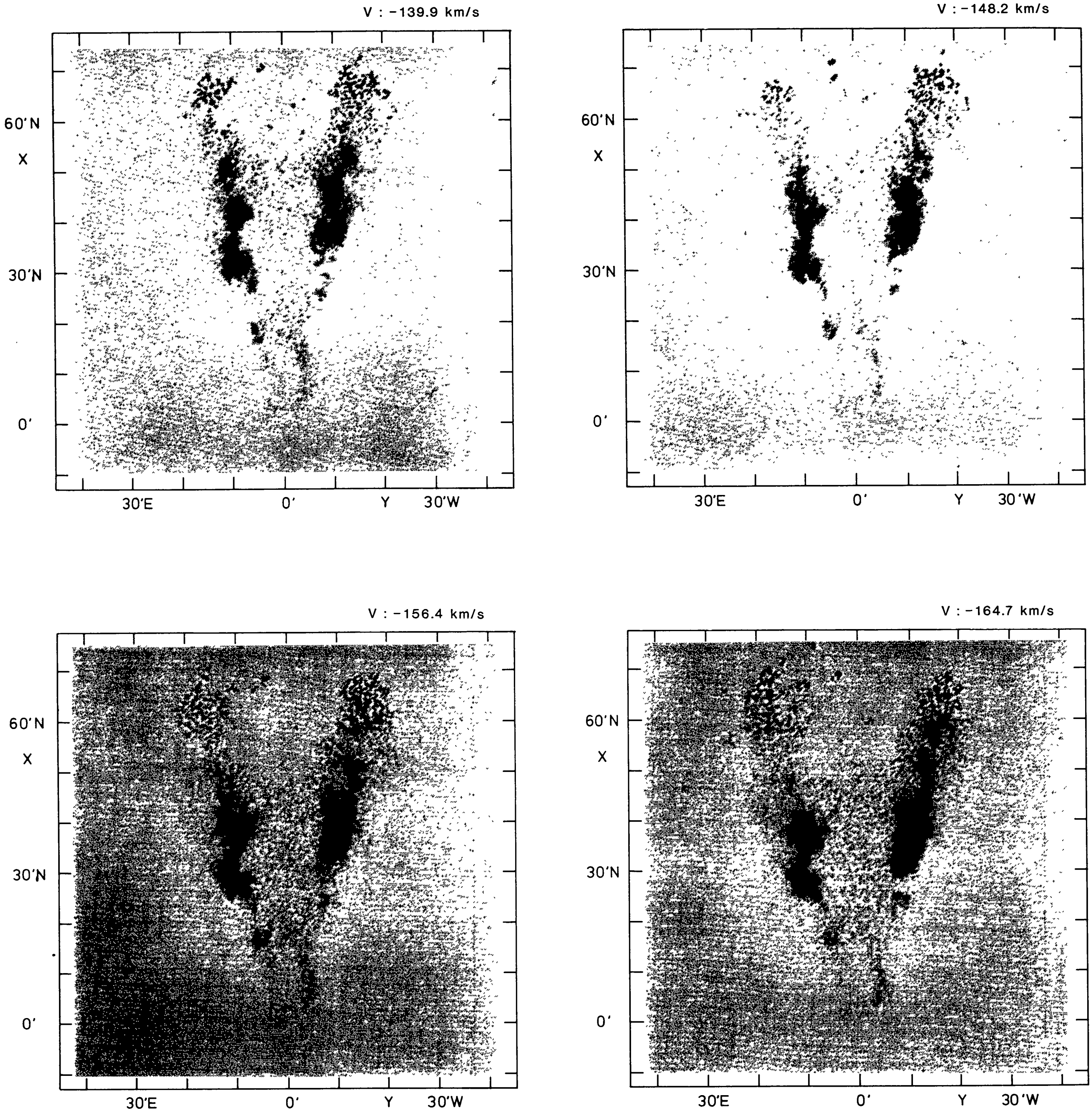

FIGURE 6 *(continued)*.

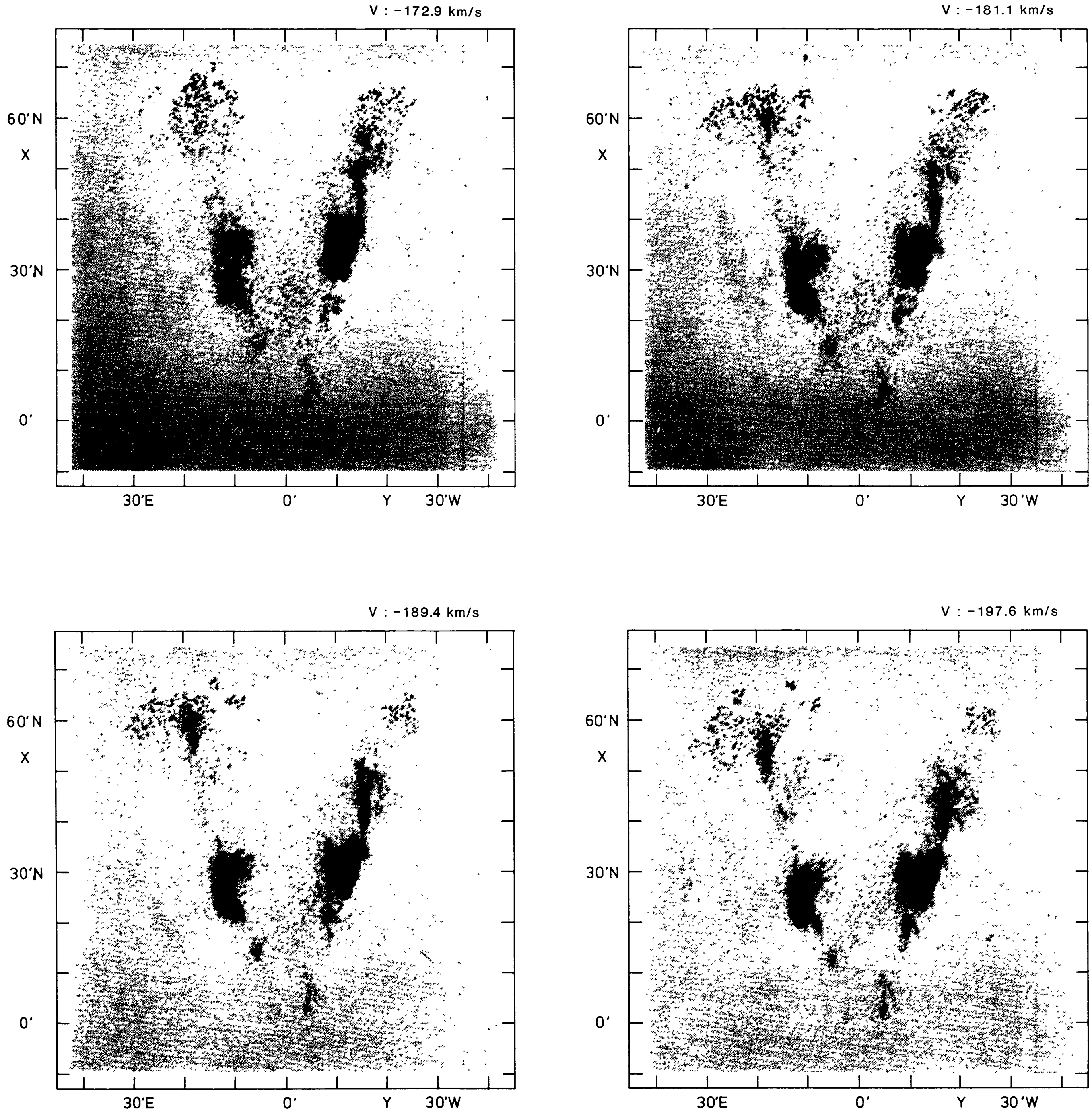

FIGURE 6 *(continued)*.

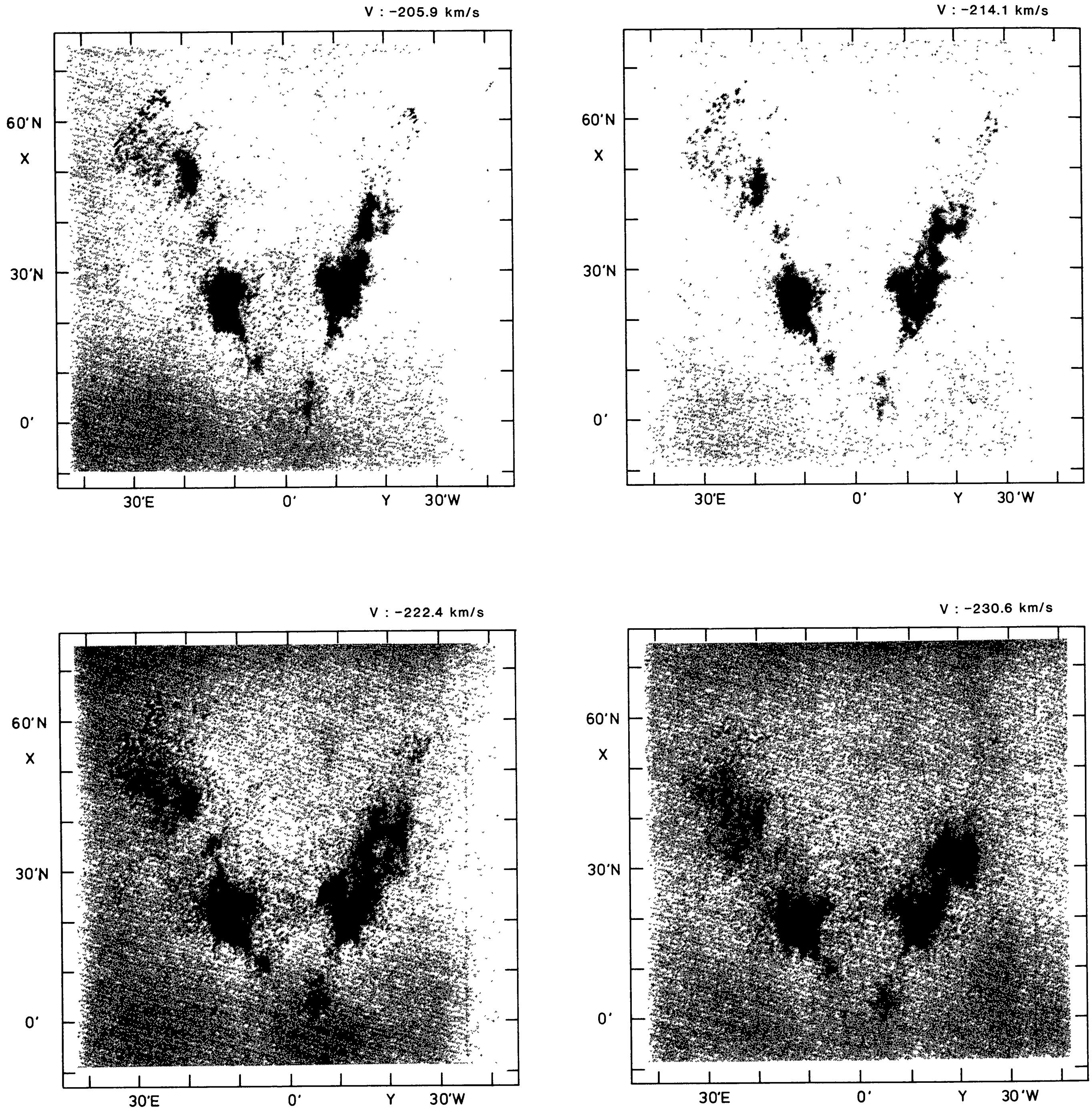

FIGURE 6 *(continued)*.

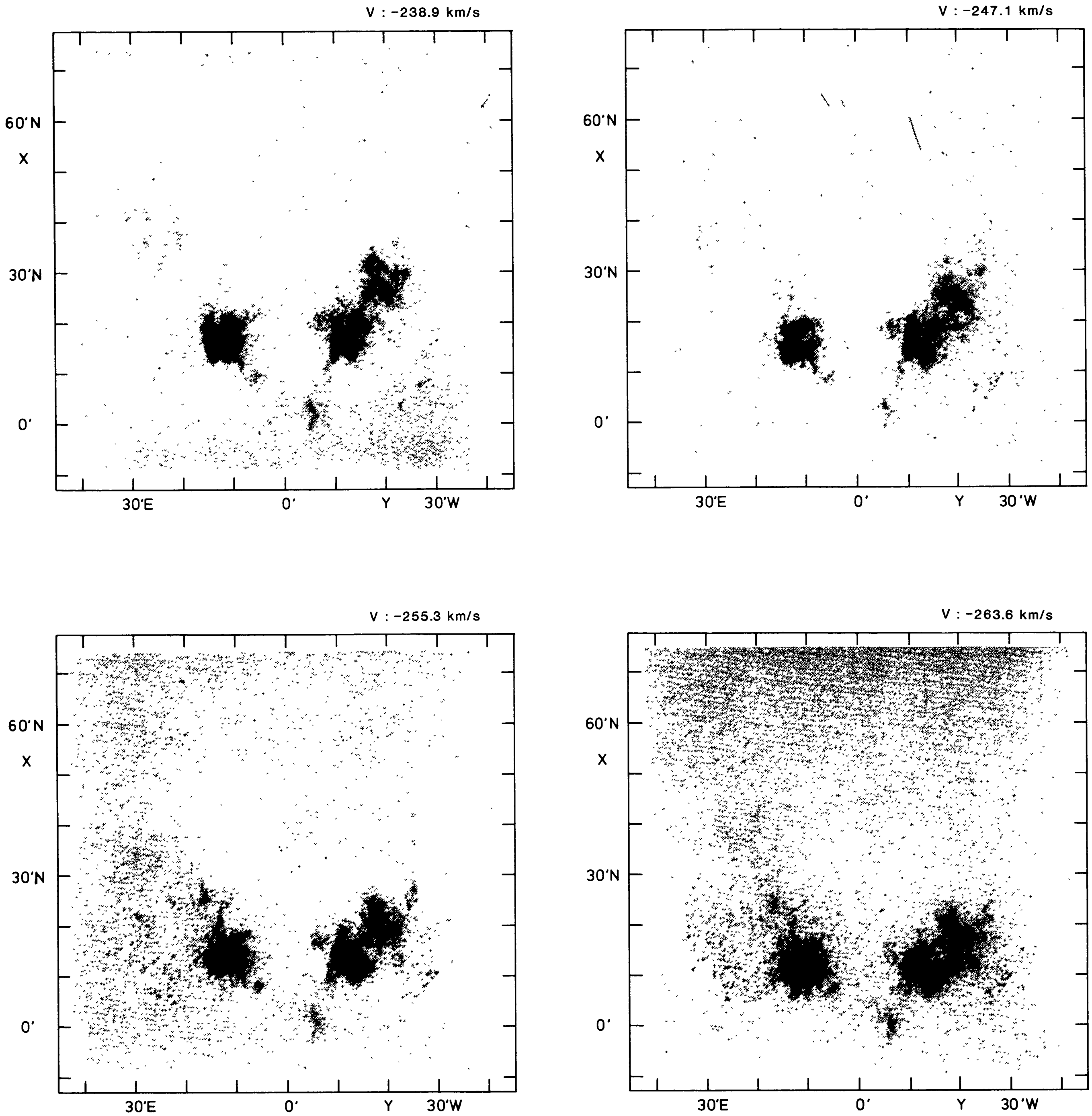

FIGURE 6 *(continued)*.

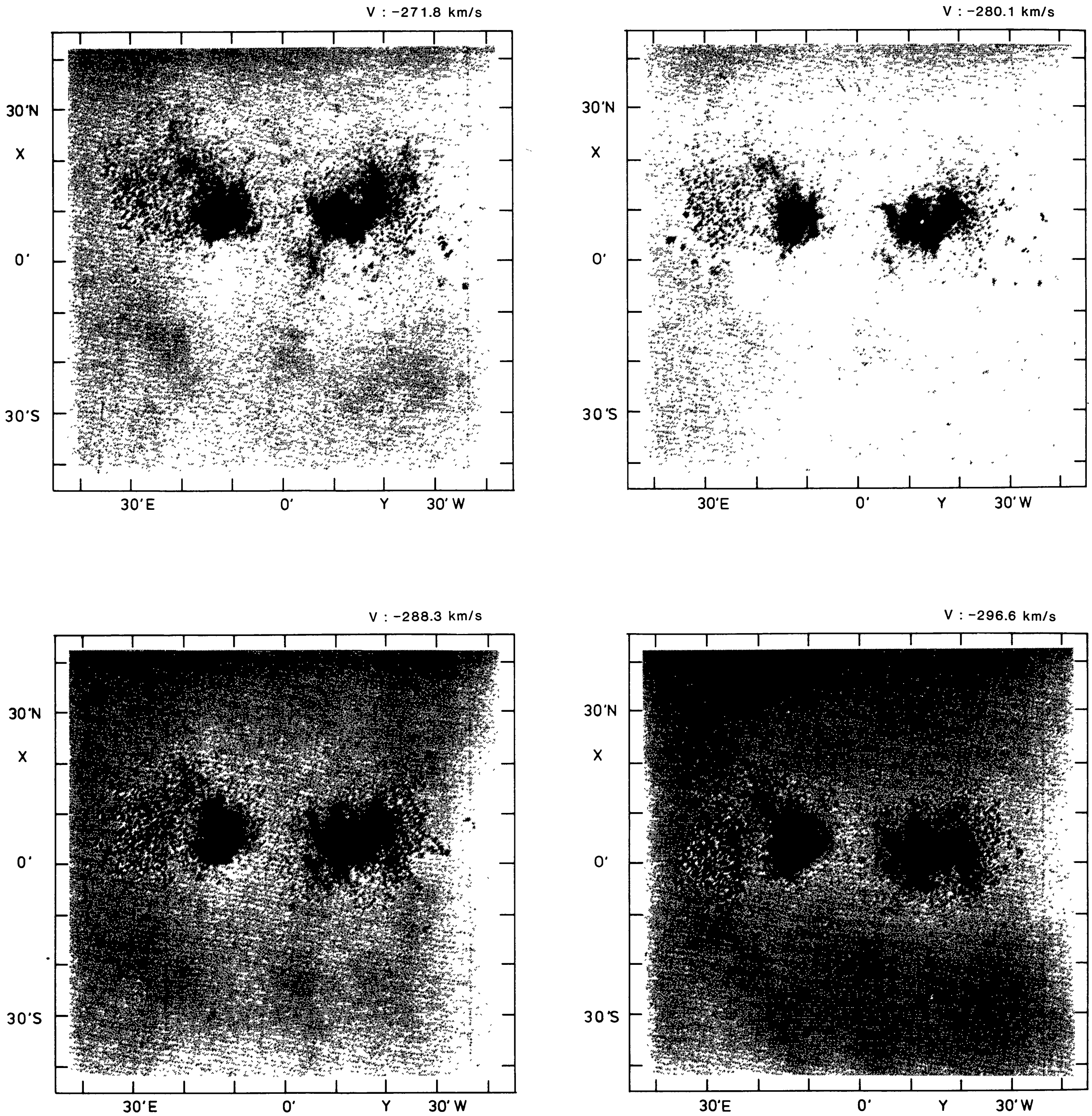

FIGURE 6 *(continued)*.

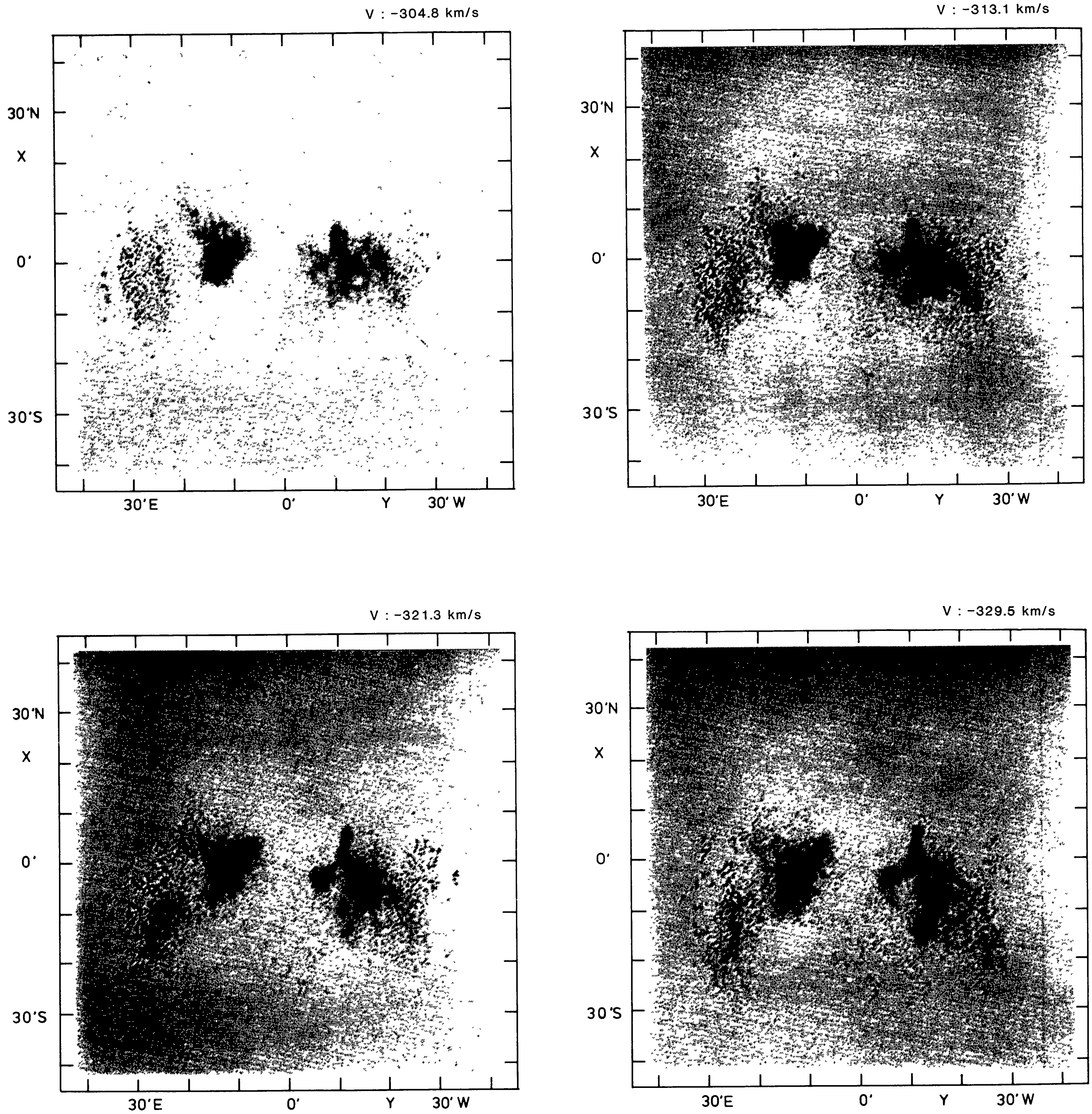

FIGURE 6 *(continued)*.

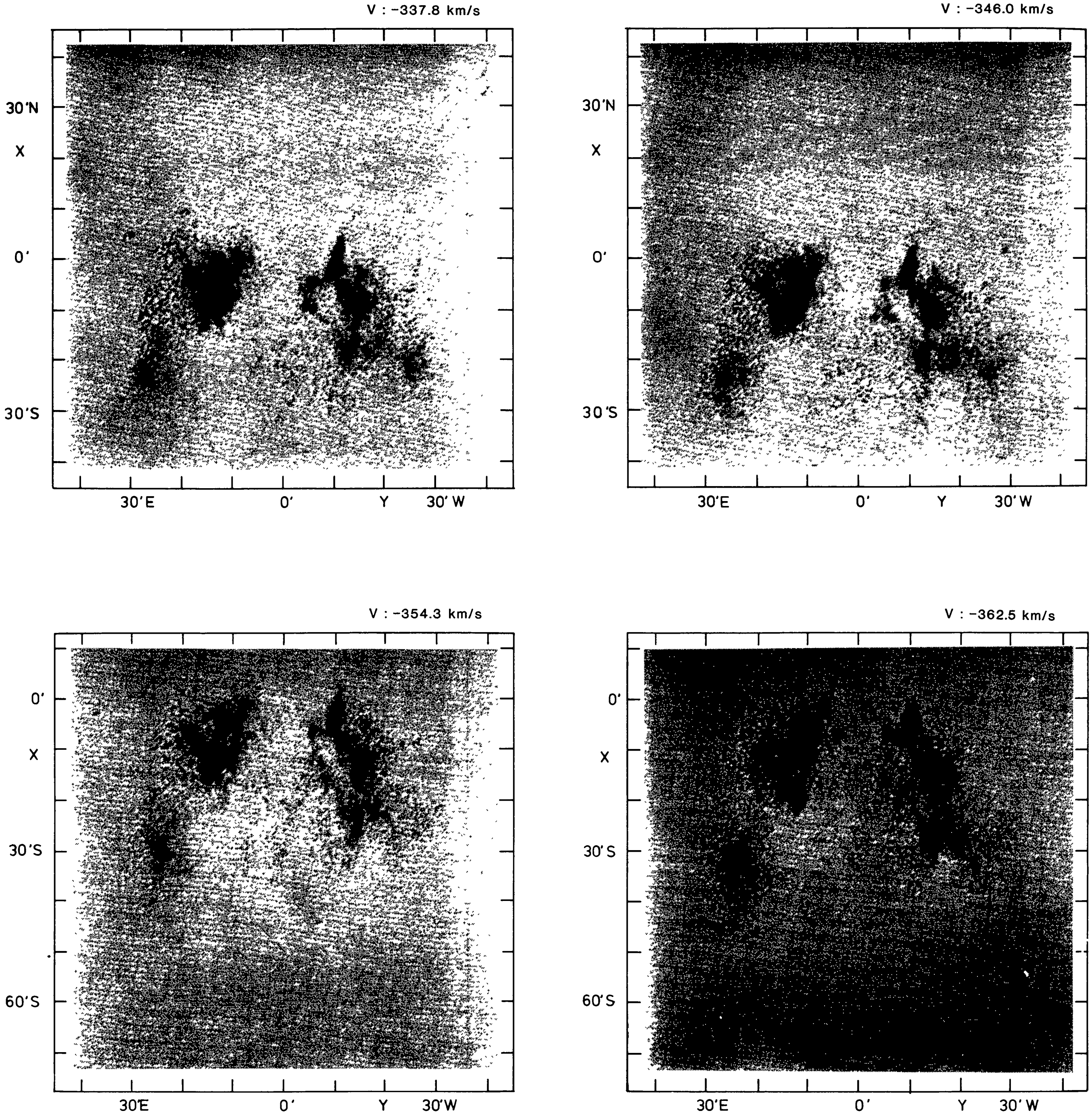

FIGURE 6 *(continued)*.

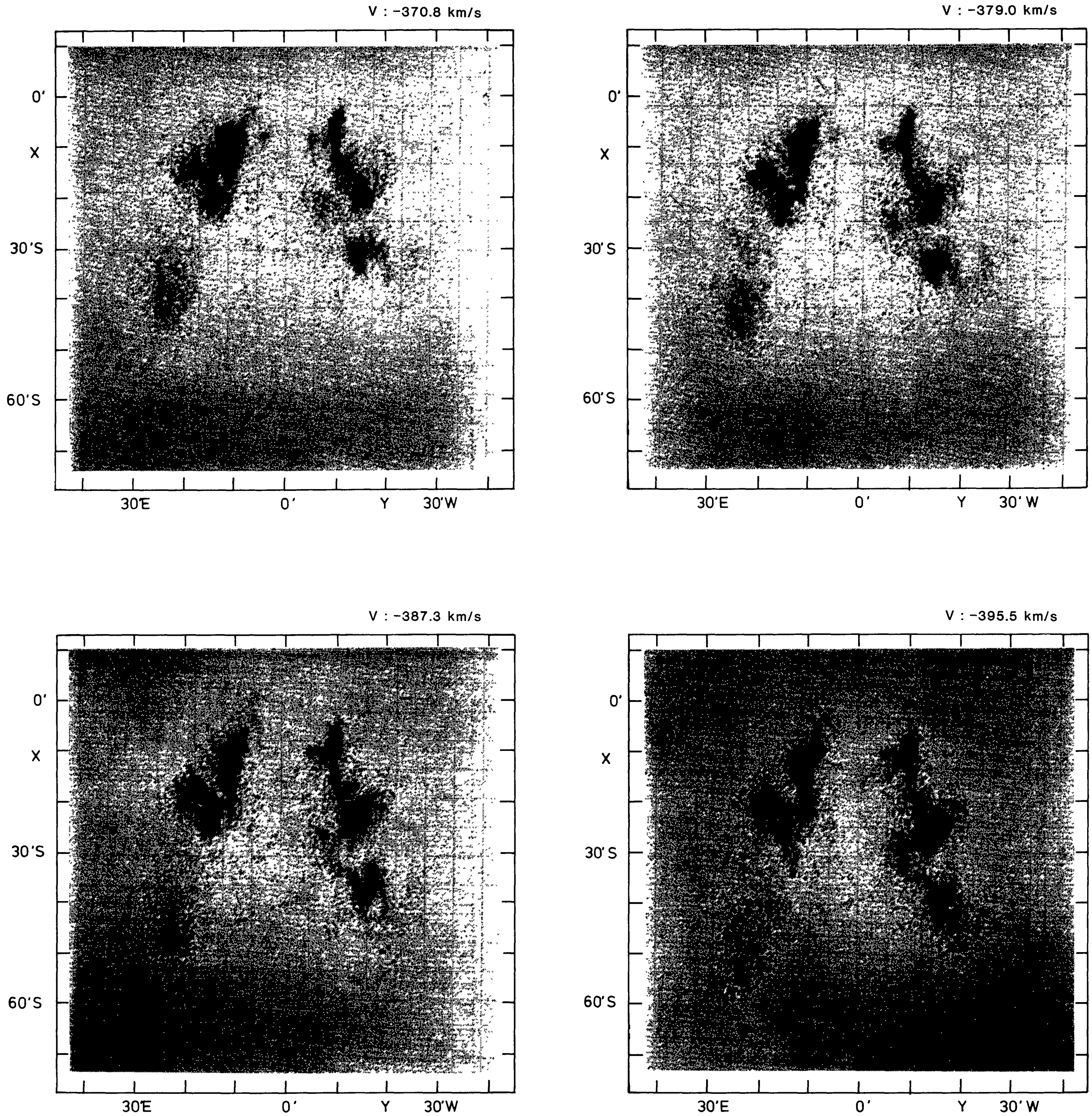

FIGURE 6 *(continued)*.

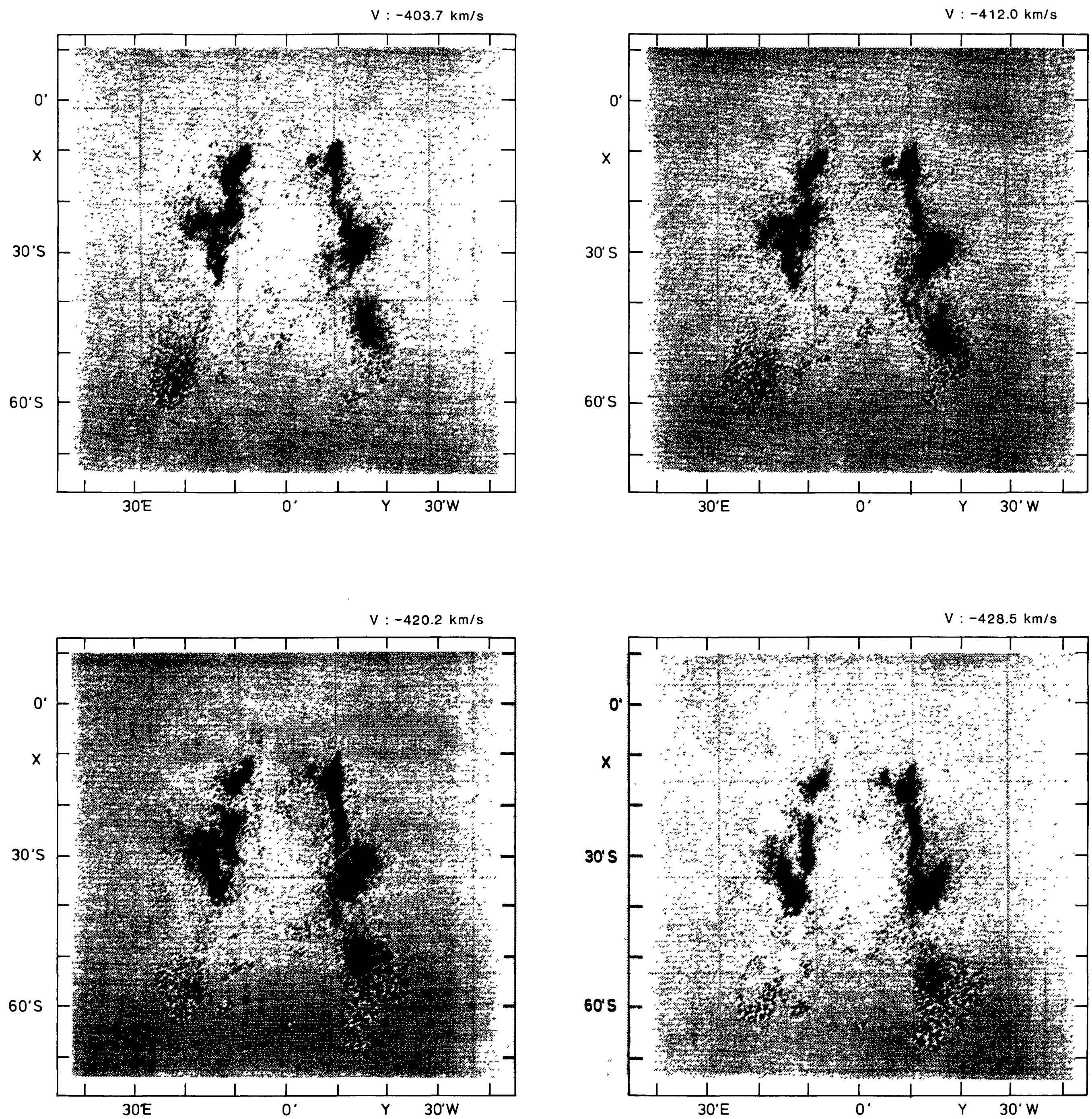

FIGURE 6 *(continued)*.

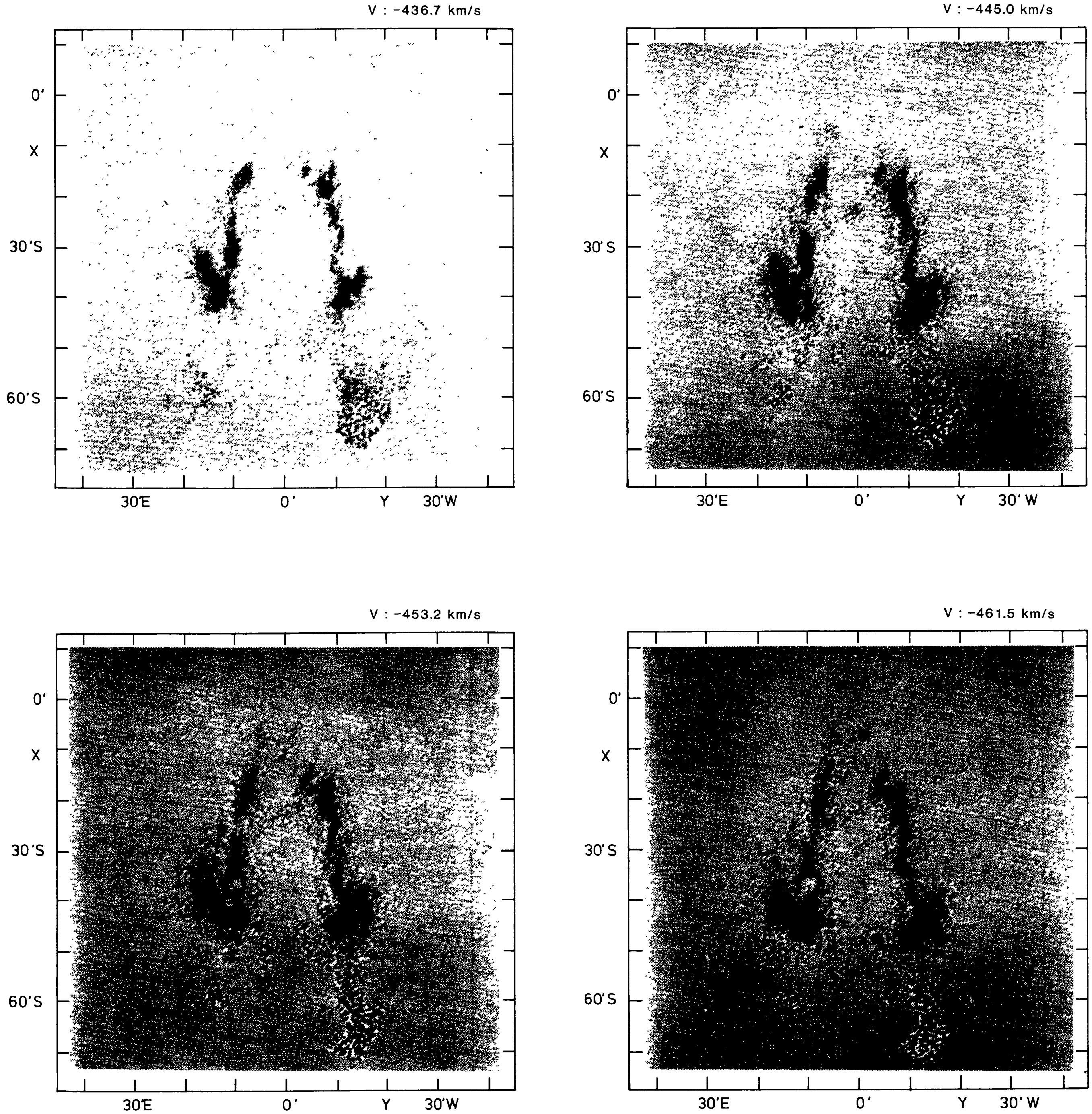

FIGURE 6 *(continued)*.

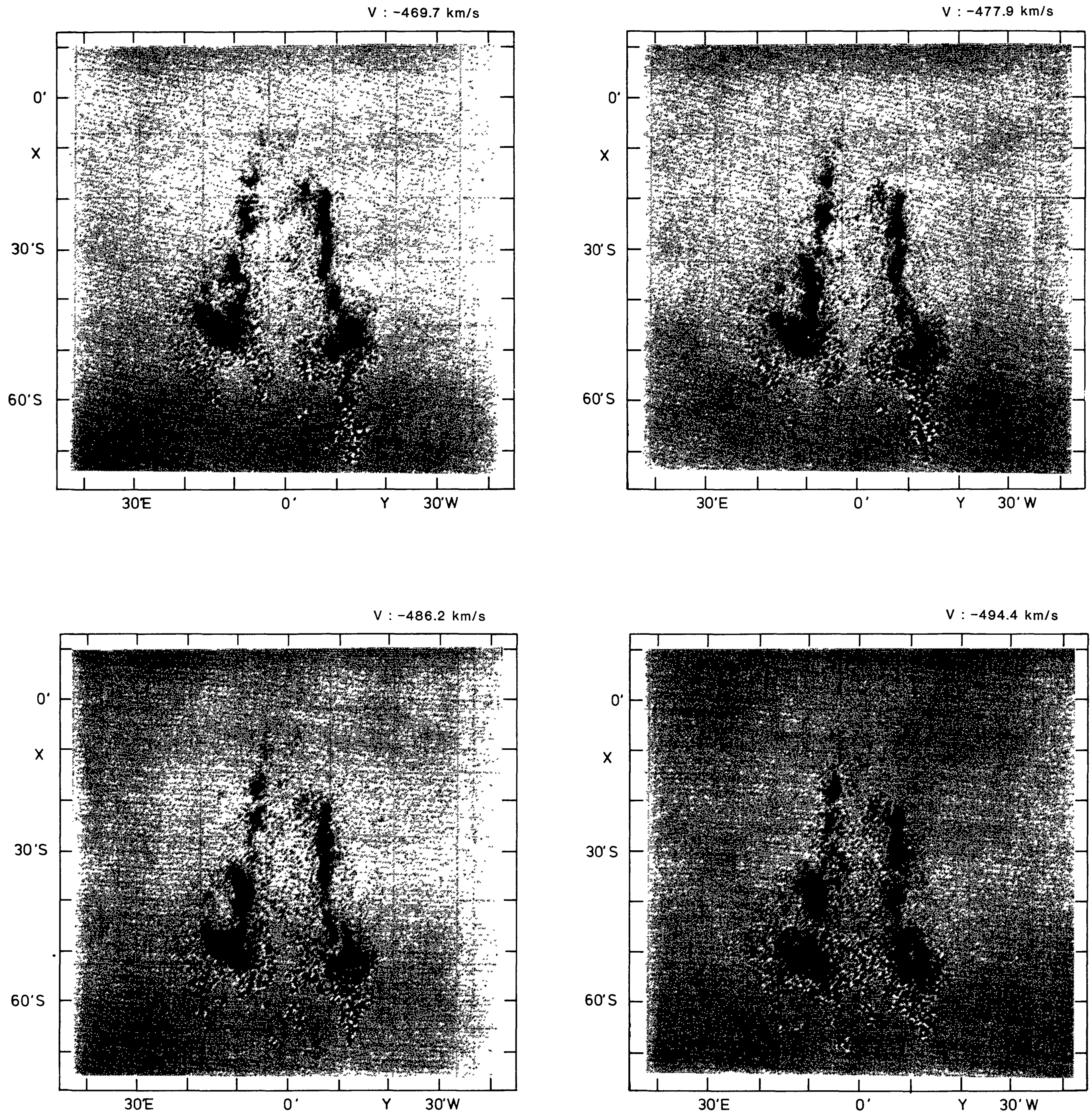

FIGURE 6 *(continued)*.

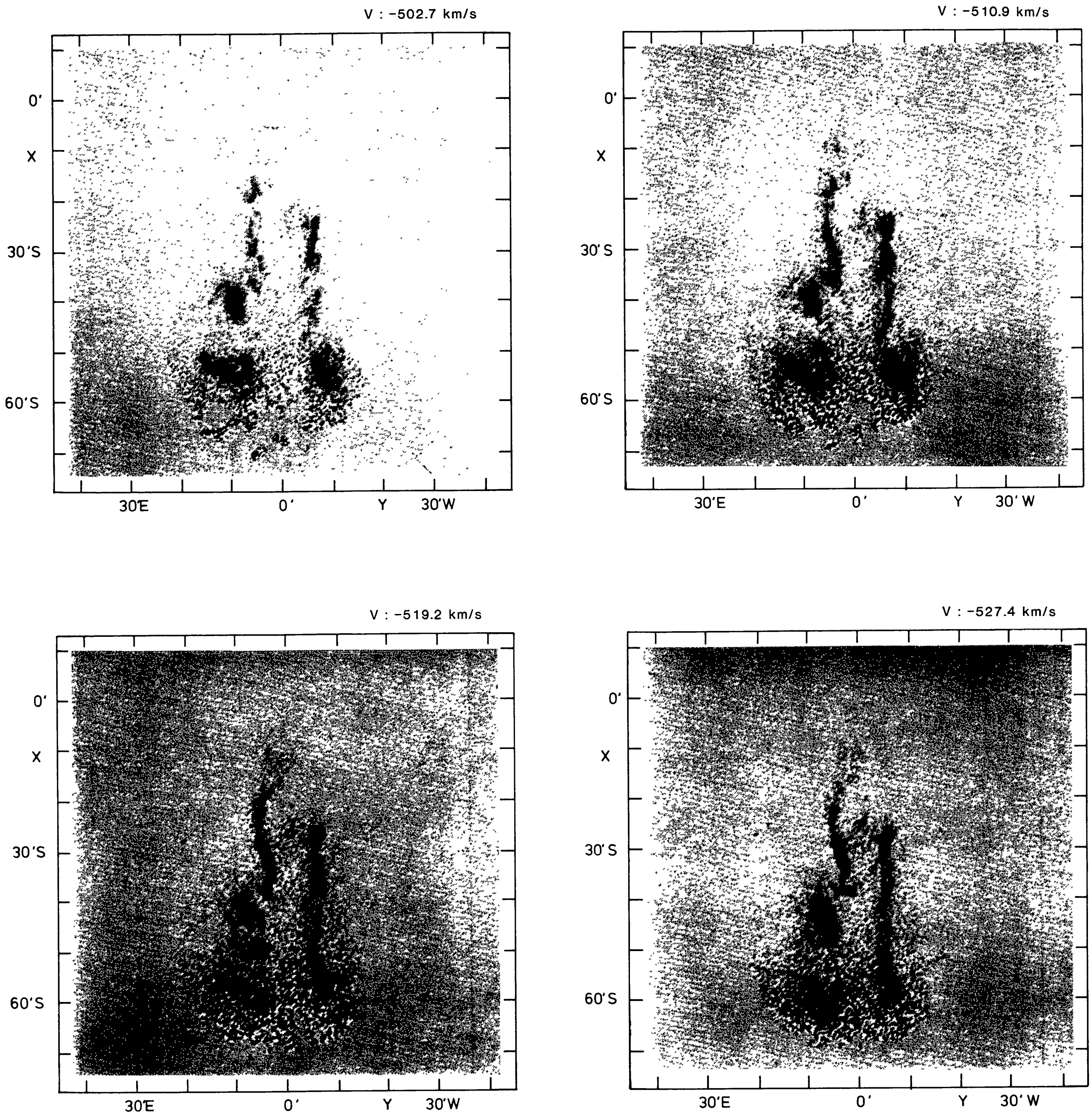

FIGURE 6 *(continued)*.

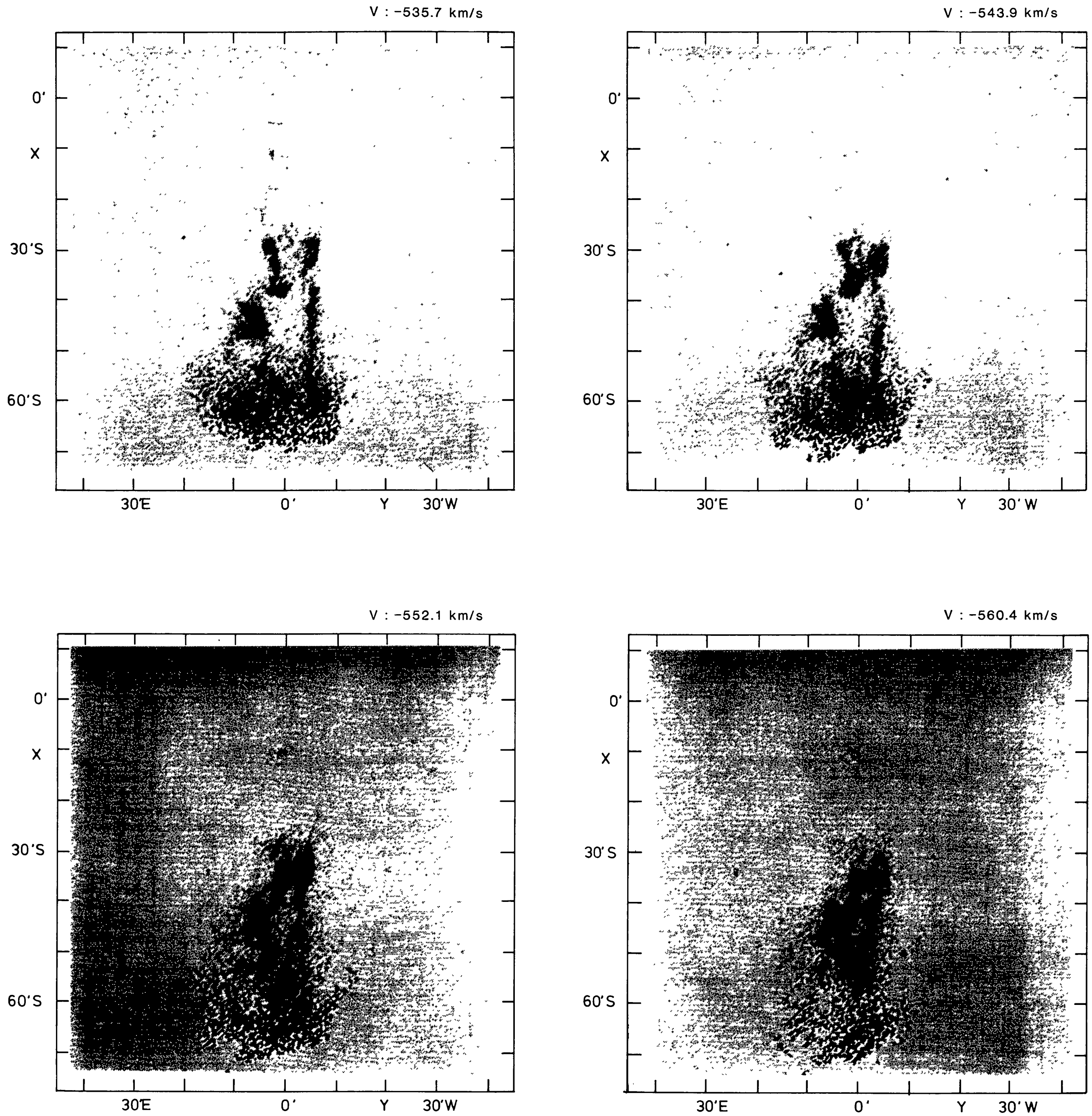

FIGURE 6 *(continued)*.

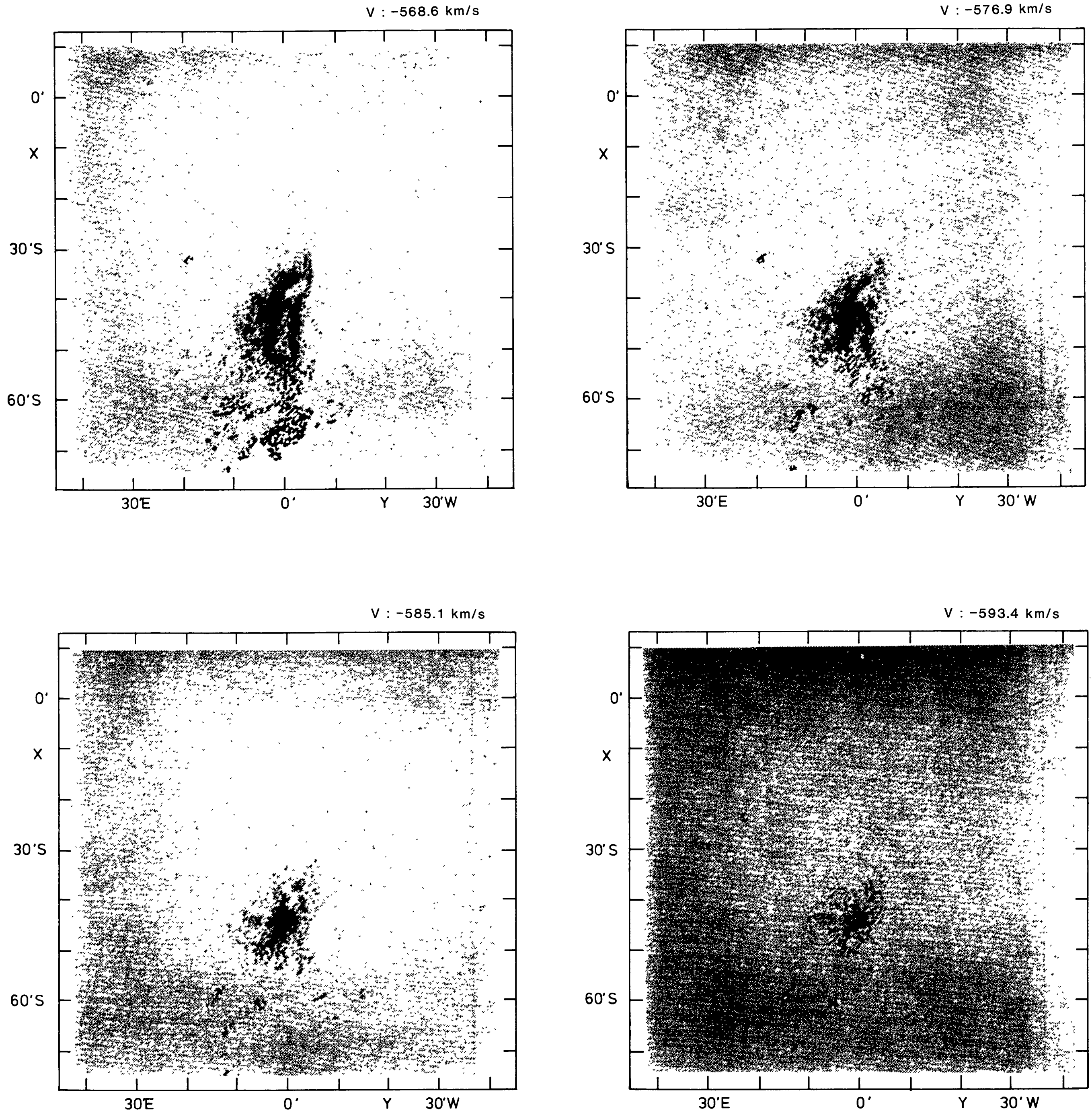

FIGURE 6 *(continued)*.

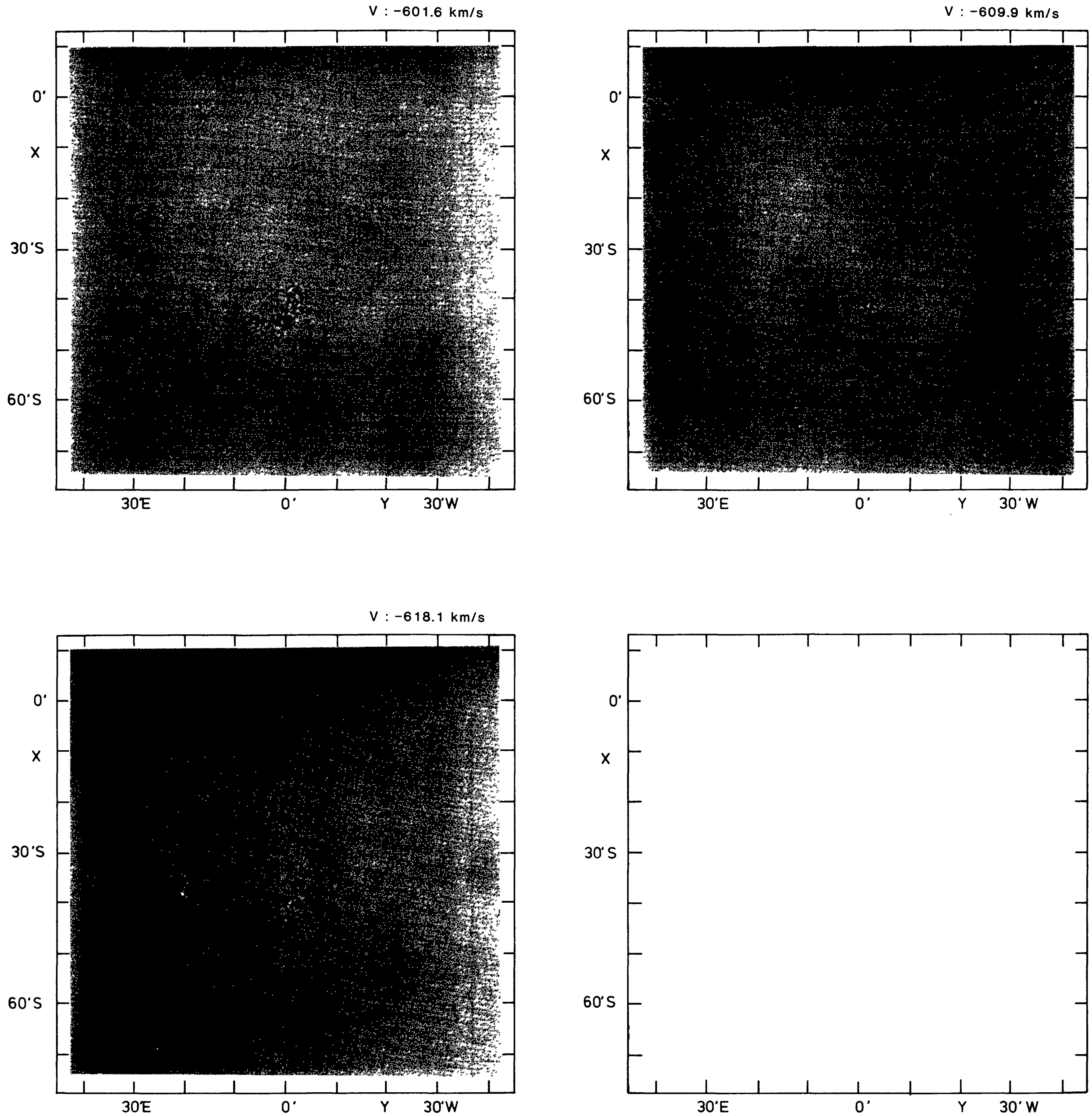

FIGURE 6 *(continued)*.

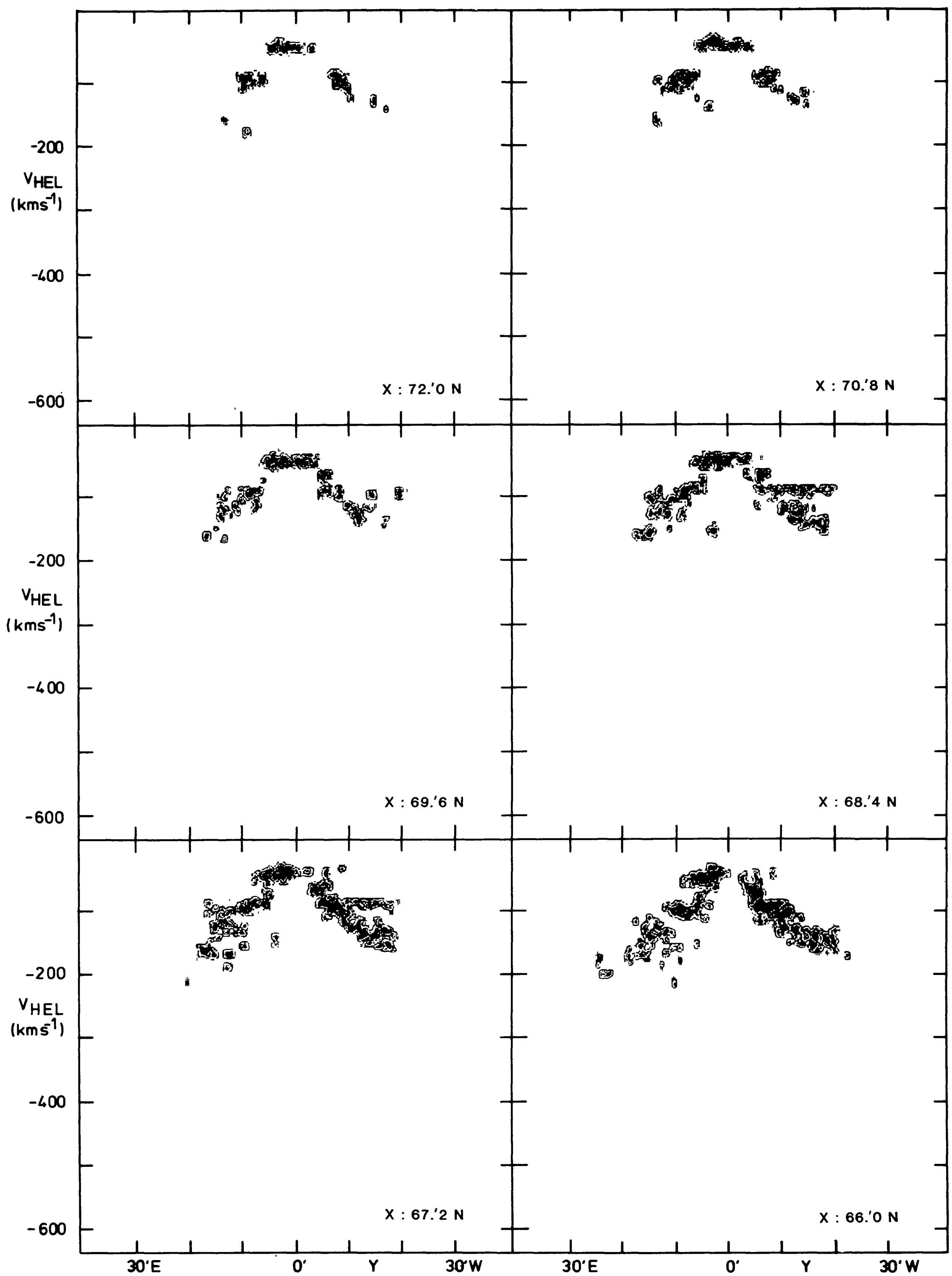

FIGURE 7. — Position-velocity maps with a resolution of 54″ × 8.2 km s^{-1} made parallel to the minor axis. The interval between cross cuts is 1.2 arcmin. The maps were constructed from maps smoothed to twice the original resolution of the survey and have an r.m.s. noise of 0.60 K. The gray scale levels are at 1.0, 1.5, 2.5, 5, 10, 25 and 50 K; the contour levels are at 2.5, 5, 10, 25 and 50 K.

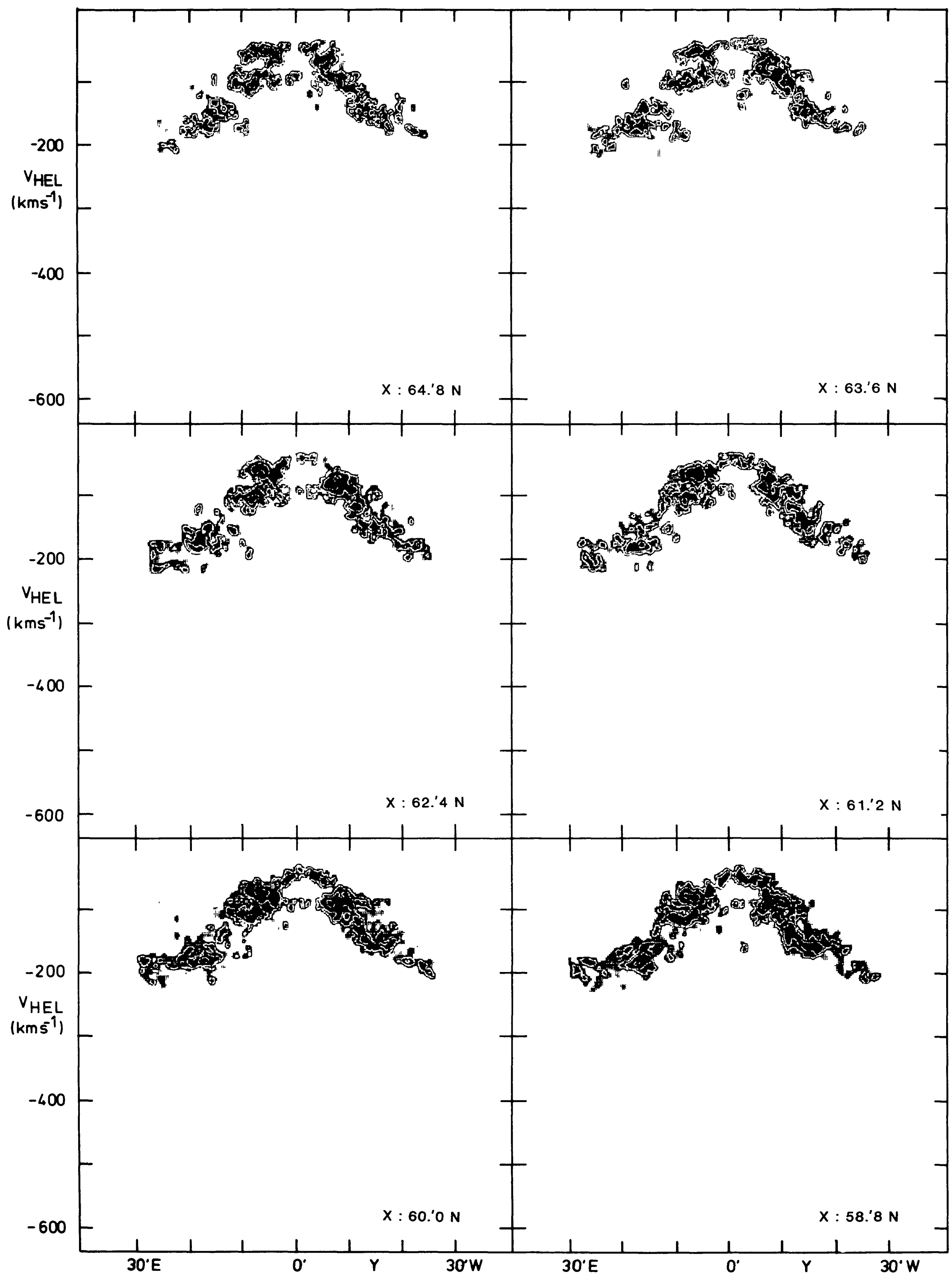

FIGURE 7 *(continued)*.

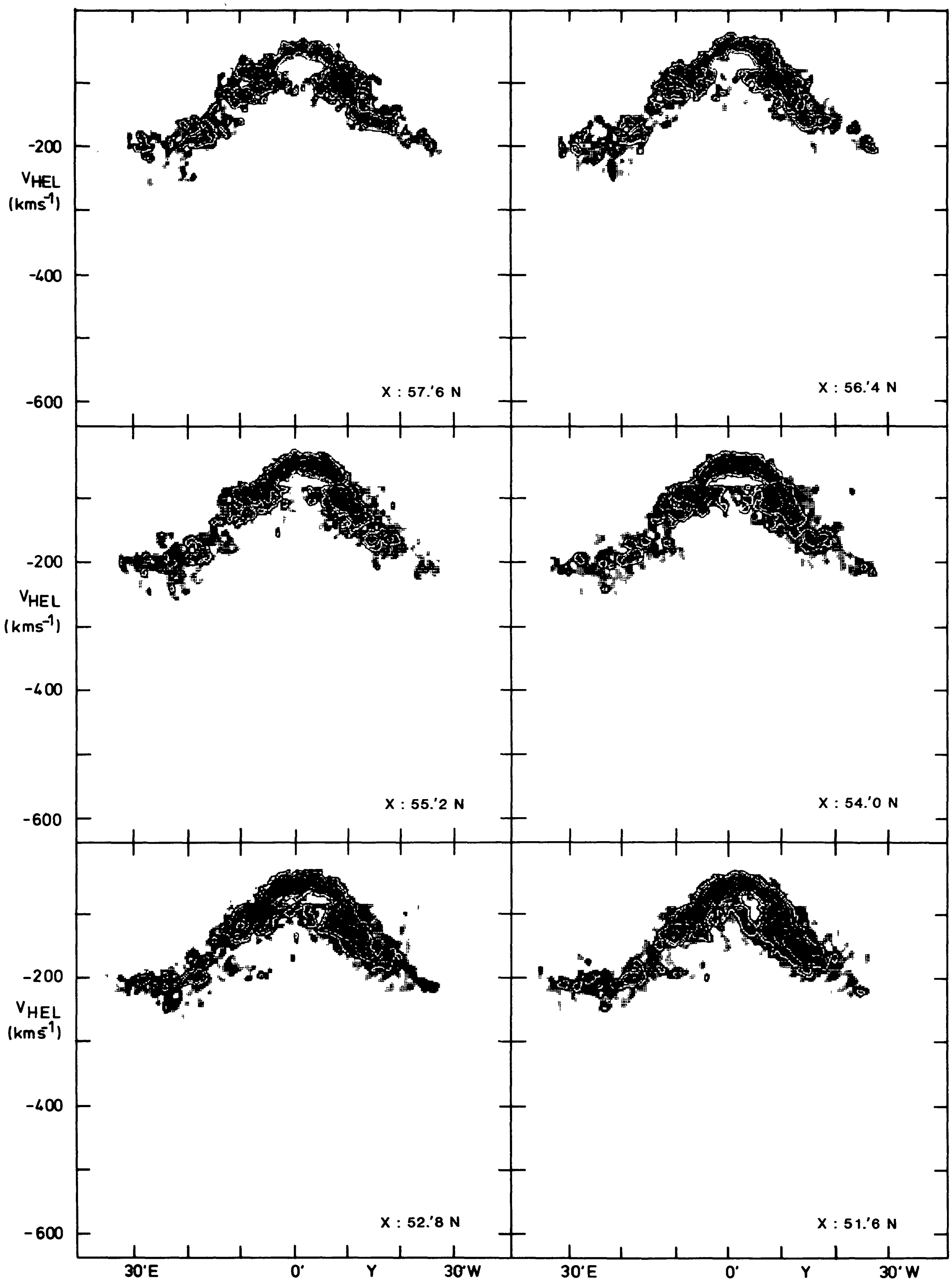

FIGURE 7 *(continued)*.

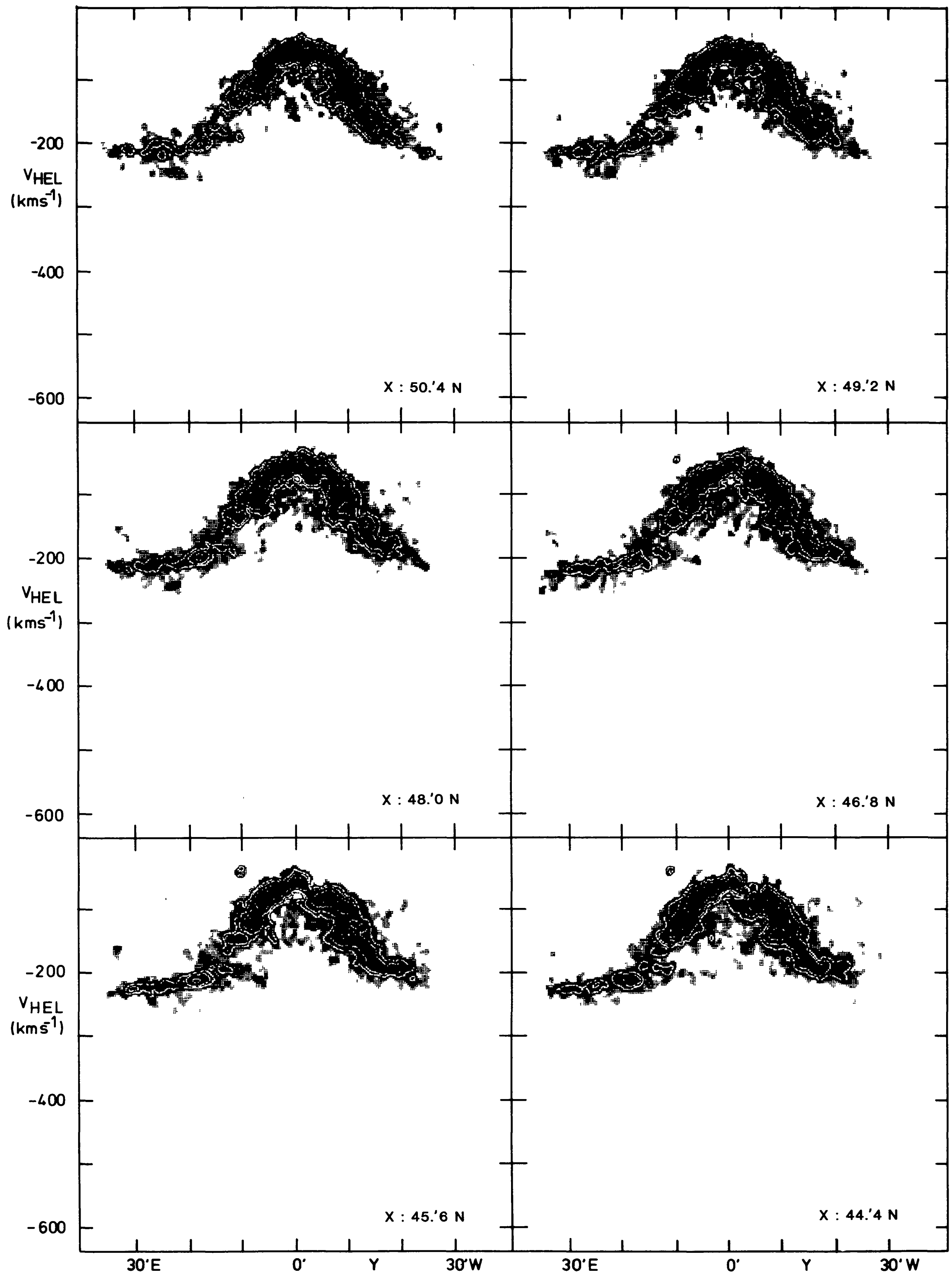

FIGURE 7 *(continued)*.

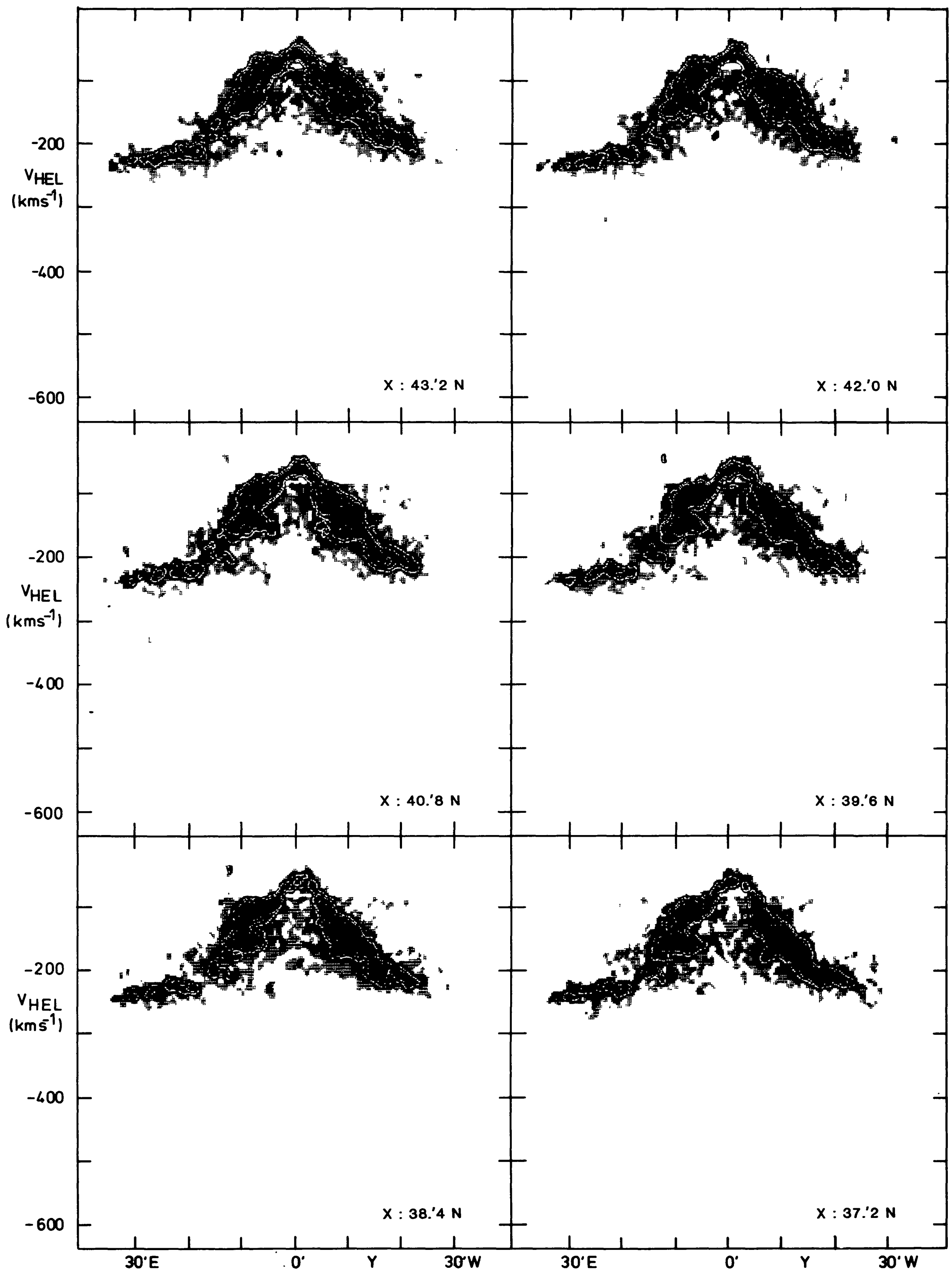

FIGURE 7 *(continued)*.

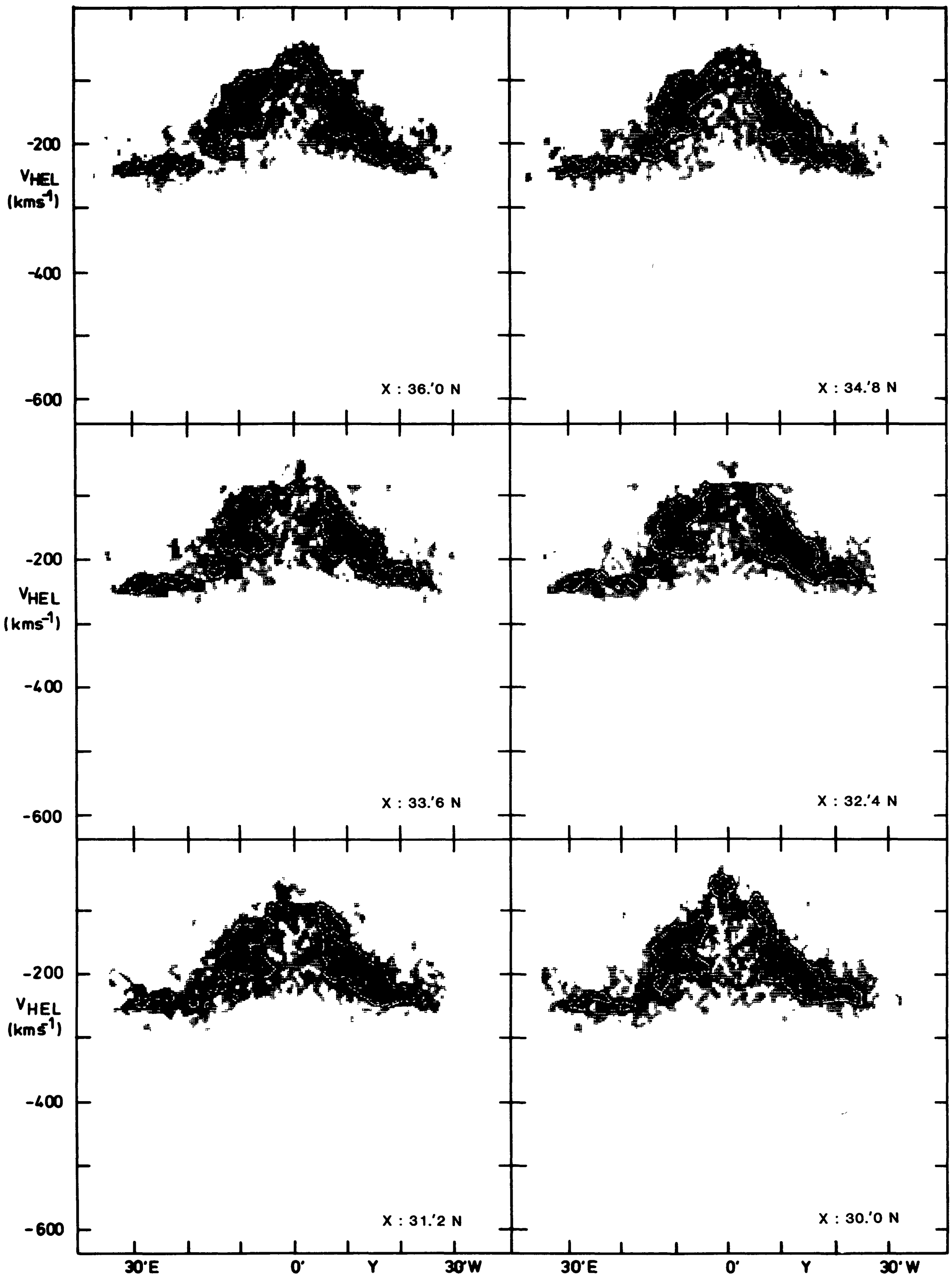

FIGURE 7 *(continued)*.

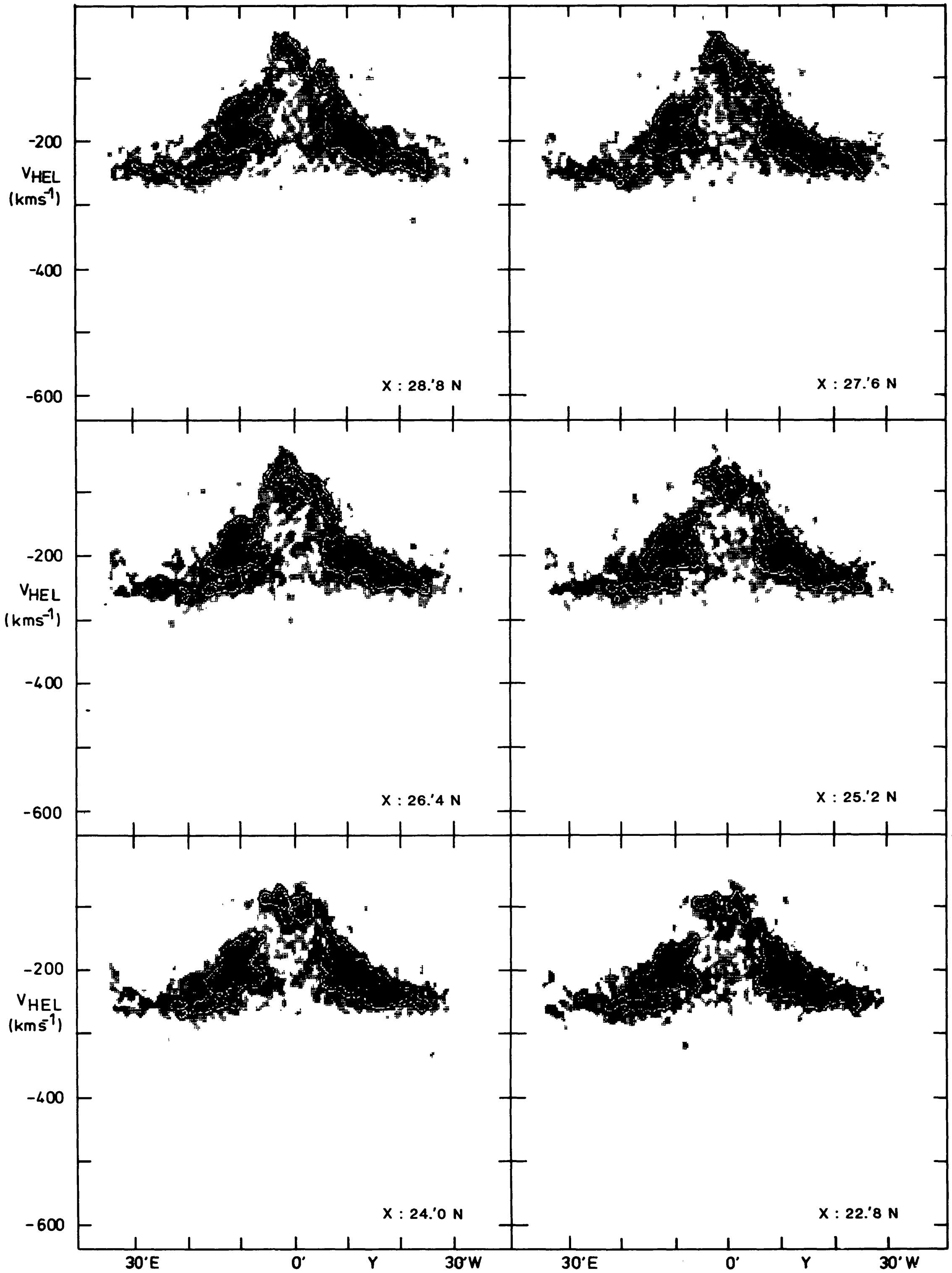

FIGURE 7 *(continued)*.

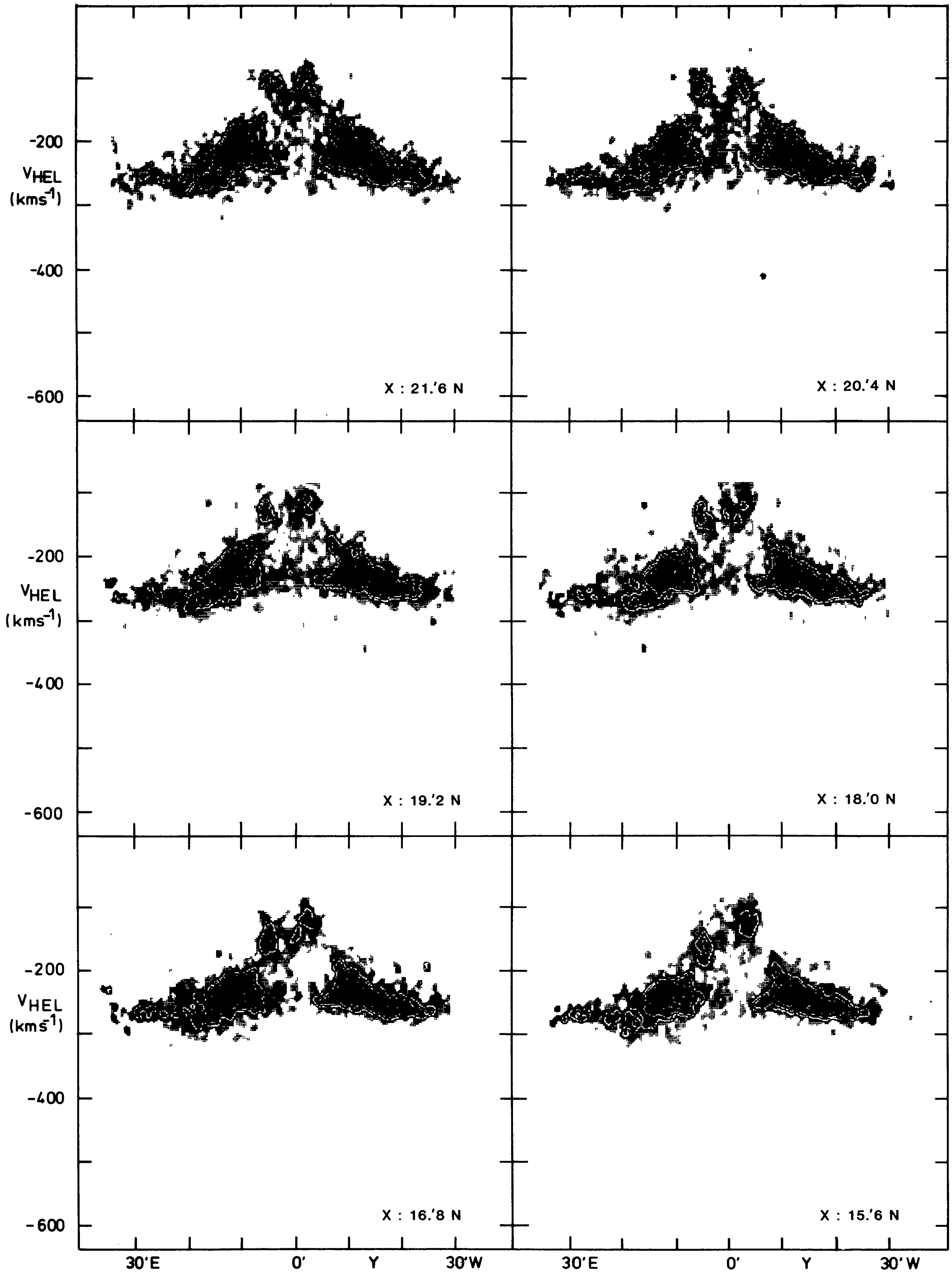

FIGURE 7 *(continued)*.

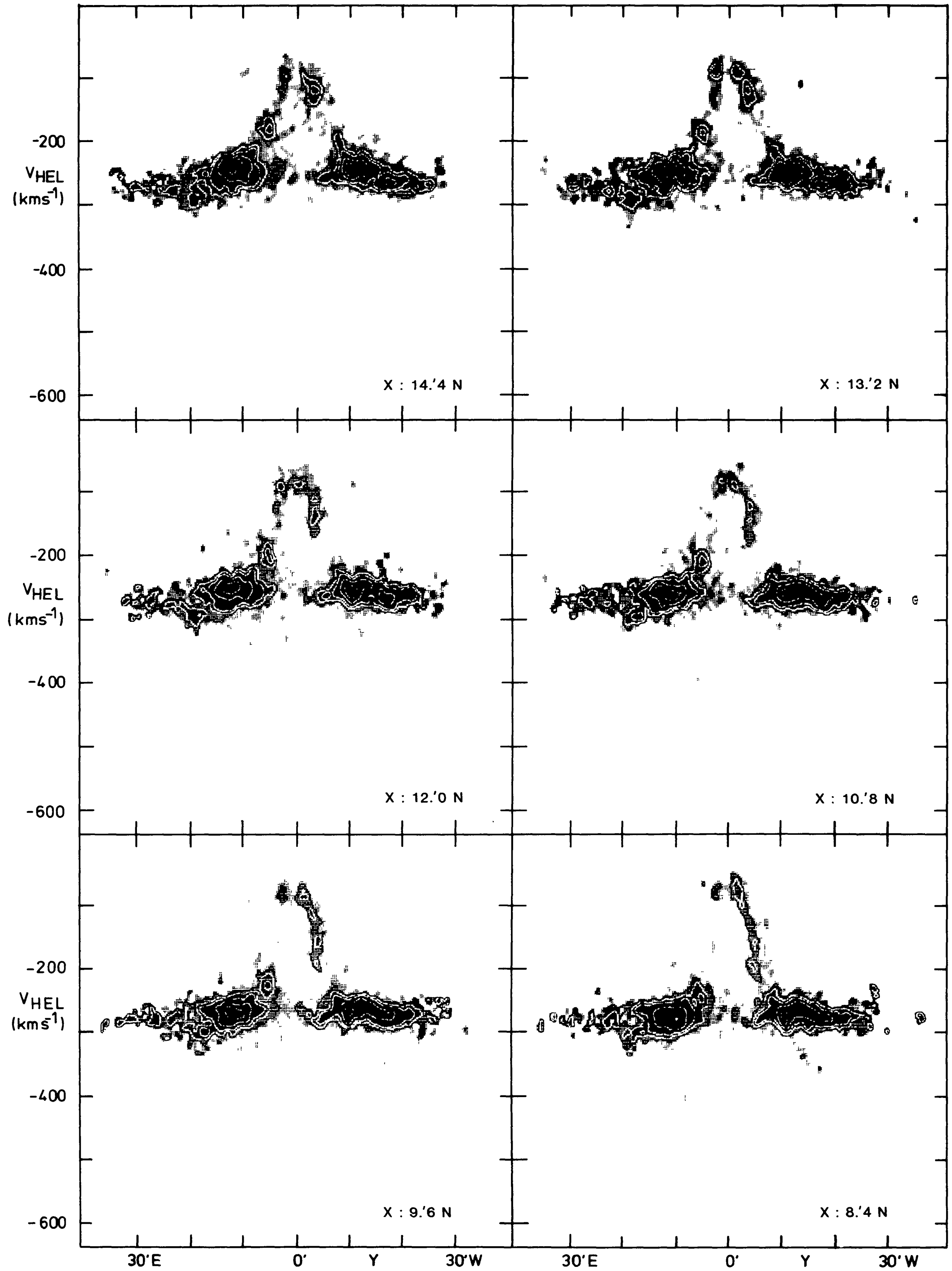

FIGURE 7 *(continued)*.

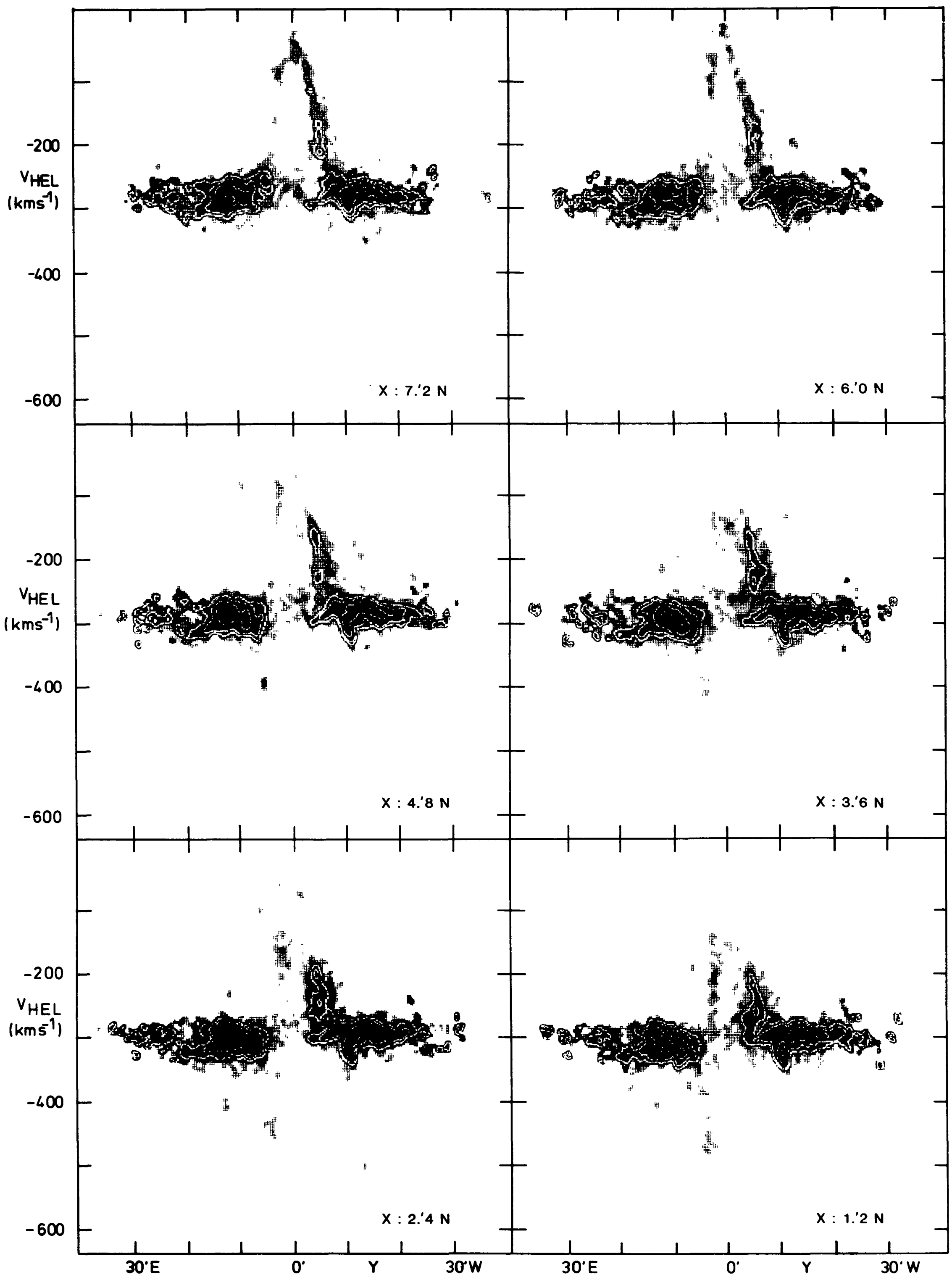

FIGURE 7 *(continued)*.

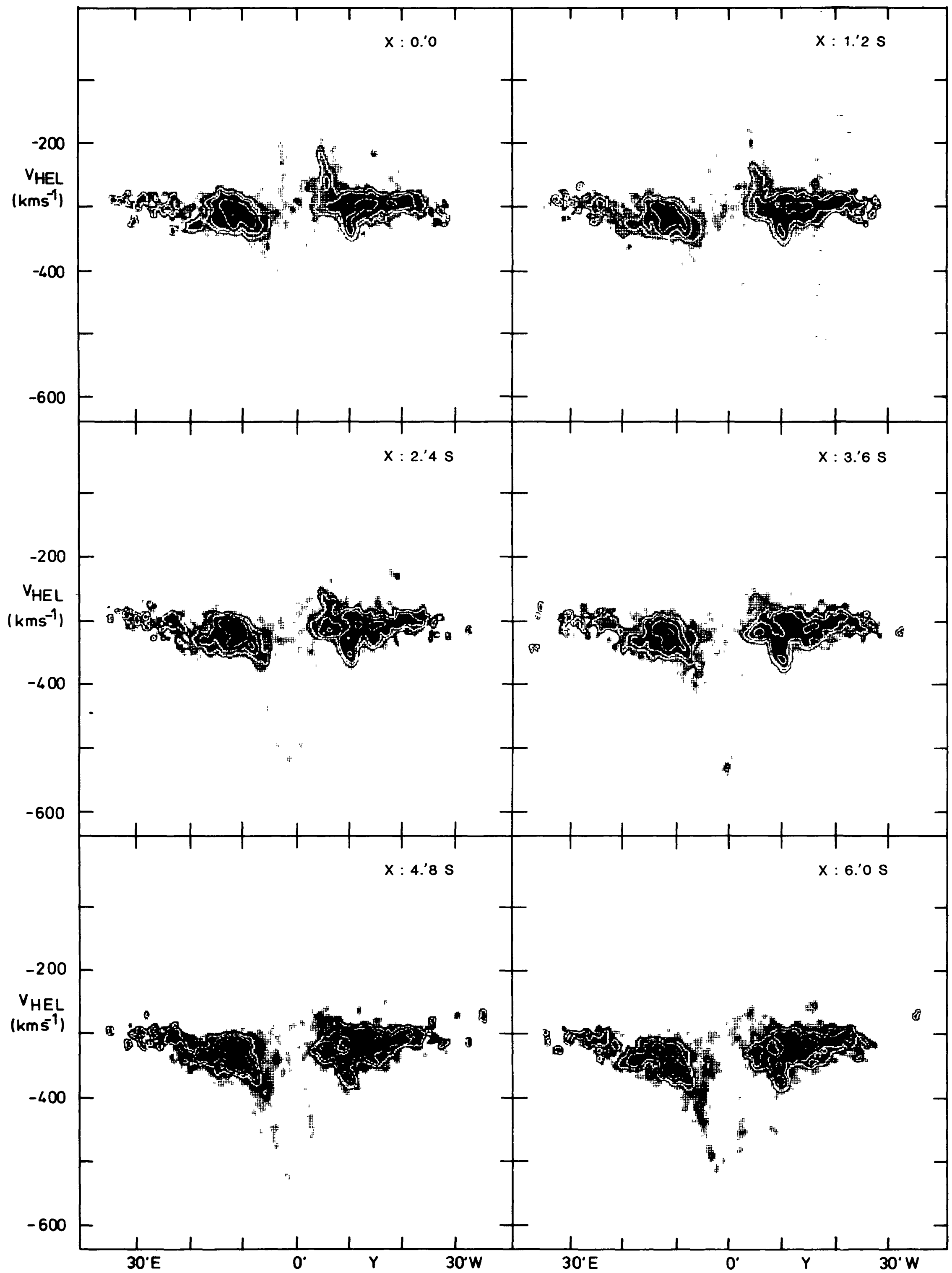

FIGURE 7 *(continued)*.

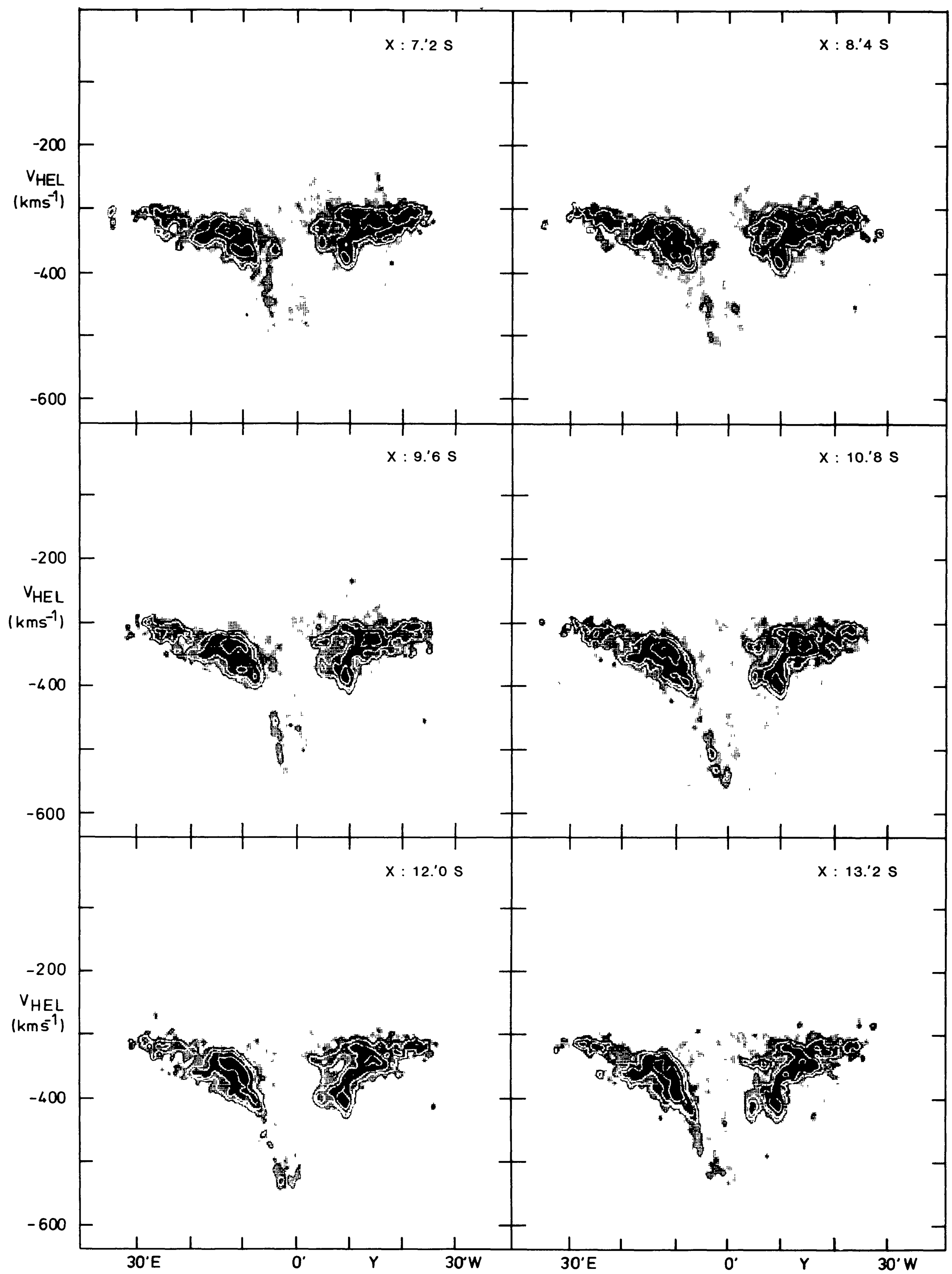

FIGURE 7 *(continued)*.

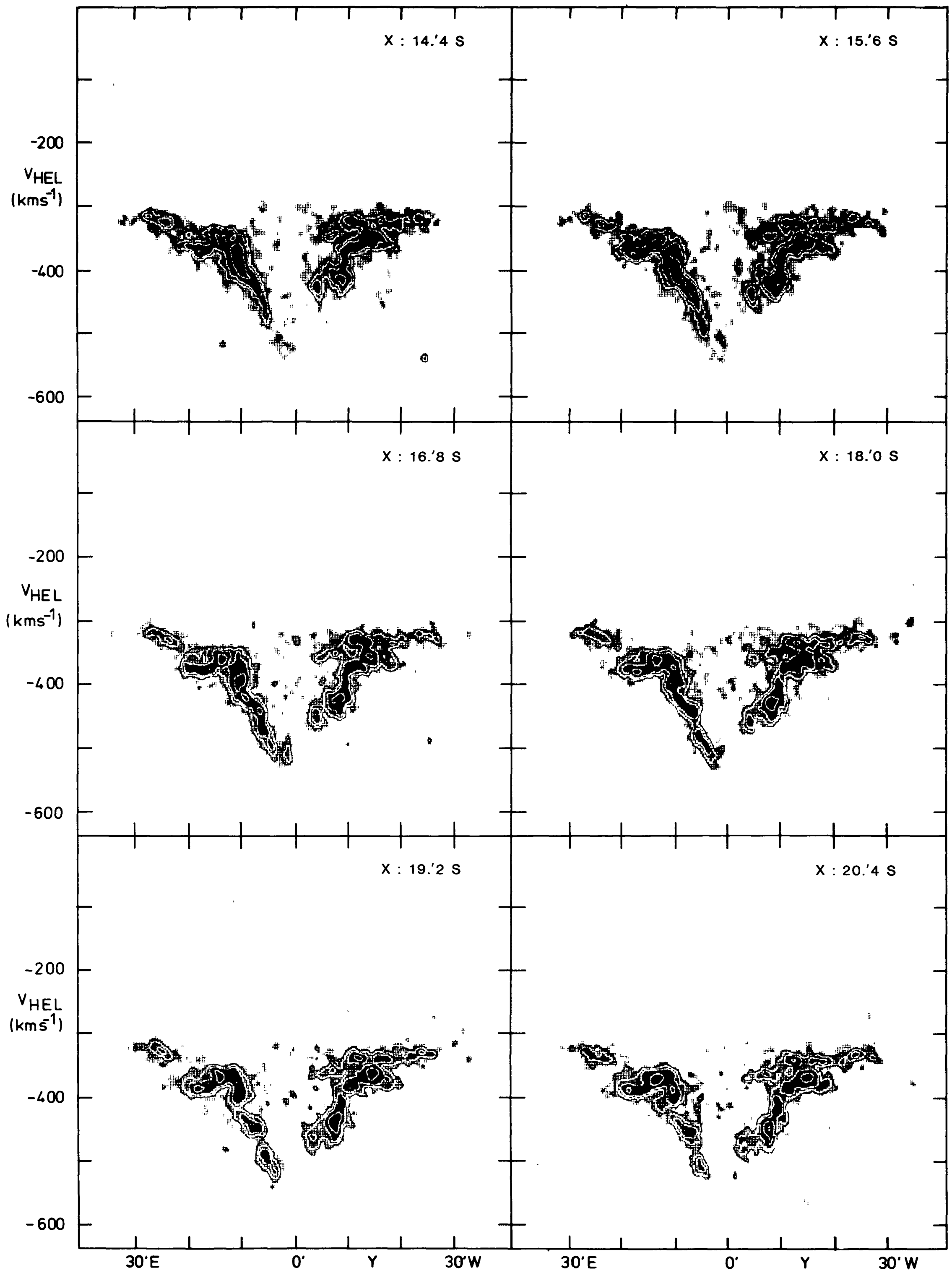

FIGURE 7 *(continued)*.

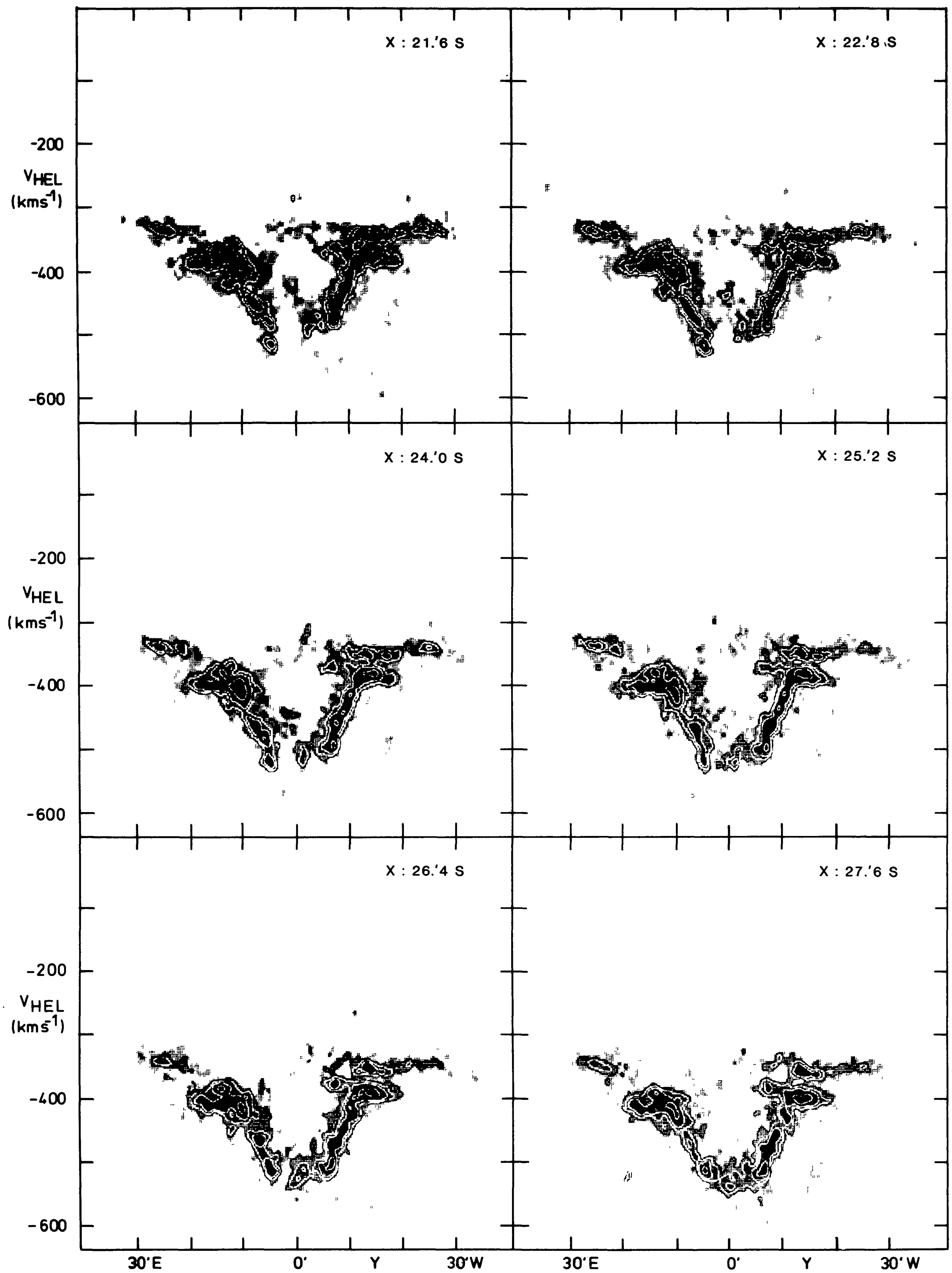

FIGURE 7 *(continued)*.

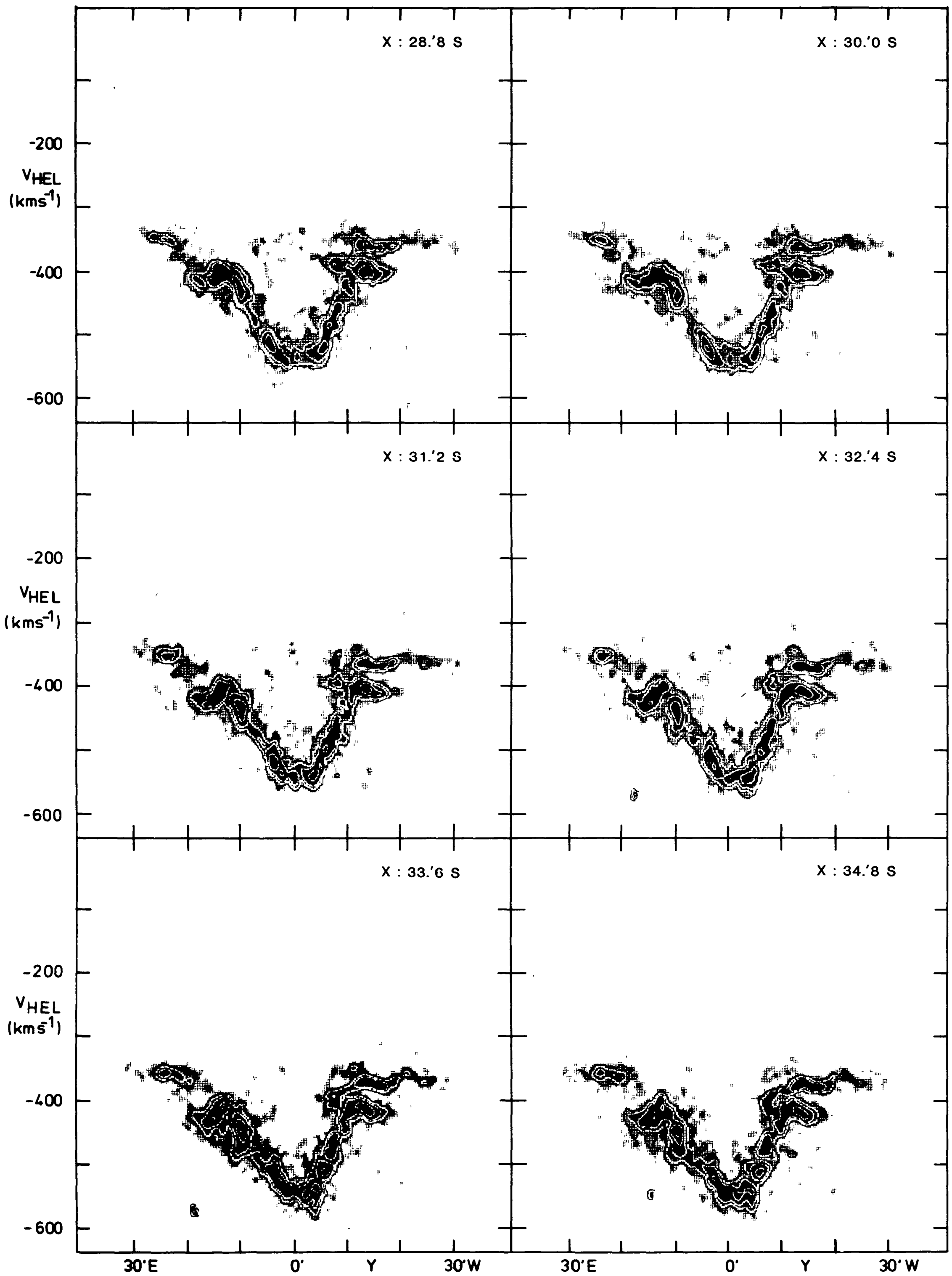

FIGURE 7 *(continued)*.

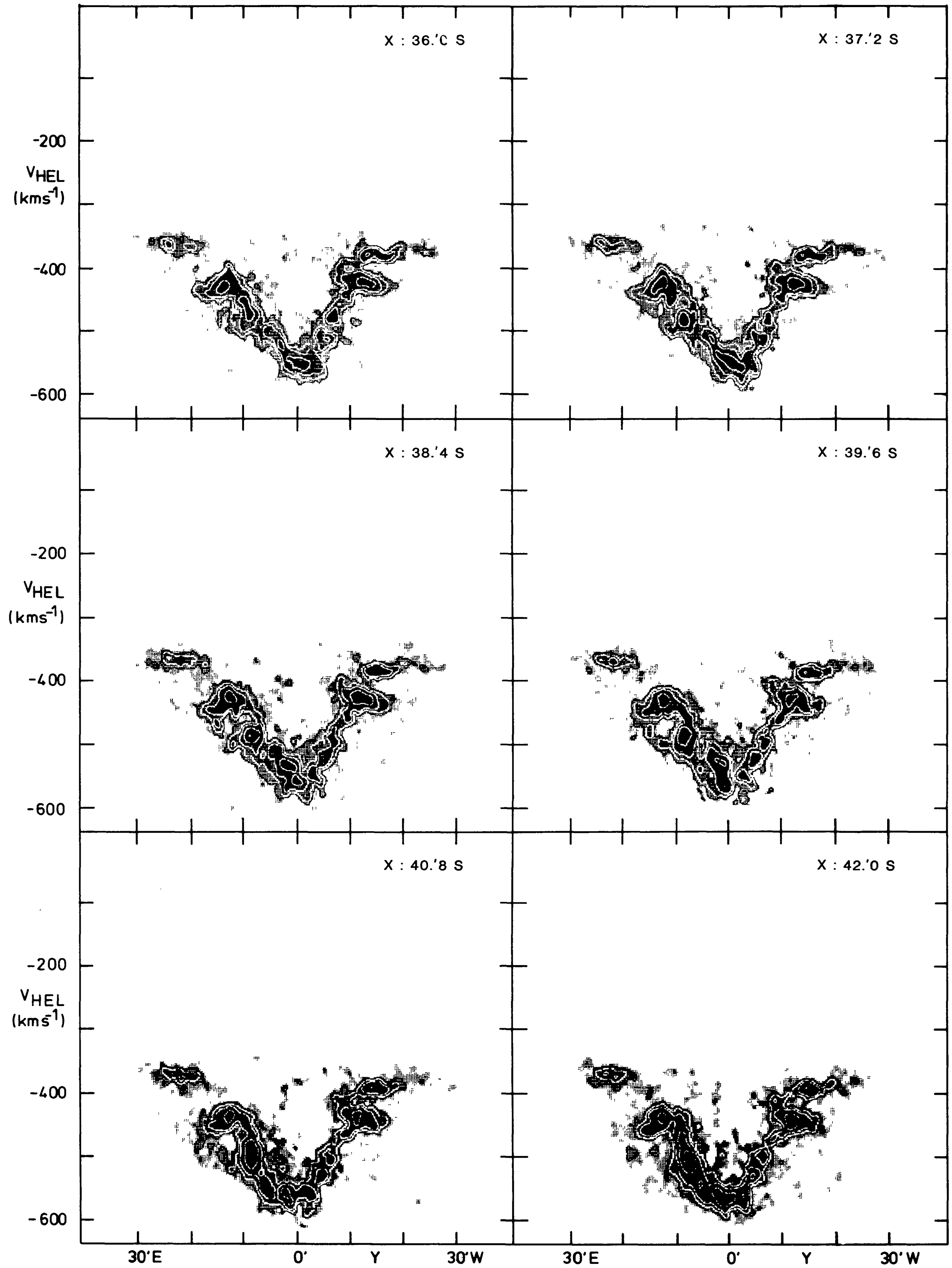

FIGURE 7 *(continued)*.

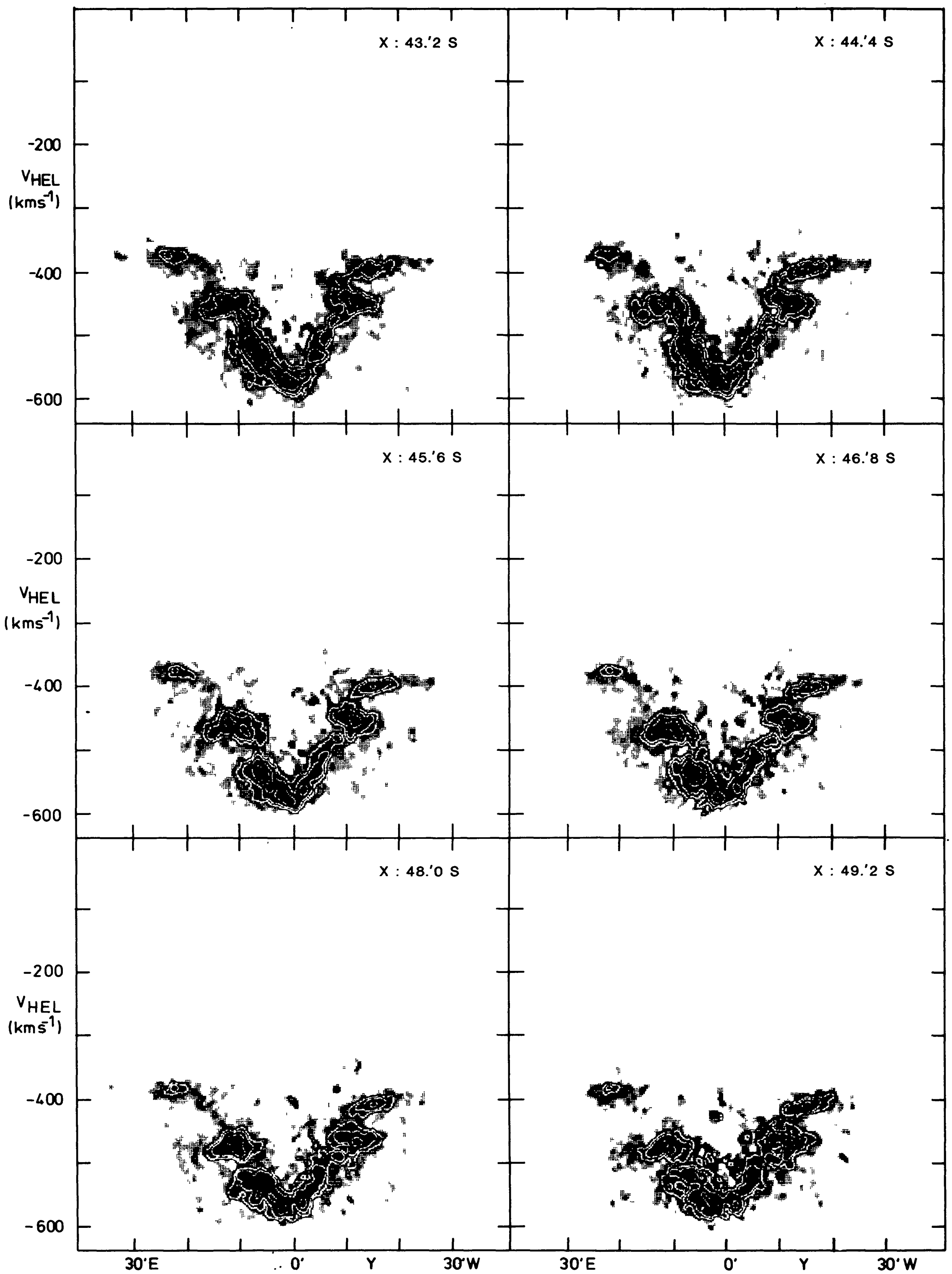

FIGURE 7 *(continued)*.

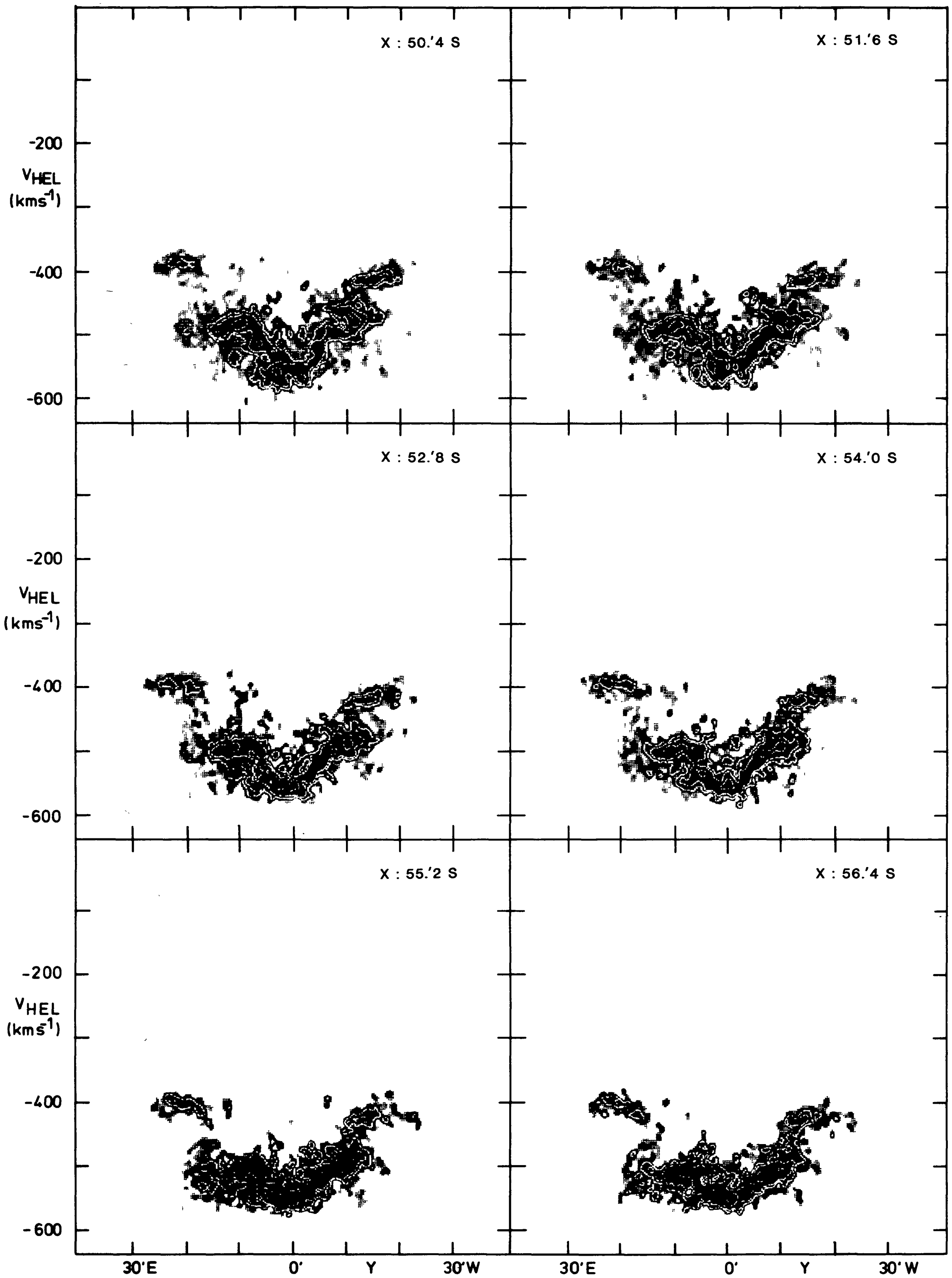

FIGURE 7 *(continued)*.

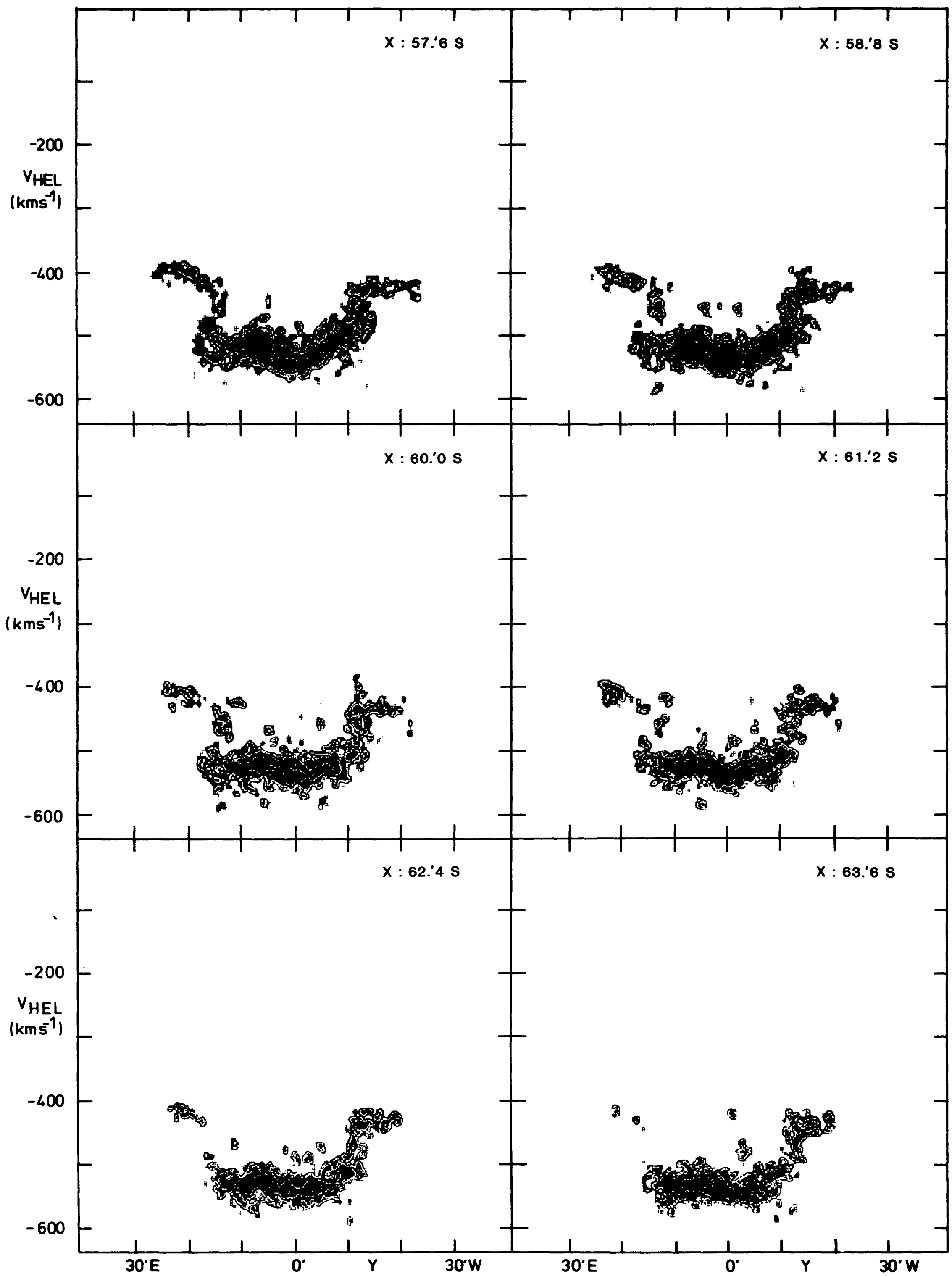

FIGURE 7 *(continued)*.

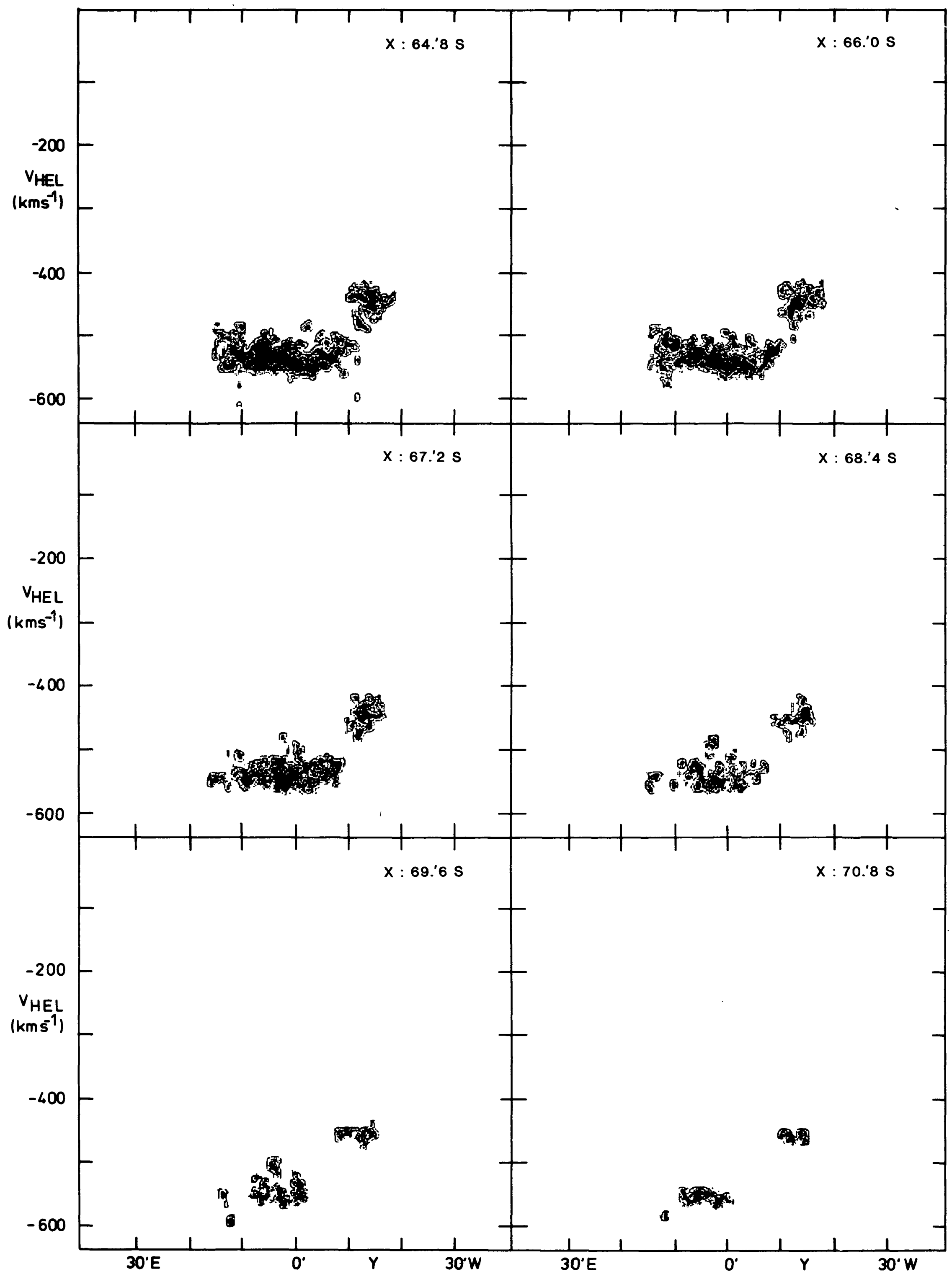

FIGURE 7 *(continued)*.

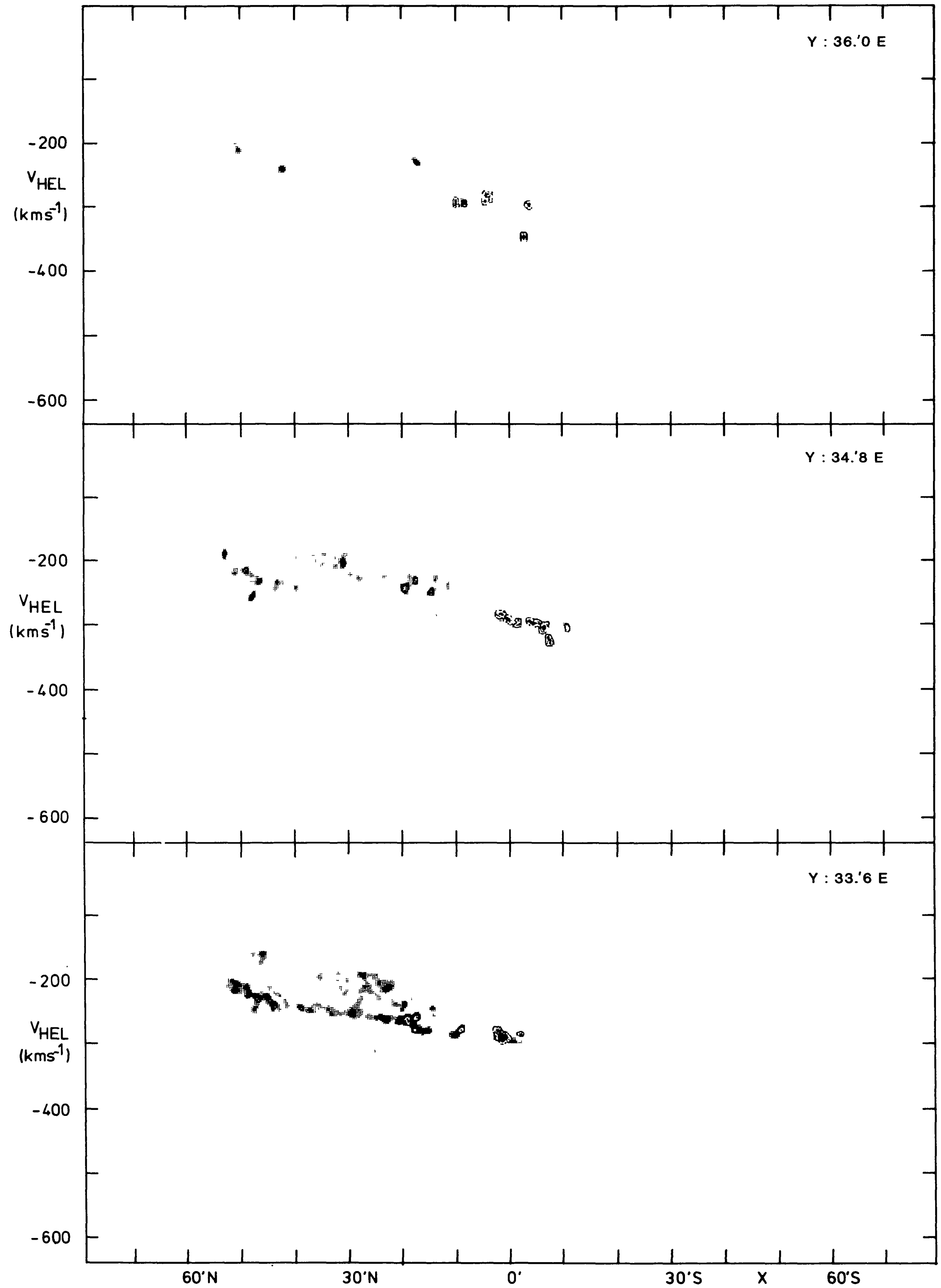

FIGURE 8. — Position-velocity maps made parallel to the major axis. The specifications are the same as for figure 7. The resolution is 60″ × 8.2 km s^{-1}.

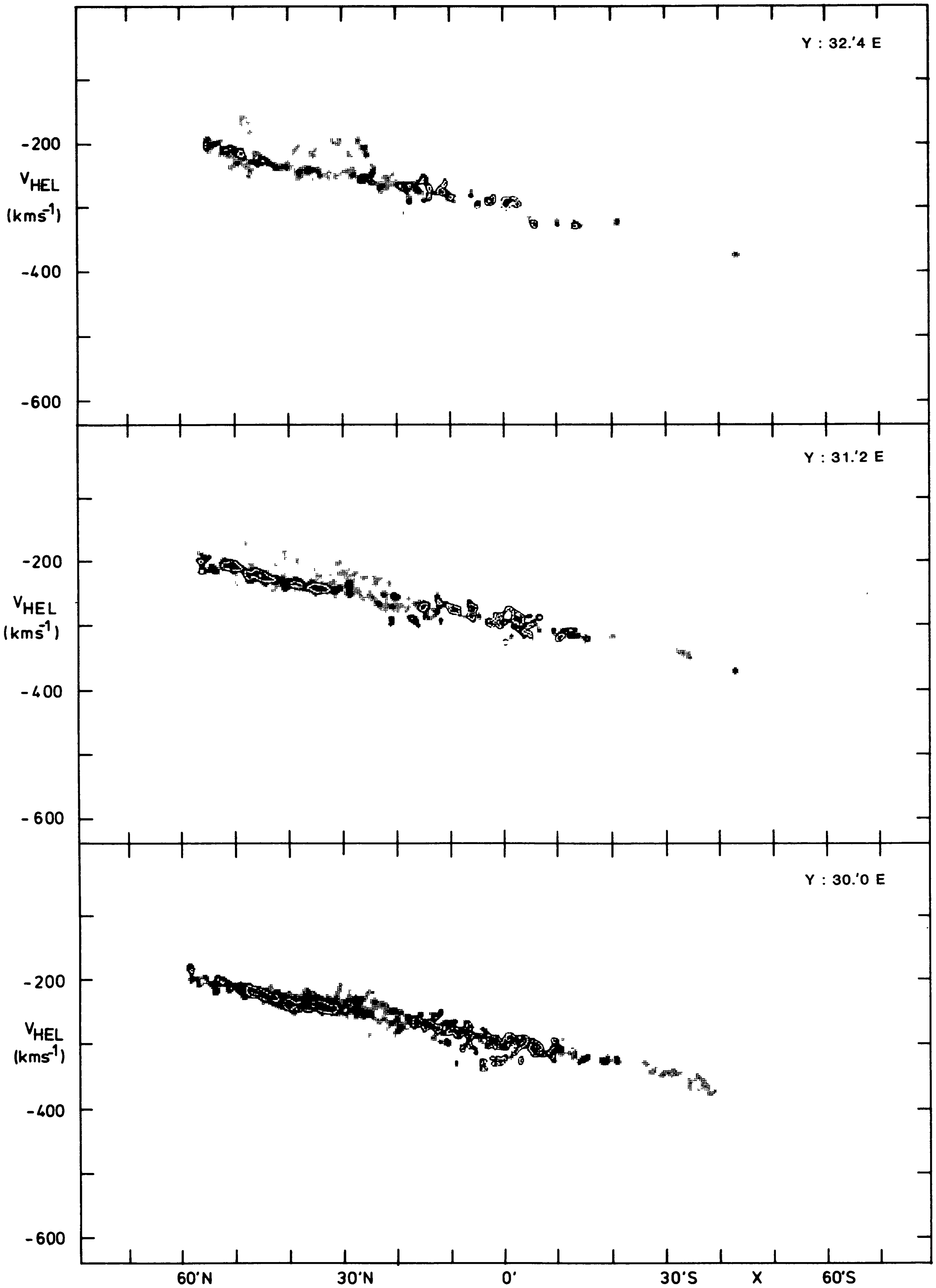

FIGURE 8 *(continued)*.

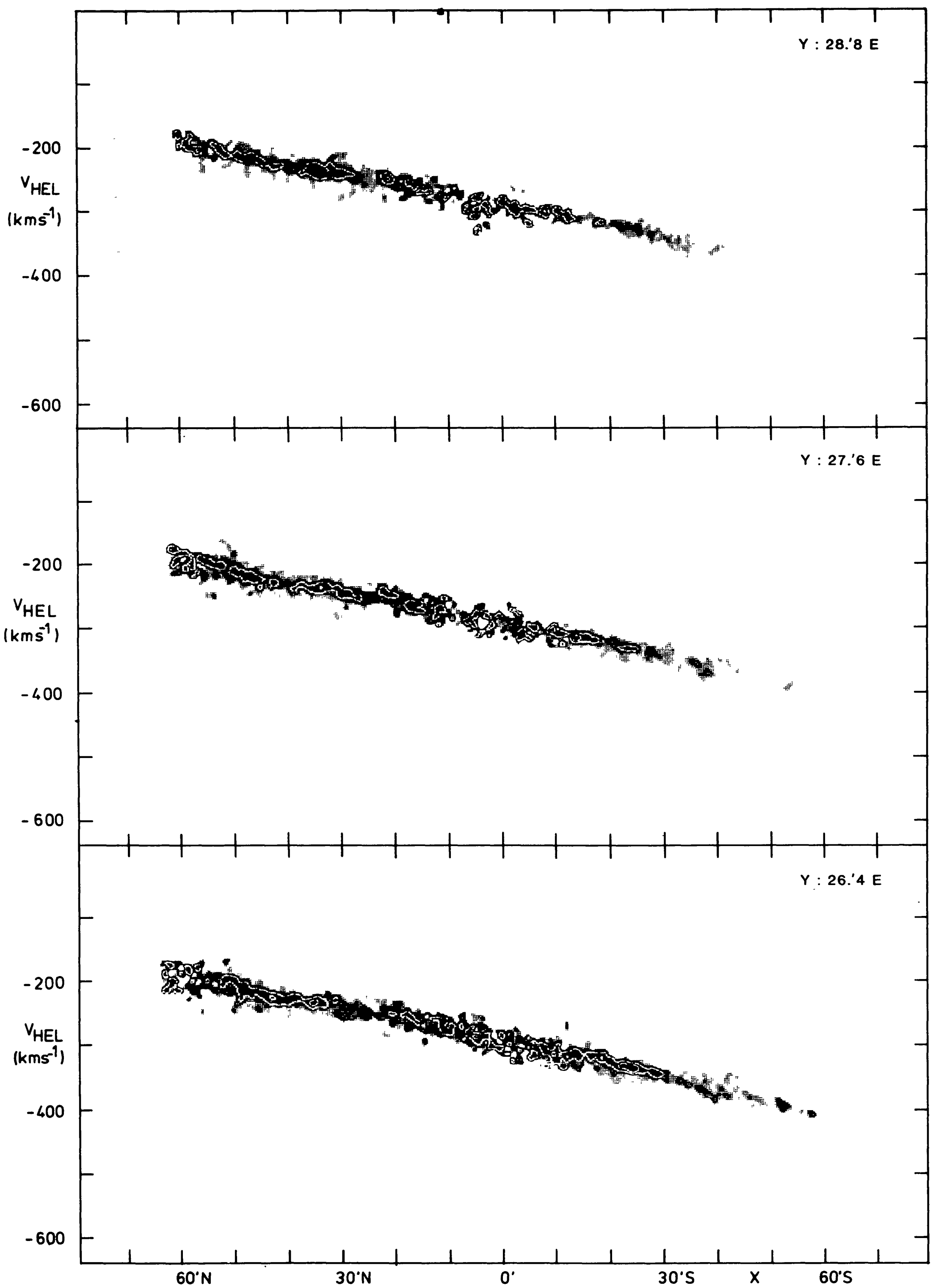

FIGURE 8 *(continued)*.

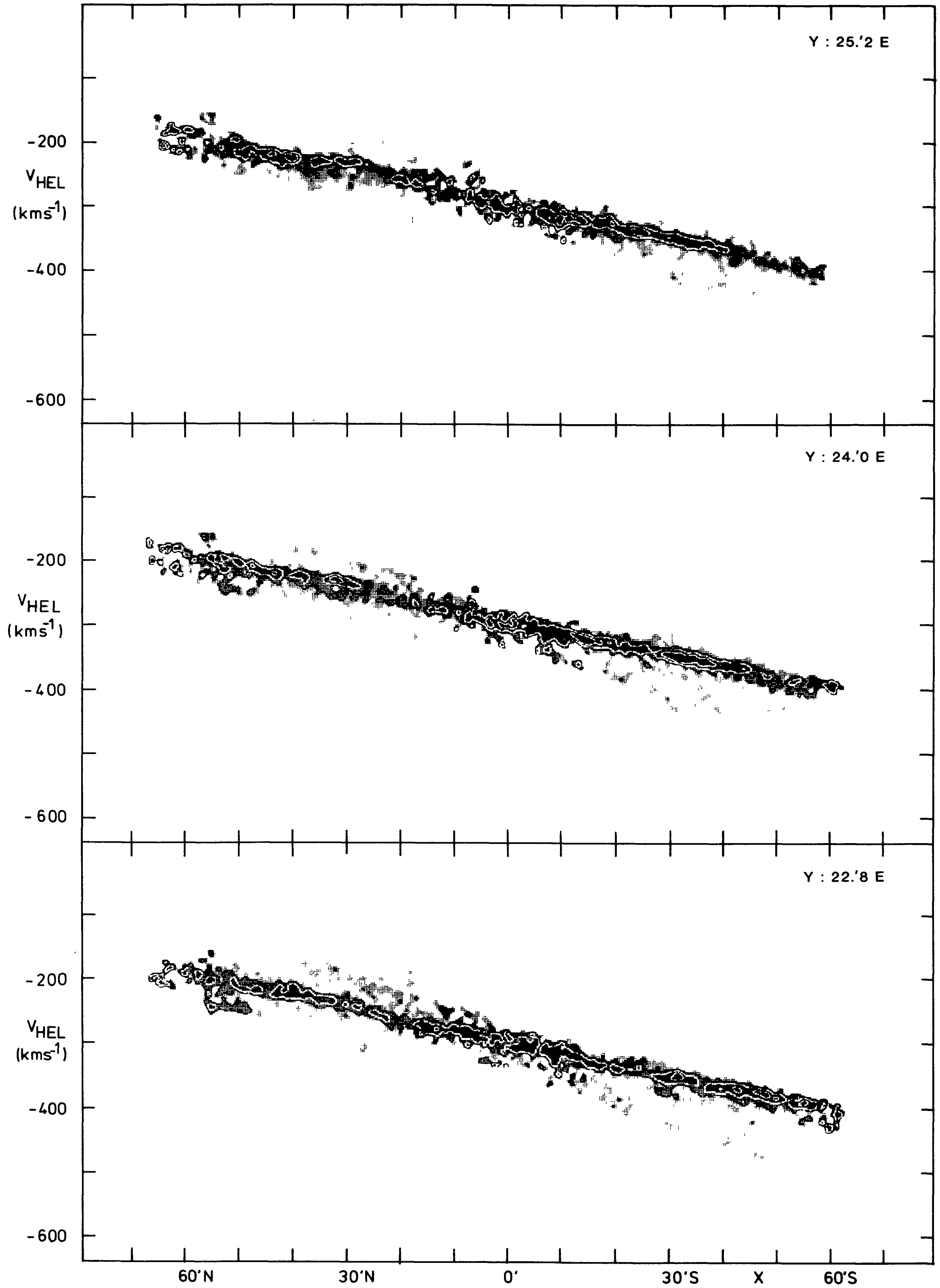

FIGURE 8 *(continued)*.

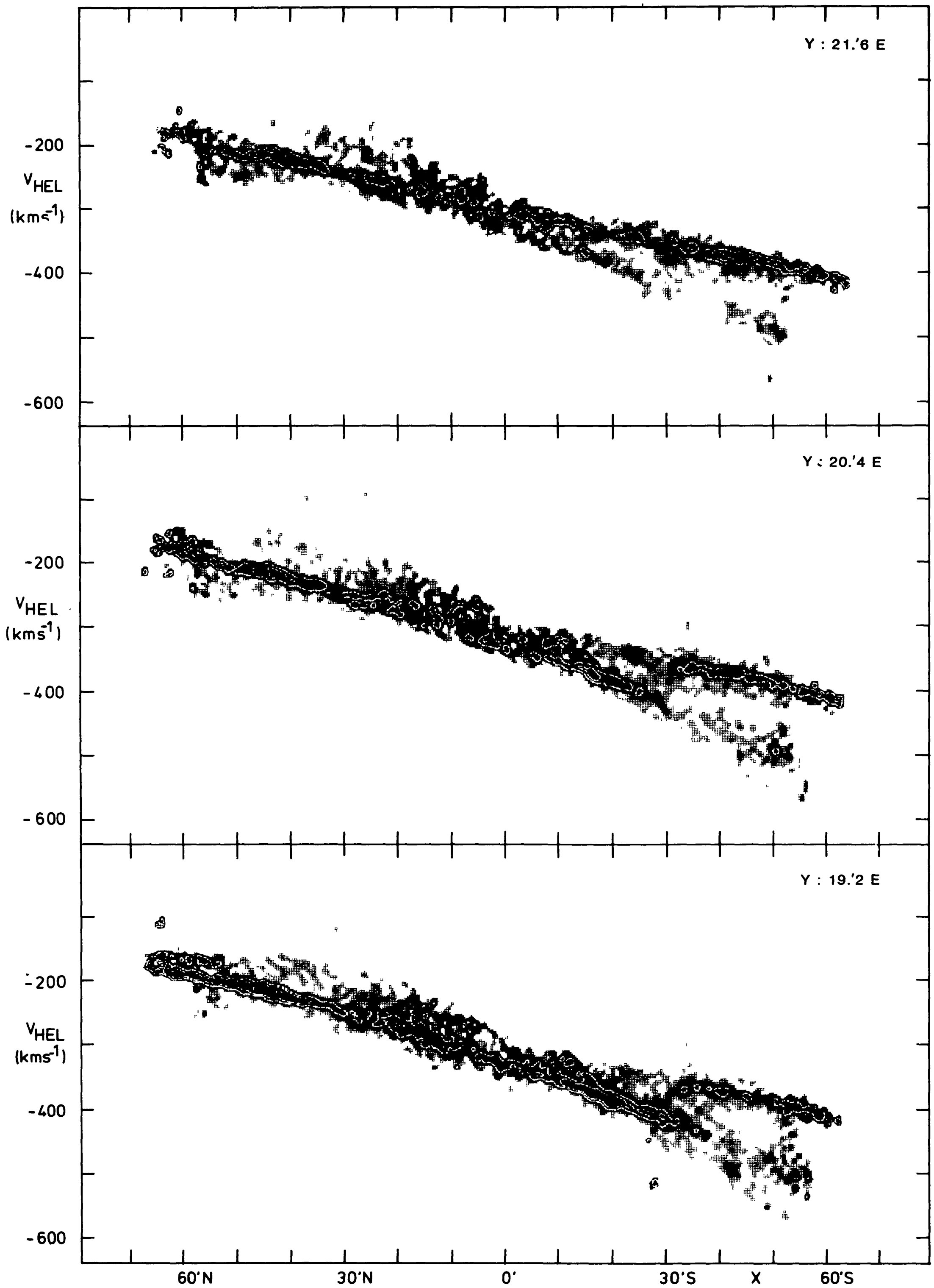

FIGURE 8 *(continued)*.

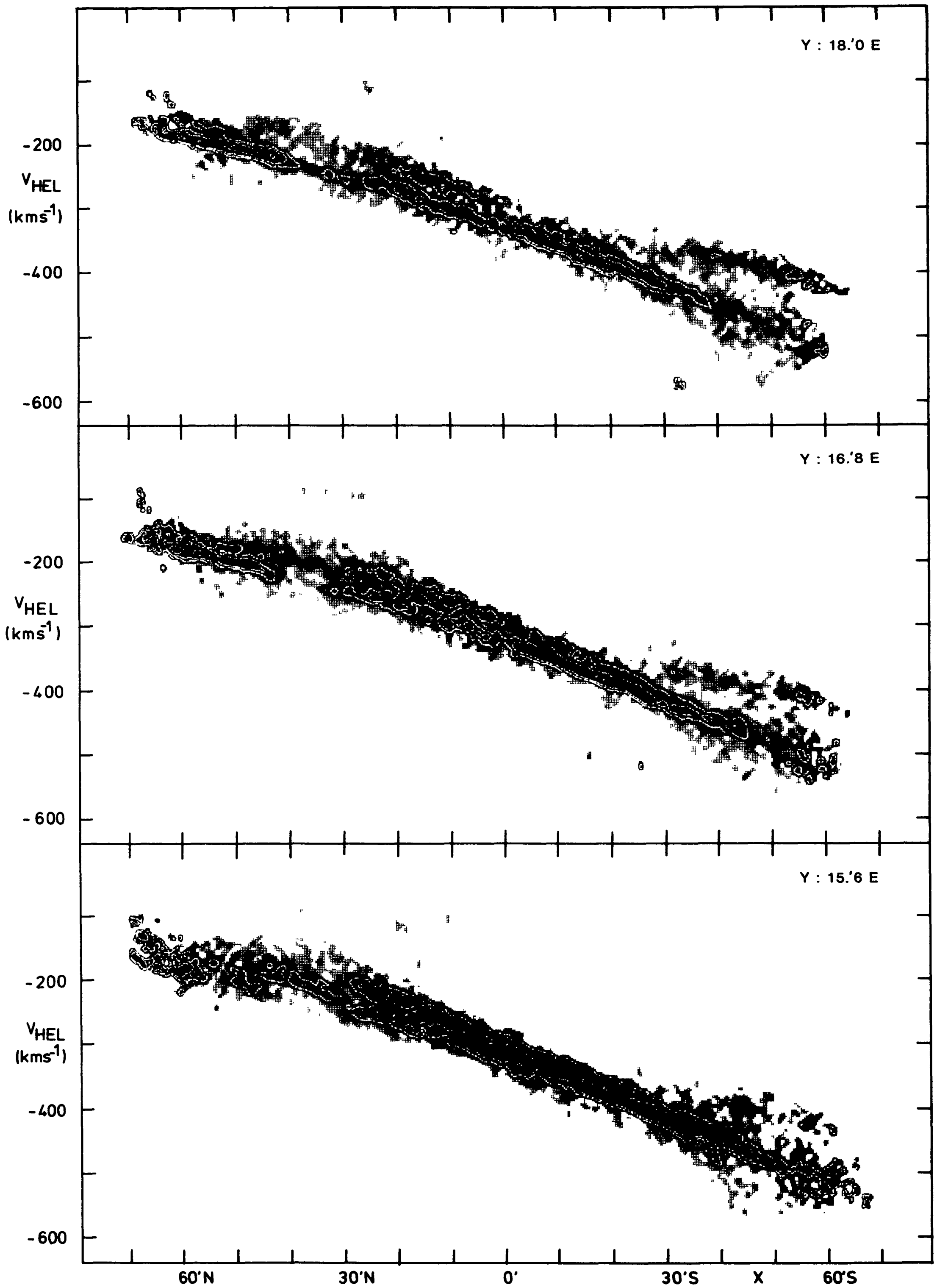

FIGURE 8 *(continued)*.

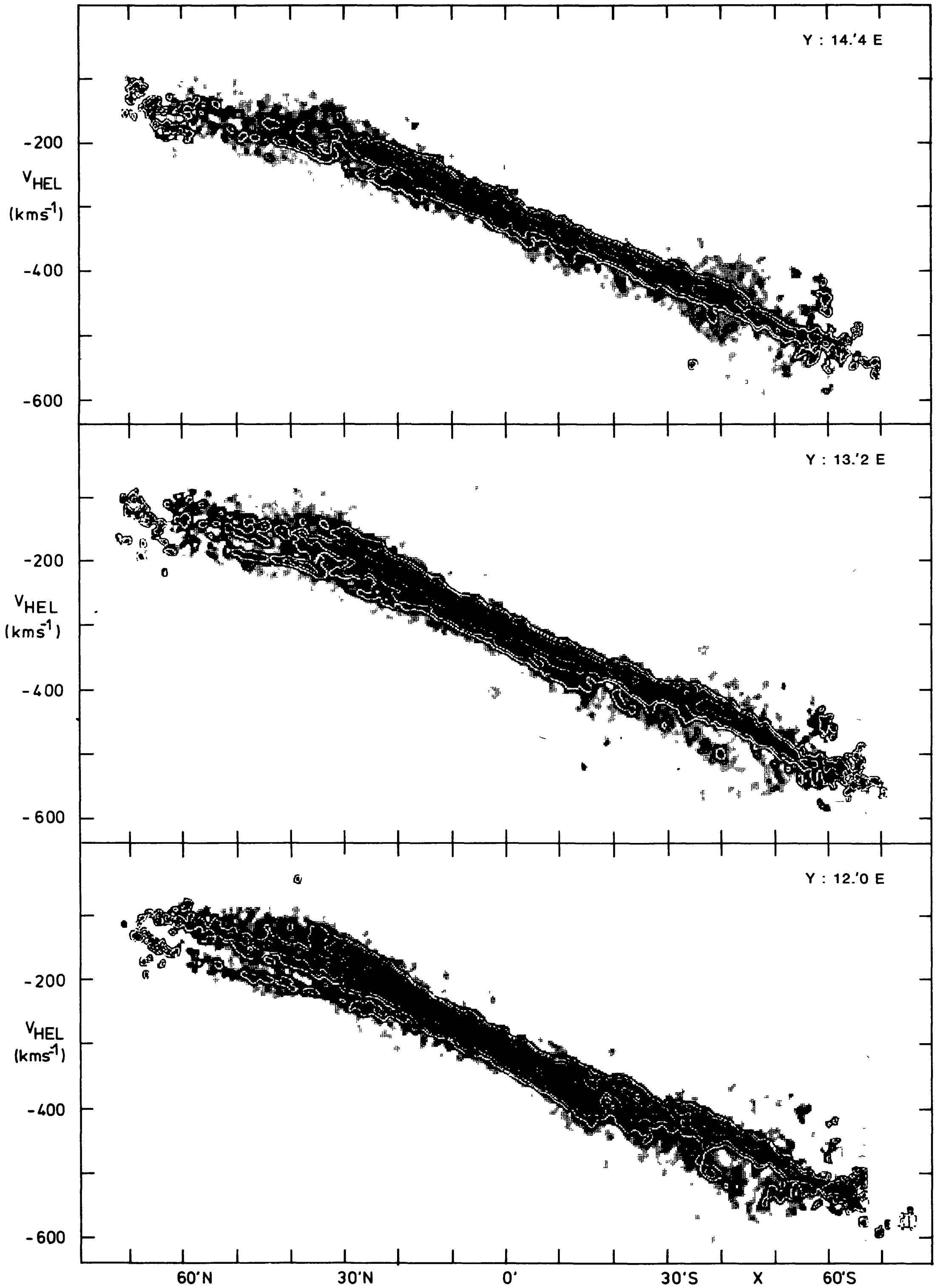

FIGURE 8 *(continued)*.

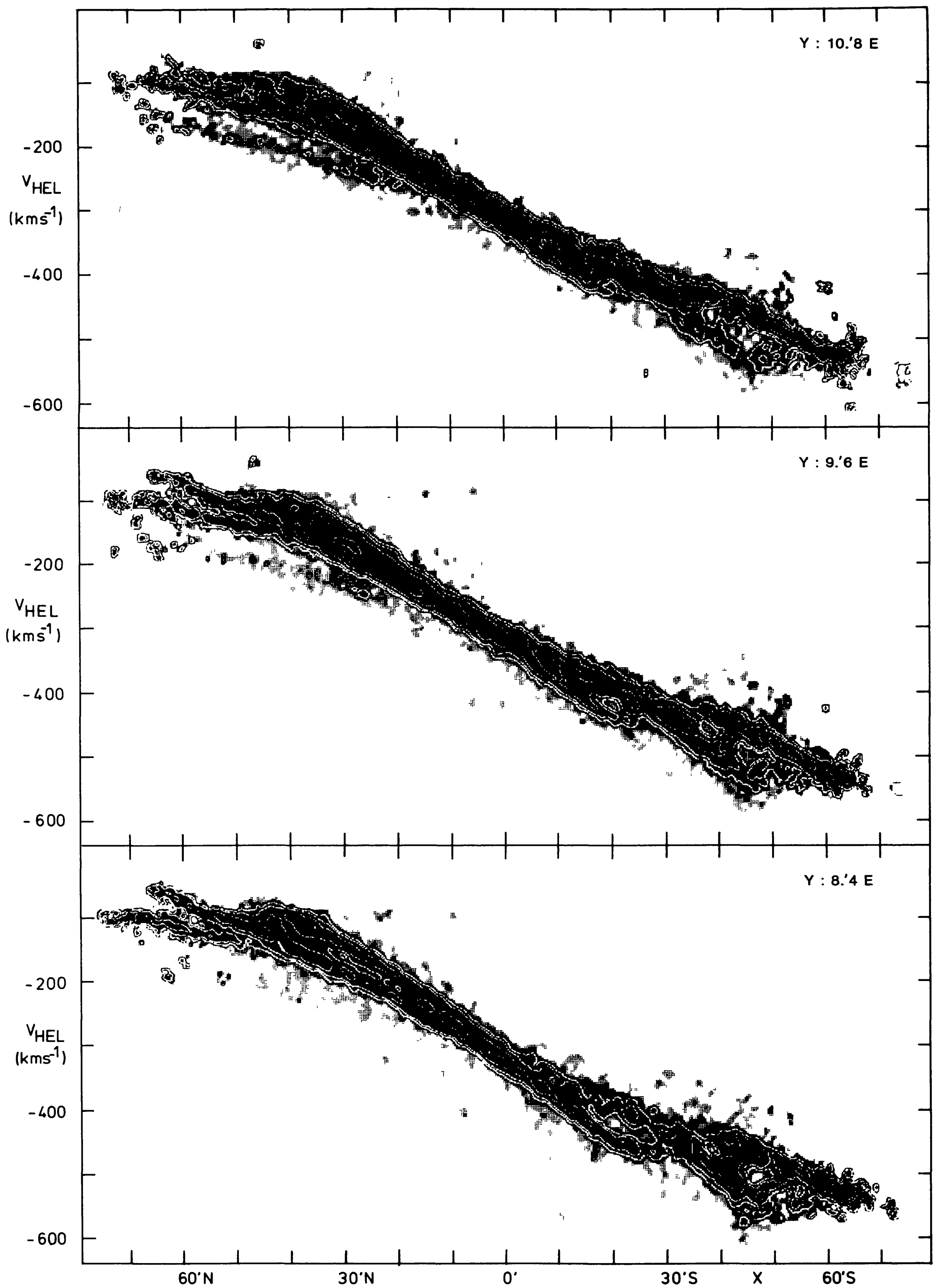

FIGURE 8 *(continued)*.

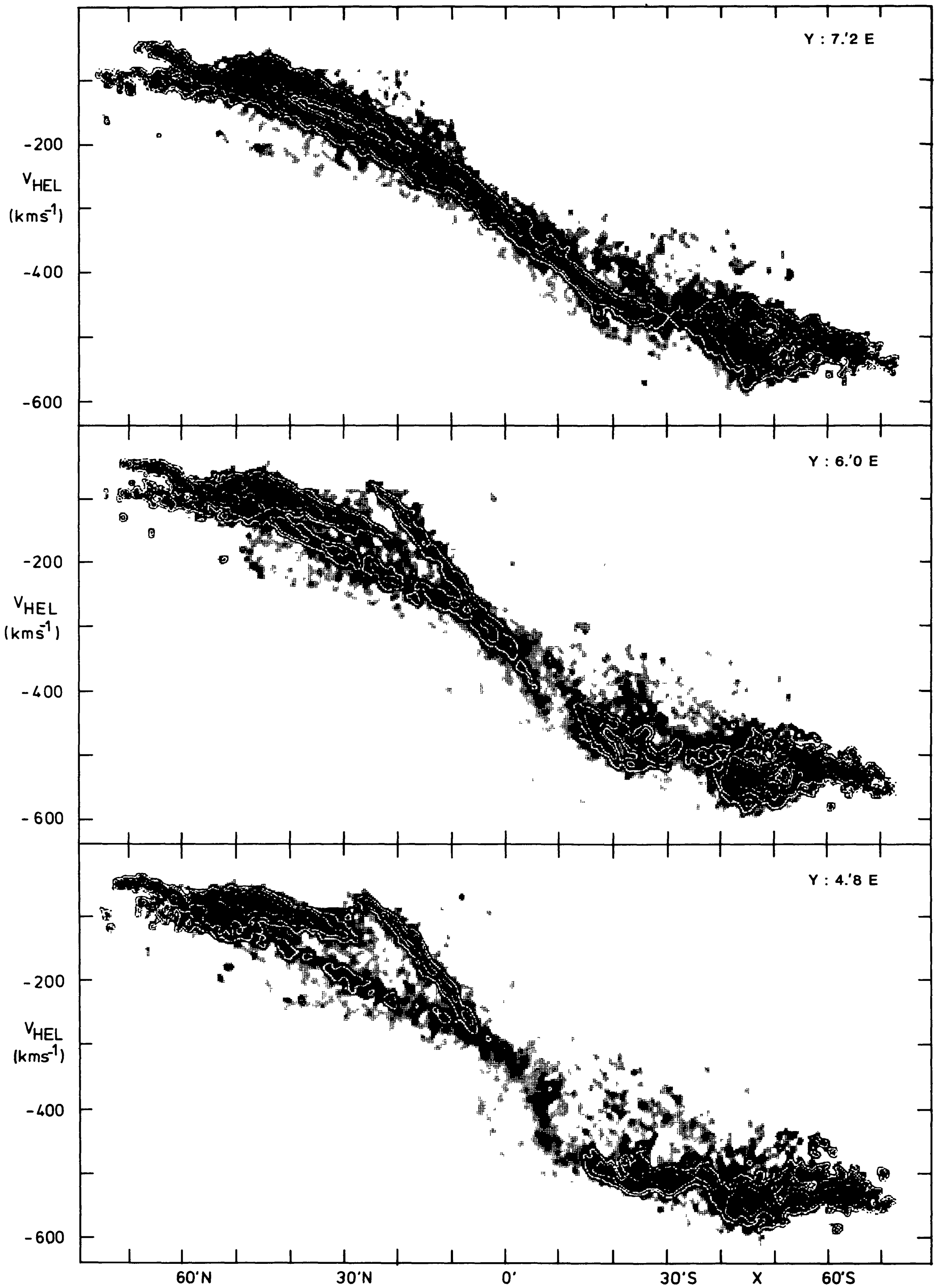

FIGURE 8 *(continued)*.

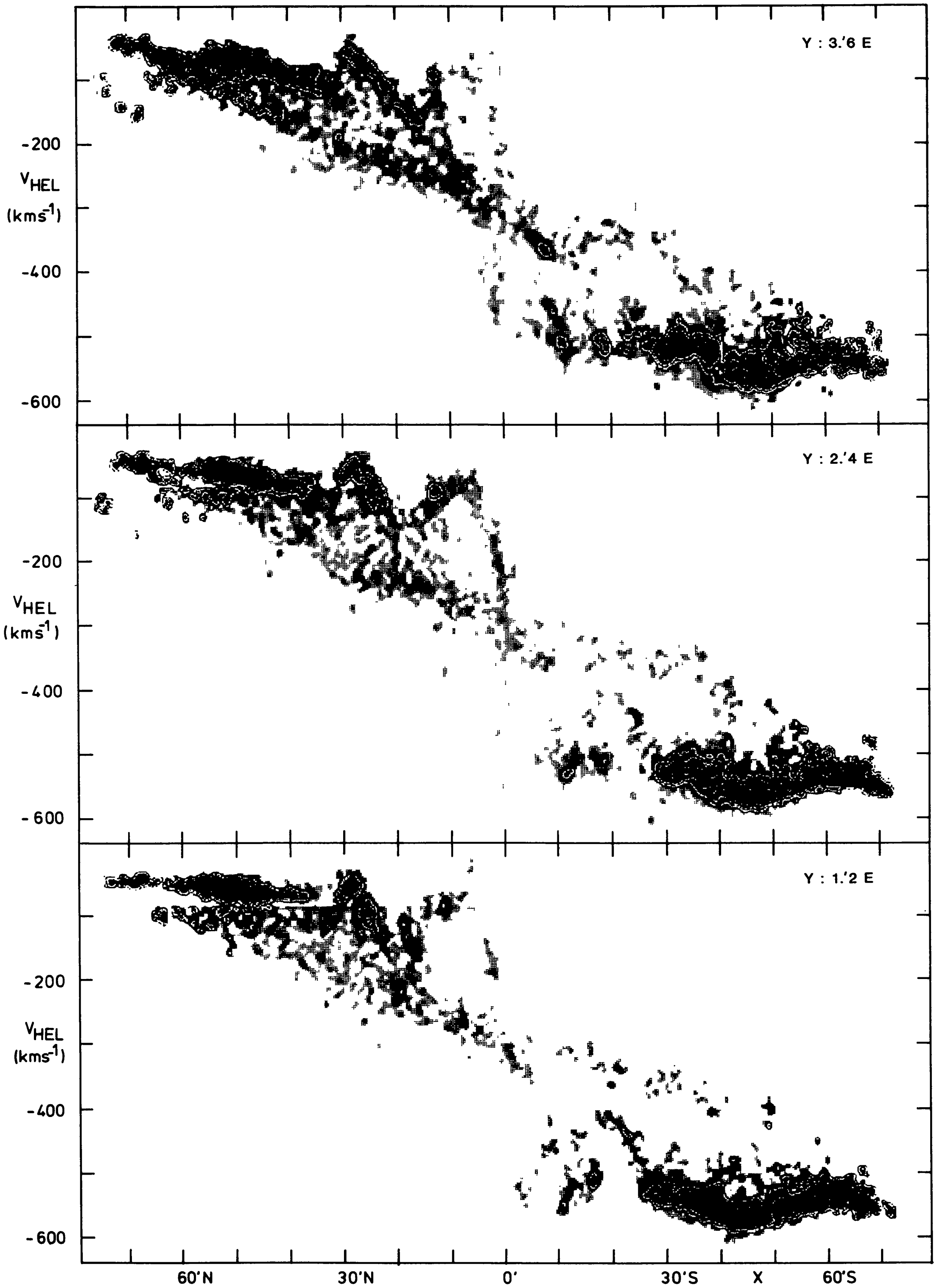

FIGURE 8 *(continued)*.

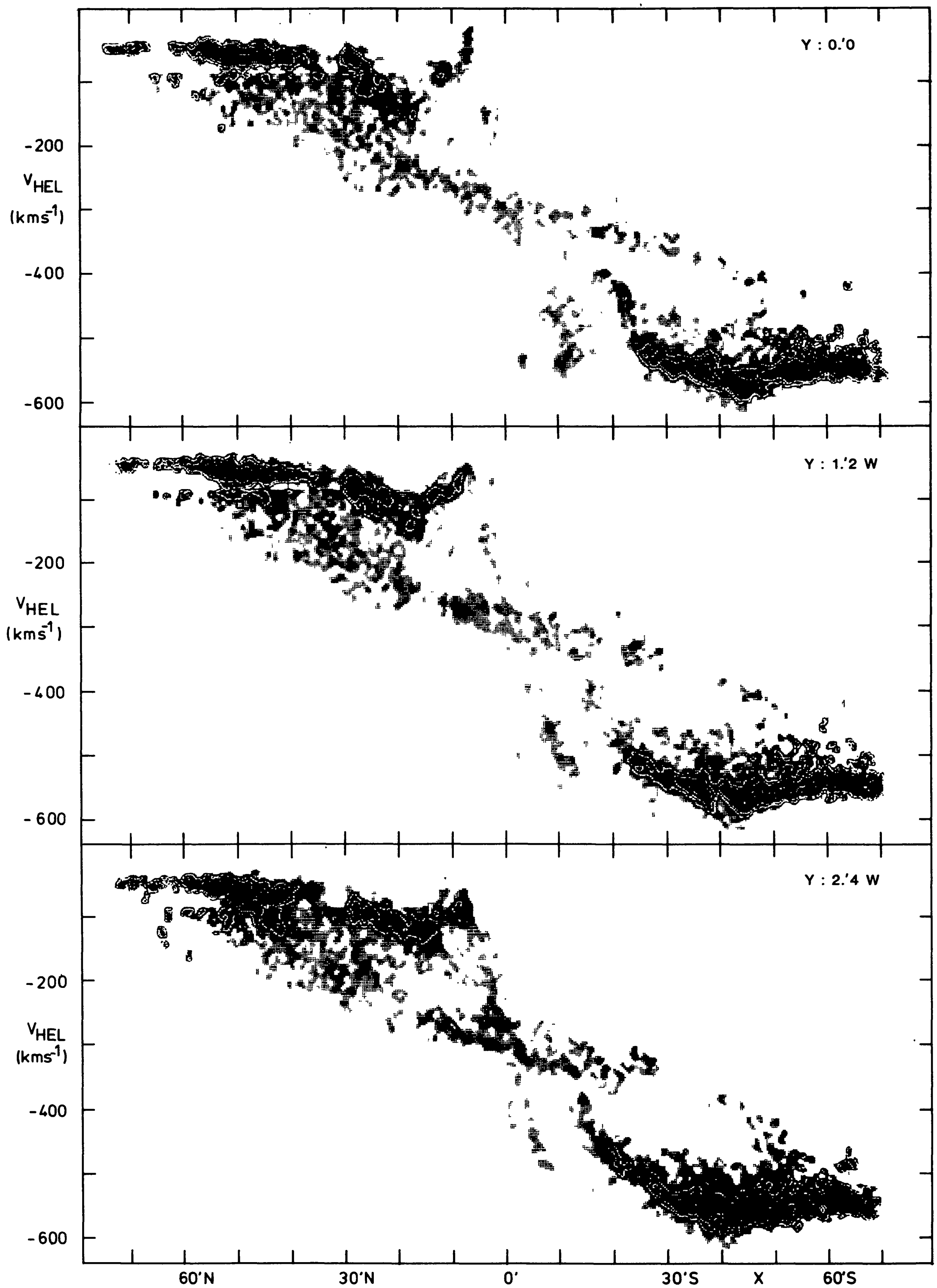

FIGURE 8 *(continued)*.

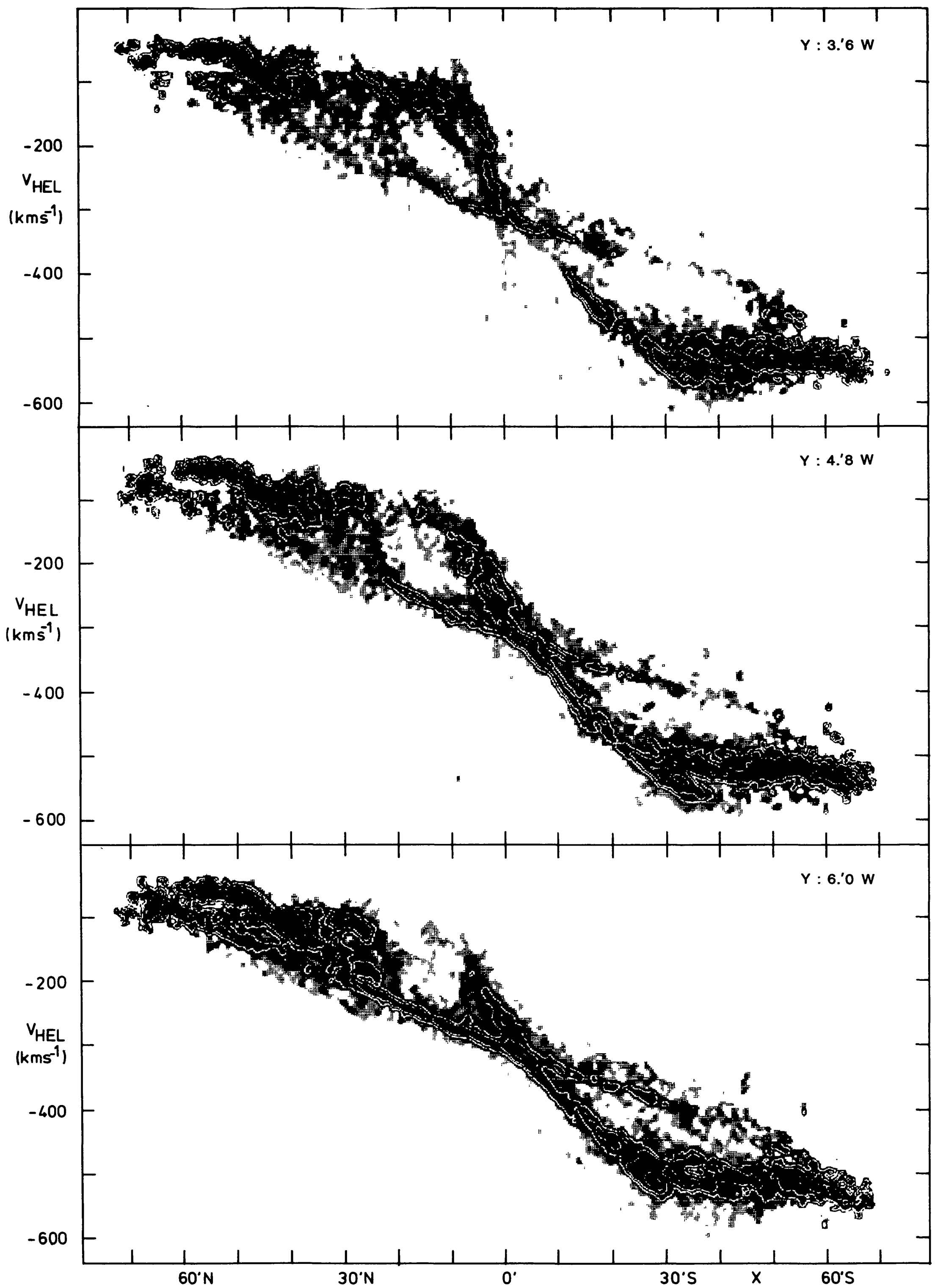

FIGURE 8 *(continued)*.

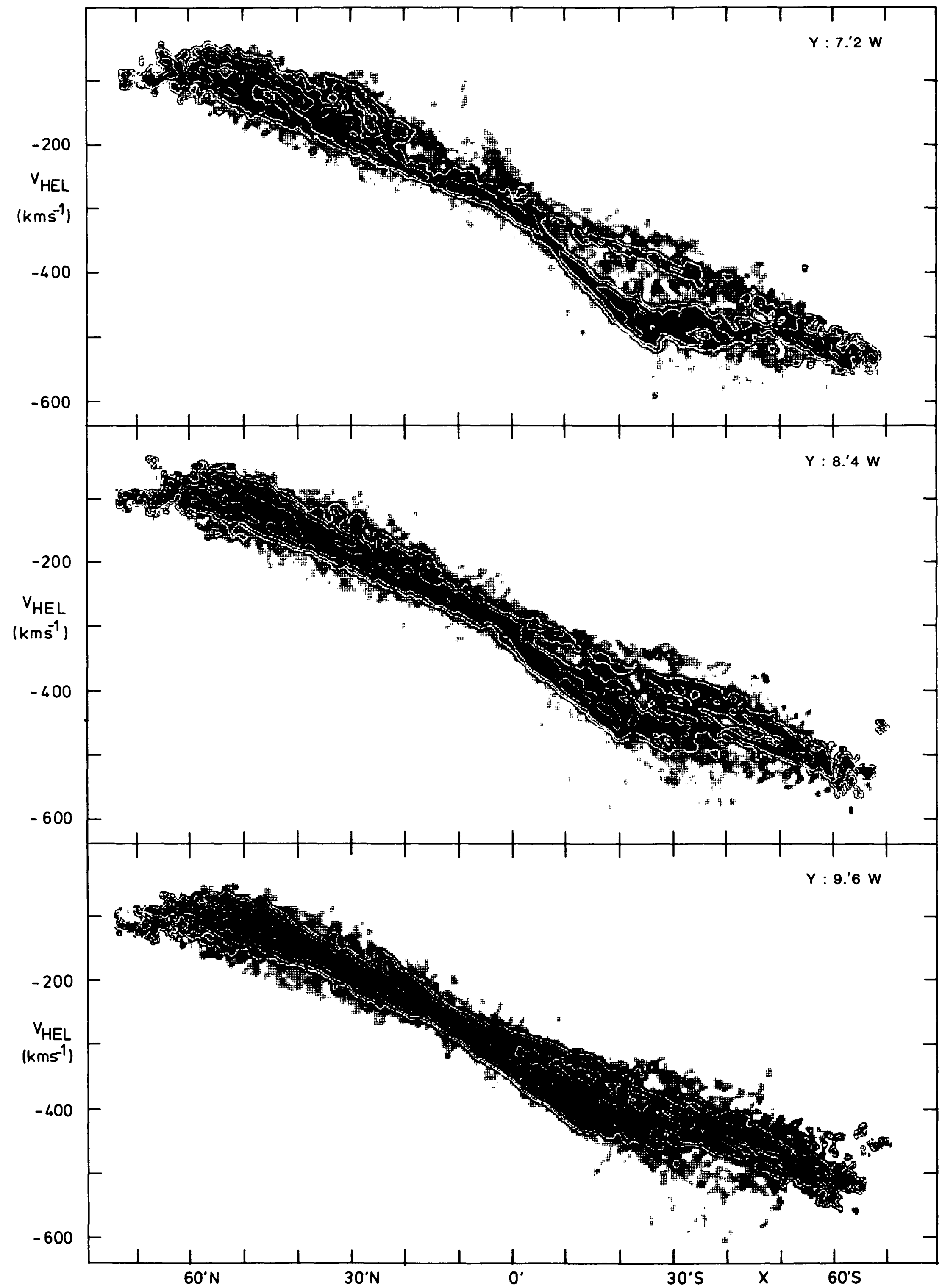

FIGURE 8 *(continued)*.

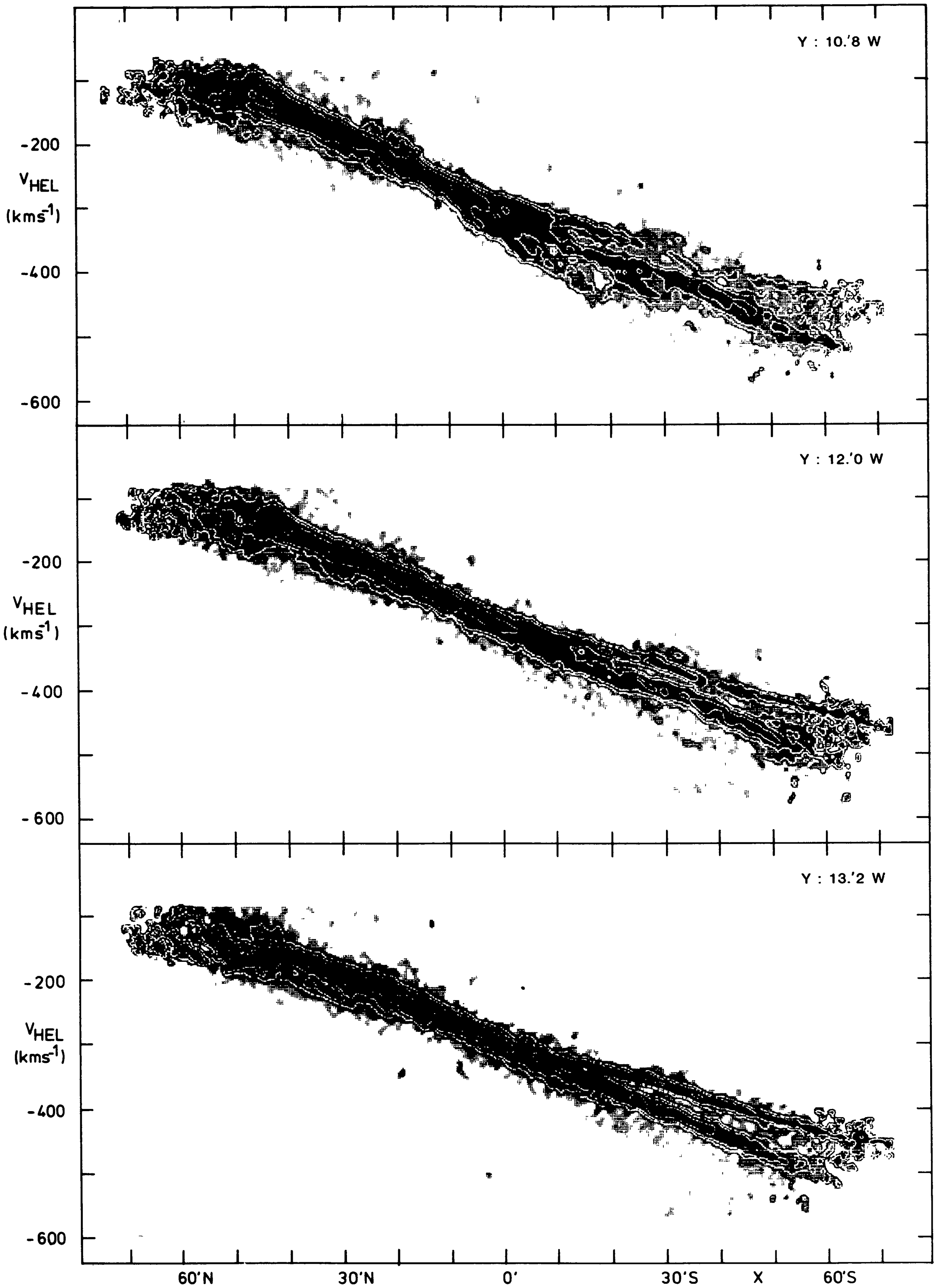

FIGURE 8 *(continued)*.

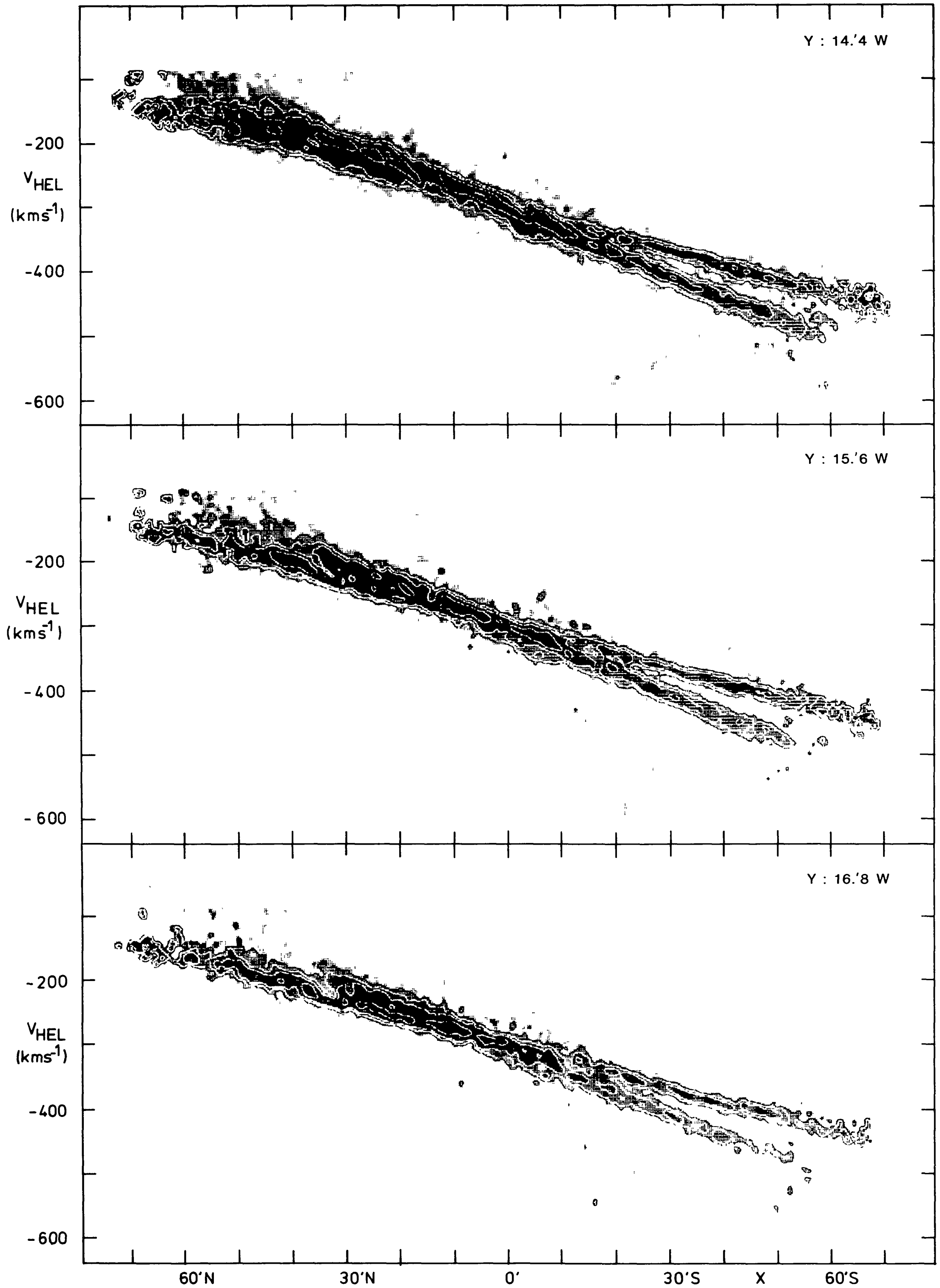

FIGURE 8 *(continued)*.

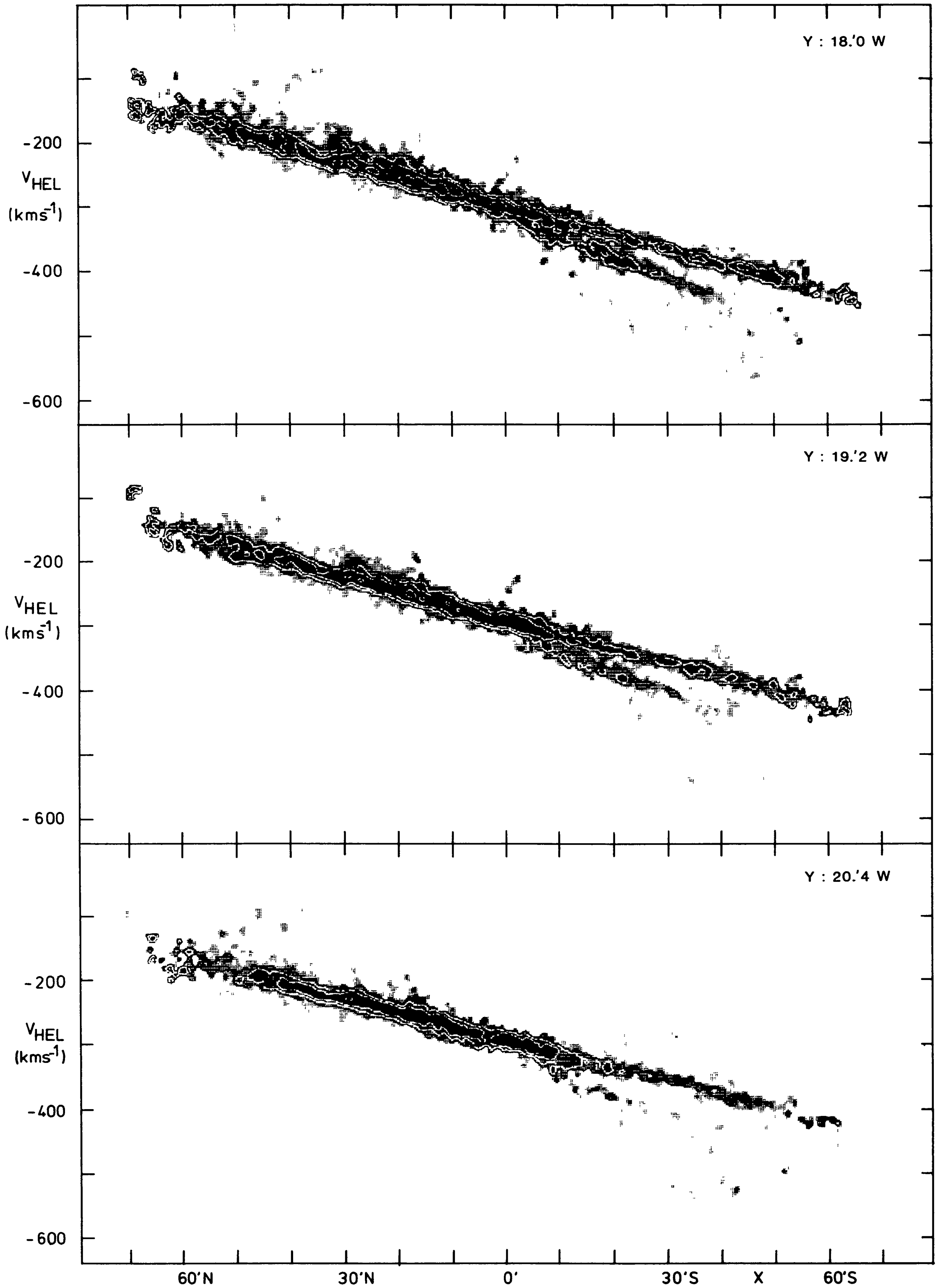

FIGURE 8 *(continued)*.

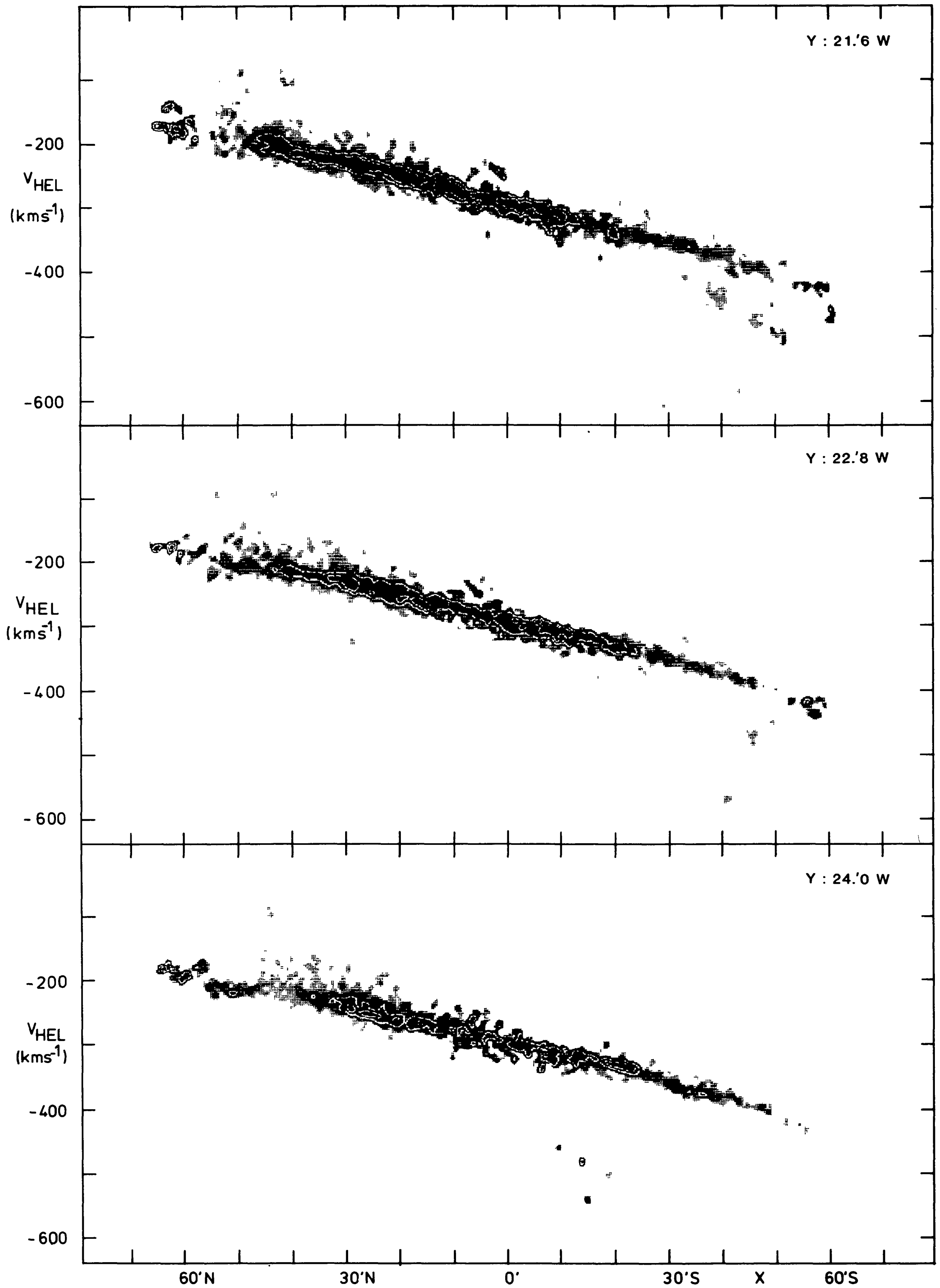

FIGURE 8 *(continued)*.

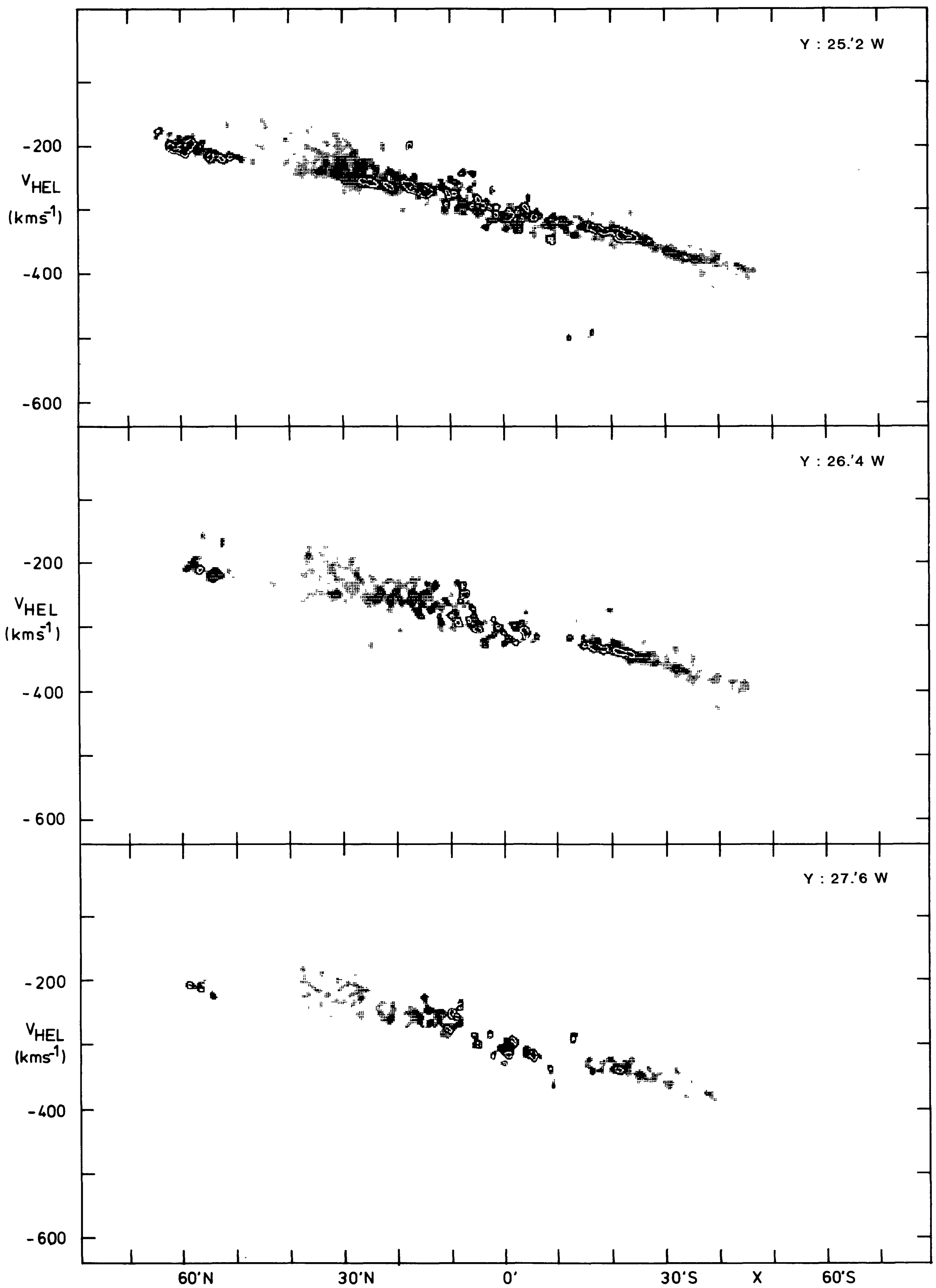

FIGURE 8 *(continued)*.

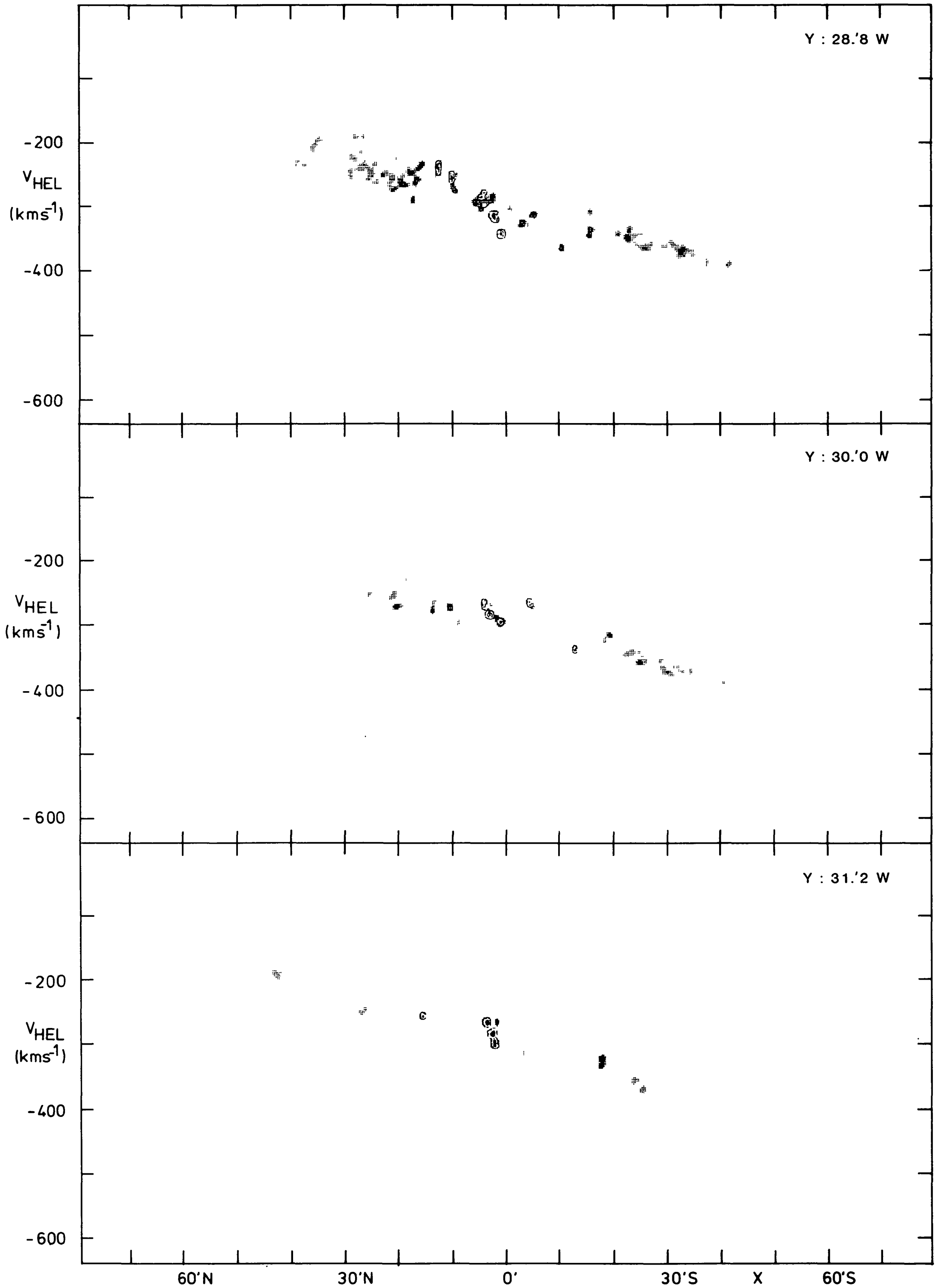

FIGURE 8 *(continued)*.

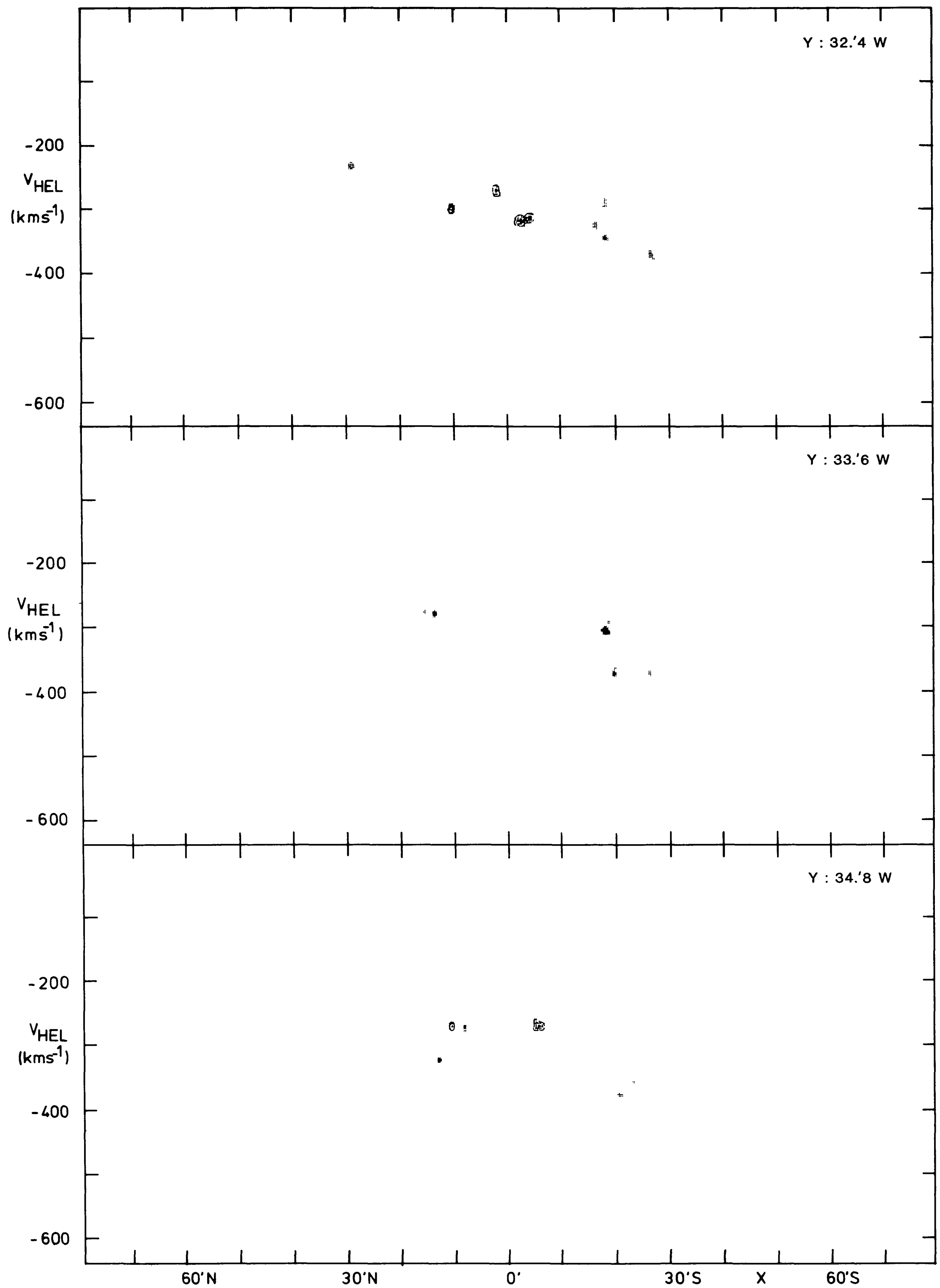

FIGURE 8 *(continued)*.

FIGURE 9. — Map of the total HI surface density at a resolution of 24″ × 36″. The map is a composition of two photographs taken from the LIPS-monitor. As in figure 6, the coordinates are only approximate. The white spot at about (7.5 N, 12.1 W) is caused by absorption against the strong background continuum source 5C3.107 (Pooley, 1969). Due to the limited coverage, the noise increases rapidly towards the northern and southern ends of the major axis.